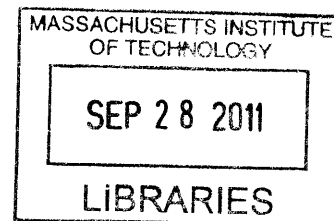


Amyloid Fibril Structure of Peptides and Proteins
by Magic Angle Spinning NMR Spectroscopy
and Dynamic Nuclear Polarization

by

Galia Tzvetanova Debelouchina

B.A., Colby College (2005)



ARCHIVES

Submitted to the Department of Chemistry
in Partial Fulfillment of the Requirements for the Degree of

Doctor of Philosophy in Chemistry

at the

MASSACHUSETTS INSTITUTE OF TECHNOLOGY

September 2011

© 2011 Massachusetts Institute of Technology. All rights reserved.

Signature of Author.....

Department of Chemistry
August 2nd, 2011

Certified by

Robert G. Griffin
Professor of Chemistry
Thesis Supervisor

Accepted by

Robert W. Field
Chairman, Departmental Committee on Graduate Students

This Doctoral thesis has been examined by a Committee of the Department of Chemistry as follows:

Professor Troy Van Voorhis
Chairman

Professor Robert G. Griffin.....
Thesis Supervisor

Professor Mounji G. Bawendi
.....

Amyloid Fibril Structure of Peptides and Proteins by Magic Angle Spinning NMR Spectroscopy and Dynamic Nuclear Polarization

by
Galia Tzvetanova Debelouchina

Submitted to the Department of Chemistry on August 26, 2011
in Partial Fulfillment of the Requirements for the
Degree of Doctor of Philosophy in Chemistry

ABSTRACT

Amyloid fibrils are insoluble, non-crystalline protein filaments associated with a number of diseases such as Alzheimer's and Type II diabetes. They can have a functional role in different organisms and many proteins and peptides have been found to form amyloid fibrils *in vitro*. We have used magic angle spinning (MAS) NMR spectroscopy to investigate the structure of two amyloid fibril systems – an 11-residue segment from the disease-related protein transthyretin (TTR); and β_2 -microglobulin (β_2m), a 99-residue protein associated with dialysis-related amyloidosis. The TTR(105-115) case exemplifies our efforts to characterize the hierarchy of structures present in the fibril form, including the organization of the β -strands into β -sheets (tertiary structure), the β -sheet interface that defines each protofilament (quaternary structure), and the protofilament-to-protofilament contacts that lead to the formation of the complete fibril. Our efforts were guided by information obtained from other methods such as cryo-electron microscopy and atomic force microscopy, and resulted in the very first atomic resolution structure of a complete amyloid fibril. We have extended the methods used in the TTR(105-115) structure determination procedure to the fibrils formed by β_2m , a process complicated not only by the much larger size of the protein involved but also by the high degree of dynamics exhibited in these fibrils. Nevertheless, we were able to characterize the secondary structure of the protein in the fibril form, and the tertiary and quaternary interactions within the fibrils. In addition, we have compared at the molecular level β_2m fibrils formed under different conditions, in an effort to characterize the origins of fibril polymorphism for this protein sequence. Our work on amyloid fibrils has also benefited extensively from the development of dynamic nuclear polarization, a method used to enhance the sensitivity of MAS NMR experiments, leading to unprecedented gains in signal-to-noise ratios and acquisition times.

Thesis Supervisor: Robert G. Griffin
Title: Professor of Chemistry

Dedicated to Mom, Dad and Ivan.

Acknowledgements

The work presented in this dissertation would not have been possible without the support and encouragement of my advisor, Robert Griffin, who allowed me to work independently on many interesting and exciting projects, to pursue my ideas and to learn from my mistakes in the course of this research. He made sure I became a well-rounded scientist, not afraid to take probes apart when things went wrong, or embark on new scientific journeys when opportunities presented themselves.

I would like to thank Dr. Marvin Bayro for being a great collaborator in many of the projects presented in this dissertation, and for teaching me much of what I know about the experimental and theoretical aspects of MAS NMR. He was also a great mentor, who contributed tremendously to my scientific growth, and helped me navigate the sometimes confusing world of science.

During my time at MIT, I have had the pleasure of working with many great collaborators, including Prof. Sheena Radford, Dr. Geoffrey Platt, Theodoros Karamanos and Dr. Claire Sarell at the University of Leeds, who provided me with a different perspective as to the importance of our work on β_2 -microglobulin fibrils, and very patiently met our demands for more and more samples. I have learnt a great deal from Dr. Anthony Fitzpatrick and Prof. Chris Dobson at the University of Cambridge, UK, while Dr. Kendra Frederick at the Whitehead Institute has been a true scientific “rock star” in tackling some of the most difficult amyloid proteins an NMR spectroscopist can imagine. Many thanks are also due to Melanie Rosay, Werner Maas, Shane Pawsey and Jochem Struppe at Bruker BioSpin who made sure our DNP experiments there ran as smoothly as possible.

I am indebted to many present and past members of the Griffin group for their ideas, support and encouragement during my time in the lab. I would like to thank Matthew Eddy, Loren Andreas, Patrick van der Wel, Gael de Paepe, Eugenio Daviso, Vladimir Michaelis and Marc Caporini for many productive discussions regarding protein NMR spectroscopy; Andy Smith, Bjorn Corzilius, Thorsten Maly, Alexander Barnes and Kan-Nian Hu for helping me understand the not so obvious aspects of DNP; and last but not the least Ajay Thakkar, Dave Ruben, Jeffrey Bryant, Ron DeRocher and Mike Mullins for taking great care of our spectrometers and probes.

My time at MIT would not have been the same without “Muddy Wednesday” and the “Wingers Crew”. I thank Marvin, Becky, Marc, Leo, Ziad, Beans, Bert, Bj and Jason for making Wednesday a day to look forward to. I am also very grateful to Nina for making my first year at MIT much more welcoming, and my friends Vasi, Magi and Tsveti for always being there when I needed them.

My parents and my brother, Ivan, supported me through this experience with much love, patience and understanding, and it is to them that this work is dedicated.

Table of Contents

Acknowledgements	9
List of Figures	14
List of Tables	17
Chapter 1. Introduction	19
1.1. Preface.....	19
1.2. Amyloid fibrils.....	19
1.3. Basics of MAS NMR spectroscopy	22
1.3.1. <i>The Zeeman interaction</i>	<i>23</i>
1.3.2. <i>The chemical shift interaction</i>	<i>24</i>
1.3.3. <i>The scalar interaction.....</i>	<i>25</i>
1.3.4. <i>The dipolar interaction.....</i>	<i>25</i>
1.3.5. <i>The radio-frequency Hamiltonian</i>	<i>28</i>
1.3.6. <i>The effect of MAS.....</i>	<i>28</i>
1.4. Protein Structure Determination with MAS NMR Spectroscopy	29
1.4.1. <i>Resonance assignments</i>	<i>29</i>
1.4.2. <i>Distance measurements</i>	<i>31</i>
1.5. Thesis outline	32
Chapter 2. Dynamic Nuclear Polarization at High Magnetic Fields	39
2.1. Introduction	40
2.2. Polarizing mechanisms in DNP experiments.....	42
2.2.1. <i>The solid effect.....</i>	<i>43</i>
2.2.2. <i>Cross-effect/thermal mixing.....</i>	<i>44</i>
2.3. Polarization agents.....	46
2.3.1. <i>Polarizing agents for the SE.....</i>	<i>48</i>
2.3.2. <i>Polarizing agents for TM and CE.....</i>	<i>48</i>
2.4. Instrumentation.....	50
2.4.1. <i>Gyrotrons.....</i>	<i>50</i>
2.4.2. <i>Low temperature MAS NMR probes.....</i>	<i>52</i>
Chapter 3. Dynamic Nuclear Polarization Studies of Amyloid Fibrils	59
3.1. Introduction	60
3.2. DNP enhancements of amyloid fibrils.....	61
3.3. Effects of temperature and TOTAPOL on spectral resolution	64
3.4. Effects of temperature and TOTAPOL on experimental efficiency	68
3.4.1. <i>¹H-¹³C cross polarization.....</i>	<i>68</i>
3.4.2. <i>Transverse relaxation.....</i>	<i>69</i>
3.5. Comparison of GNNQQNY crystals and amyloid fibrils.....	70
3.5.1. <i>DNP of GNNQny monoclinic crystals</i>	<i>70</i>
3.5.2. <i>Temperature dependent structural changes</i>	<i>73</i>
3.5. Conclusions	76
3.6. Materials and methods	76
3.6.1. <i>Sample preparation</i>	<i>76</i>
3.6.2. <i>DNP experiments</i>	<i>77</i>
3.6.3. <i>Room temperature experiments</i>	<i>78</i>
Chapter 4. Hierarchical Structure of an Amyloid Fibril Determined by MAS NMR and DNP-Enhanced Distance Measurements.....	83

4.1. Introduction	84
4.2. Results and Discussion	86
4.2.1. <i>Intra-sheet arrangement</i>	86
4.2.2. <i>Inter-sheet contacts</i>	89
4.2.3. <i>Protofilament arrangement</i>	97
4.2.5. <i>Combining MAS NMR, cryoEM, AFM and STEM to obtain the full structure of the fibril</i>	102
4.3. Conclusions	104
4.4. Methods	104
4.4.1. <i>Sample Preparation</i>	104
4.4.2. <i>DNP Experiments</i>	105
4.4.3. <i>Room Temperature MAS NMR Experiments</i>	105
4.4.4. <i>Data Fitting</i>	106
Appendix I	112
Chapter 5. Secondary Structure Analysis of β_2-Microglobulin Amyloid Fibrils Formed at pH 2.5	113
5.1. Introduction	114
5.2. Resonance assignment of LS β_2m fibrils	115
5.3. Dynamics of the N-terminus of LS β_2m fibrils	121
5.4. Chemical shift analysis of LS β_2m fibrils	122
5.5. The majority of residues are involved in the rigid core structure of LS β_2m fibrils	124
5.6. β_2m is organized in a non-native manner in amyloid-like fibrils	126
5.7. Conclusions	128
5.8.1. <i>Protein Expression and Purification</i>	129
5.8.2. <i>Fibril formation</i>	129
5.8.3. <i>Solid-state NMR spectroscopy</i>	129
Chapter 6. Intermolecular Alignment in β_2-Microglobulin Amyloid Fibrils	137
6.1. Introduction	138
6.2. Detection of backbone-to-backbone intermolecular interactions	139
6.3. Parallel, in-register β-strand arrangement in β_2m amyloid fibrils	141
6.4. Methods	143
6.4.1. <i>Sample Preparation</i>	143
6.4.2. <i>MAS NMR Spectroscopy</i>	143
Chapter 7. Long-Range Structural Constraints in β_2-Microglobulin Amyloid Fibrils	147
7.1. Introduction	148
7.2. Alternating labeling scheme	149
7.3. Experiments for efficient recoupling of long-range correlations	150
7.3.1. <i>BASE-RFDR</i>	150
7.3.2. <i>PDSD/DARR</i>	151
7.3.3. <i>Efficient recoupling of aromatic residues</i>	153
7.3.4. <i>TSAR-based experiments</i>	156
7.4. Specific labeling for unambiguous assignments	159
7.5. Distinguishing between <i>inter</i>-molecular and <i>intra</i>-molecular interactions	160
7.6. Summary of observed quaternary structural constraints in β_2m fibrils	164
Chapter 8. Structural Comparison of Three Distinct β_2-Microglobulin Amyloid Fibril Morphologies	169
8.1. Fibril polymorphism	170
8.2. Comparison of LS and WL fibrils	171

8.3. Comparison of LS and ΔN6 fibrils	175
8.4. Materials and Methods.....	178
8.4.1. <i>Protein Expression and Purification</i>	178
8.4.2. <i>Fibril Formation</i>	178
8.4.3. <i>MAS NMR Spectroscopy</i>	178
CURRICULUM VITAE	183

List of Figures

Figure 1.1. Examples of 2D Dipolar Correlation Experiments.

Figure 1.2. N(CO)CA and N(CA)CB correlations.

Figure 2.1. Energy level diagrams for the SE.

Figure 2.2. Energy level diagrams for the CE.

Figure 2.3. Chemical structures of DNP polarizing agents.

Figure 2.4. Low temperature MAS NMR probe for DNP experiments.

Figure 3.1. DNP-enhanced ^{13}C CP spectra of amyloid fibrils.

Figure 3.2. DNP-enhanced and room temperature ^{13}C CP spectra of $\beta_2\text{m}$ amyloid fibrils.

Figure 3.3. ^{13}C CP spectra of monoclinic GNNQQNY crystals recorded with and without DNP.

Figure 3.4. DNP-enhanced PDSD correlation spectrum of monoclinic GNNQQNY crystals.

Figure 3.5. DNP-enhanced ZF-TEDOR spectra of monoclinic GNNQQNY crystals.

Figure 3.6. Crystal lattice of monoclinic GNNQQNY.

Figure 3.7. Low temperature and room temperature chemical shift comparison of GNNQQNY monoclinic crystals and amyloid fibrils.

Figure 4.1. High-resolution structure of the TTR(105-115) monomer in amyloid fibrils.

Figure 4.2. Intrashet arrangement of TTR(105-115) amyloid fibrils.

Figure 4.3. PDSD spectrum of TTR(105-115) fibrils.

Figure 4.4. PAIN-CP spectrum of TTR(105-115) fibrils.

Figure 4.5. ZF-TEDOR buildup curves used for quantitative distance determination.

Figure 4.6. ZF-TEDOR and R2TRW mixing experiments of TTR(105-115) fibrils.

Figure 4.7. Summary of the observed quantitative contacts constraining the odd-even-odd-even anti-parallel β -sheet interface in TTR(105-115) fibrils.

Figure 4.8. Protofilament-to-protofilament arrangement in TTR(105-115) fibrils.

Figure 4.9. Structural complexity in the TTR(105-115) fibril spectra.

Figure 4.10. One-bond NCA correlation spectrum of a TTR(105-115) sample.

Figure 4.11. Atomic resolution structures of three different TTR(105-115) fibril classes as determined by MAS NMR, cryoEM, AFM and STEM.

Figure 5.1. RFDR correlation spectrum of U- β_2 m fibrils.

Figure 5.2. NCACX and NCOCX experiments of U- β_2 m fibrils.

Figure 5.3. One-bond ZF-TEDOR correlation spectra of 2- β_2 m and 1,3- β_2 m β_2 m fibrils.

Figure 5.4. Two-bond ZF-TEDOR correlation spectra of 2- β_2 m and 1,3- β_2 m fibrils.

Figure 5.5. RFDR correlation spectrum of VYL β_2 m fibrils.

Figure 5.6. INEPT-TOBSY correlation spectrum obtained of U- β_2 m fibrils.

Figure 5.7. TALOS and chemical shift analysis of the assigned residues in β_2 m fibrils.

Figure 5.8. Secondary structure comparison of β_2 m fibrils and native crystals.

Figure 6.1. ^{13}C CP and 1D ZFTEDOR spectra of mixed 2- β_2 m fibrils.

Figure 6.2. 1D ZF-TEDOR buildup experiments of mixed 2- β_2 m fibrils.

Figure 6.3. Comparison of the ^{15}N - ^{13}C region of correlation spectra obtained with ZF-TEDOR mixing for mixed and 100% labeled 2- β_2 m fibrils.

Figure 6.4. Summary of identified residues involved in parallel, in-register intermolecular interactions.

Figure 7.1. BASE-RFDR spectrum of a 2- β_2 m amyloid fibril sample.

Figure 7.2. The aliphatic region of a long-mixing PDS spectrum obtained with a 1,3- β_2 m amyloid fibril sample.

Figure 7.3. The aromatic regions long-mixing PDS spectra obtained with 1,3- β_2 m and 2- β_2 m amyloid fibril samples.

Figure 7.4. PAIN-CP spectra of 1,3- β_2 m and 2- β_2 m amyloid fibril samples.

Figure 7.5. PAR spectrum of a VYL- β_2 m amyloid fibril sample.

Figure 7.6. Comparison of long-mixing PDS spectra of a 100% labeled 2- β_2 m sample and a dilute 2- β_2 m sample.

Figure 7.7. Comparison of long-mixing PDS spectra of a 100% labeled 1,3- β_2 m sample and a dilute 1,3- β_2 m sample.

Figure 8.1. CryoEM images of β_2m fibrils in three distinct morphologies.

Figure 8.2. Comparison of ^{13}C CP and INEPT spectra of LS and WL U- b_2m fibrils.

Figure 8.3. Comparison of RFDR correlation spectra of WL and LS U- b_2m fibrils.

Figure 8.4. Comparison of RFDR correlation spectra of $\Delta N6$ and LS U- b_2m fibrils.

Figure 8.5. Comparison of TEDOR correlation spectra of $\Delta N6$ and LS U- b_2m fibrils.

List of Tables

Table 3.1. DNP enhancement ε and polarization buildup time τ for the fibril signals measured for several different fibril systems and preparations.

Table 3.2. Cross-polarization times necessary to obtain maximum signal intensity for the $C\alpha$ sites ($C\alpha$ max), the CO sites (CO max), and the value chosen to perform the CP experiments (CP opt). If measured, T_2' for the samples are also reported.

Table A1. Intra-sheet NMR restraints obtained for TTR(105-115) amyloid fibrils.

Table A2. Inter-sheet NMR restraints obtained for TTR(105-115) amyloid fibrils.

Chapter 1. Introduction

1.1. Preface

In the last decades, the importance of magic angle spinning^{1,2} (MAS) NMR in the field of structural biology has grown tremendously and the technique has already become the tool of choice in the atomic resolution structural investigations of complex, insoluble, non-crystalline biological systems. Starting from the explosive growth of available dipolar recoupling techniques in the 1990s and early 2000s,³⁻¹⁴ through the introduction of the alternating labeling scheme for protein sample preparation¹⁵⁻¹⁷ and the construction of MAS probes capable of spinning samples up to 60 kHz,¹⁸ to the first commercial 400 MHz dynamic nuclear polarization (DNP) spectrometer,¹⁹ the field has seen many innovations that have made possible the routine collection of high quality data for larger biological systems.

Perhaps the largest contribution of biomolecular MAS NMR so far, however, has been in the structural investigations of amyloid fibrils. Amyloid fibrils are insoluble, usually long and unbranched filaments, associated with over 20 different pathologies, including Alzheimer's disease, Type II diabetes, Parkinson's disease, dialysis-related amyloidosis, cataracts and Creutzfeldt-Jacobs disease.²⁰ They represent an outstanding biophysical problem as many proteins and peptides can form amyloid-like fibrils in vitro, while the molecular forces guiding the aggregation process are not very well understood.²¹ Amyloid fibrils with a functional role have also been identified in many different organisms, including humans.²² Therefore, understanding their structural organization and the molecular interactions that underline their remarkable stability has important implications in medicine, biology, and biophysics.

1.2. Amyloid fibrils

The term "amyloid" was first introduced in 1854 by the German physician Rudolph Virchow who examined brain tissues with a "spongy" appearance that stained blue when treated with iodine and violet upon the addition of sulfuric acid.^{23,24} As this was the standard test for starch at the time he named the abnormal brain tissue features "amyloid", as derived from the Greek word for starch or "amylon". Soon after, Friedreich and Kekule demonstrated that amyloid masses contained a very high content of nitrogen, and were therefore not of carbohydrate but of protein origin.²³ However, the term "amyloid" continued to be used for

the description of such tissue abnormalities. In the early 20th century, the availability of better technology improved the understanding of the physiochemical and structural properties of amyloid. First, the use of light microscopy showed that amyloid from different tissues shared a common preference for the histopathologic dye Congo red, resulting in a characteristic green birefringence with respect to the long axis of the deposit. In 1959, Cohen and Calkins used electron microscopy to observe that amyloid deposits from a variety of sources contain long, filamentous structures, thus providing further evidence for the presence of well-defined, shared structural characteristics among different amyloids.²⁵ Further progress allowed the isolation of amyloid fibrils from tissues and the observation of their distinctive X-ray diffraction patterns, known as “cross β ”.²⁶ This cross β diffraction pattern, observed first by L. Pauling in *Bombyx mori* silk,²⁷ contains two reflections. The first reflection corresponds to the 4.7 Å separation between β strands arranged along the fibril axis, and the second reflection to the 8-11 Å separation of the β sheets in a direction perpendicular to the fibril axis.²⁸ These three properties – the green birefringence upon Congo red binding, the filamentous appearance under electron microscopy, and the cross- β X-ray diffraction pattern – are still used today in the identification and classification of amyloid fibrils.

The amyloid fibrils found in disease are each associated with a specific protein or peptide. For example, the A β peptide forms the bulk of amyloid fibrils found in patients with Alzheimer’s disease, while the amyloid fibrils found in patients suffering from dialysis-related amyloidosis consist primarily of the 99-residue protein β_2 -microglobulin. In some cases, the amyloid forms of proteins can be infectious, causing neurodegenerative diseases such as scrapie and Creutzfeldt-Jacob disease. The revolutionary idea that a protein particle (“prion”) can be infectious was proposed by Pruisner in 1982 and awarded the Nobel Prize in Physiology or Medicine in 1997.²⁹

Amyloid fibril formation, however, is not specific only to proteins associated with disease. The serendipitous discovery of amyloid fibrils in a pH 2.0 solution containing the 86-residue SH3 domain of PI3 kinase in 1997,³⁰ a protein not associated with any known amyloid diseases, led Dobson to propose that amyloid formation may be a common property of globular proteins (under the appropriate conditions), and has important implications for the understanding of protein folding and misfolding in general.²¹ Today, *in vitro* conditions for

the aggregation of many proteins and peptides have been identified, including the addition of metal ions, high salt concentration, low pH, heating, ultrasonication, etc.

Perhaps more surprising, however, was the discovery in the late 1990s and early 2000s that amyloid fibrils can have a beneficial, functional role in many different organisms.²² Several bacterial species, for example, use extracellular amyloid fibrils, called curli, to form a proteinaceous matrix known as biofilm.^{31,32} These biofilms are important for bacterial colony growth, surface adhesion and host invasion, and make the treatment of certain infections extremely difficult. Yeast cells, on the other hand, employ prions in order to adapt to different environmental conditions.³³ For example, the protein Sup35 is a translation termination factor in *S. cerevisiae* and its aggregation leads to a different phenotype that is inherited after cell division.³⁴⁻³⁶ In humans, amyloid-like fibers formed by the protein Pmel17 provide scaffolding and sequestration of toxic intermediates during melanin synthesis.²² Understanding the molecular function of such amyloid fibrils will in no doubt require determining their atomic resolution structures.

Low resolution structural information of amyloid fibrils has been available through a variety of methods including X-ray diffraction, cryo-electron microscopy, atomic force microscopy, infra-red spectroscopy, and circular dichroism. While these techniques have provided valuable knowledge regarding the gross structural features in amyloid fibrils, true atomic resolution is necessary in order to understand and correlate the similarities and differences between the different classes of amyloid fibrils (disease amyloid, prions, functional amyloid), in order to gain an insight into their origins, stability and function, to develop therapeutic agents to combat disease, and to mimic their properties for potential new applications. MAS NMR is ideally suited to provide such detailed information and has become the leading method of choice for the structural investigation of amyloid fibrils.

The first MAS NMR studies of amyloid fibrils were conducted in the early 1990s, and focused on the fibrils formed by a 9-residue peptide from A β .³⁷⁻³⁹ The low resolution structural model obtained by ¹³C-¹³C distance measurements showed the presence of pleated antiparallel β -sheets, although the side chain conformation of the residues could not be determined at the time. Thanks to the numerous technical and experimental innovations, the field has come a long way since then. In 2004, the structure of an 11-residue fragment from the disease-related protein transthyretin (TTR) was the first published high resolution

structure of a peptide in an amyloid form.⁴⁰ Structural models are available today for a number of different systems including A β (1-40),^{41,42} Het-s(218-289),^{43,44} PI3-SH3,^{45,46} a 22-residue fragment of β_2 -microglobulin,⁴⁷ α -synuclein,⁴⁸⁻⁵⁰ the Y145Stop variant of the human prion protein,⁵¹ the GNNQQNY peptide,^{52,53} etc.

In this work, we present the first atomic resolution structure of a complete amyloid fibril formed by the TTR(105-115) segment. This includes the characterization of the protofilament interface, a feat that has been possible by combining MAS NMR with methods that can probe longer length scales, such as cryoEM and AFM. We also present structural studies of the amyloid fibrils formed by β_2 -microglobulin, a 99-residue protein associated with dialysis-related amyloidosis. In the course of this work, we have developed new methods for characterizing the different levels of amyloid fibril organization, and benefited from dynamic nuclear polarization (DNP), a method that enhances the sensitivity of MAS NMR experiments and leads to unprecedented savings in data acquisition times.⁵⁴⁻⁶⁰

1.3. Basics of MAS NMR spectroscopy

MAS NMR relies on the distance information encoded in dipolar couplings in order to provide knowledge of the spacial proximity of the atoms of interest. In principle, the ability to obtain distance information is not limited by the size of the protein or protein assembly, nor does it require macroscopic order, two clear advantages over solution NMR and X-ray crystallography, respectively. On the other hand, the anisotropic component of the spin interactions describing the system can complicate the extraction of structural information, thus making the field conceptually and technically more challenging.

The Hamiltonian describing a solid-state system consisting of spin $\frac{1}{2}$ nuclei in a magnetic field under radio-frequency (RF) irradiation has the following general form:

$$H = H_Z + H_{CS} + H_J + H_D + H_{RF}. \quad (\text{Eq. 1})$$

The first terms of the Hamiltonian describe the Zeeman, the chemical shift, the scalar and the dipolar interactions, respectively, while the last term describes the effect of the RF irradiation. The chemical shift and the dipolar interactions contain an anisotropic contribution, i.e. their effective strength depends on their angular orientation with respect to the external magnetic field. The forms of the five Hamiltonian terms will be described in some detail below, while much more detailed accounts can be found in many excellent books and reviews.⁶¹⁻⁶⁵ For

nuclei with spin other than $\frac{1}{2}$, the Hamiltonian also includes the quadrupolar interaction term, which will not be discussed further in this introduction, as the protein nuclei of interest, ^1H , ^{13}C and ^{15}N , are all spin $\frac{1}{2}$ nuclei.

1.3.1. The Zeeman interaction

The Zeeman term is the product of the magnetic field vector \mathbf{B}_0 and the nuclear angular momentum operator \mathbf{I} , i.e.

$$H_z = -\gamma\hbar\mathbf{B}_0 \cdot \mathbf{I}, \quad (\text{Eq. 2})$$

where γ and \hbar are the gyromagnetic ratio and Planck's constant, respectively. Conventionally, the external magnetic field is defined along the z-axis of the laboratory frame, and Eq. 2 is simplified to

$$H_z = -\gamma\hbar B_0 I_z. \quad (\text{Eq. 3})$$

The size of this term is in the MHz range, and the product

$$\omega_0 = \gamma B_0, \quad (\text{Eq. 4})$$

known as the nuclear Larmor frequency, describes the frequency of precession of the nuclear spin around the external magnetic field vector.

The eigenvalues of this Hamiltonian represent the energies associated with the different possible states of the nuclear spin and can be calculated using the equation

$$E_m = -\gamma\hbar B_0 m = -m\hbar\omega_0. \quad (\text{Eq. 5})$$

In the case of a nuclear spin $\frac{1}{2}$, the possible values for m are $\pm\frac{1}{2}$ and the corresponding energy levels become

$$E_m = \pm\frac{1}{2}\gamma\hbar B_0 = \pm\frac{1}{2}\hbar\omega_0 \quad (\text{Eq. 6})$$

with the $+\frac{1}{2}$ state representing the lower energy. Note that the energy difference between the two states is equal to $\hbar\omega_0$.

In a sample of non-interacting spin $\frac{1}{2}$ nuclei, each spin can exist in one of two possible states and at equilibrium the population p of state m is governed by the Boltzmann distribution

$$p_m = \frac{\exp(-E_m / kT)}{\sum_m \exp(-E_m / kT)}. \quad (\text{Eq. 7})$$

This expression can be simplified by using the Taylor expansion where

$$\exp\left(\frac{-E_m}{kT}\right) \approx 1 - \frac{E_m}{kT}. \quad (\text{Eq. 8})$$

With this approximation, the population difference, or polarization P , of the two states can be calculated and is given by the equation

$$P = \frac{\gamma \hbar B_0}{2kT}. \quad (\text{Eq. 9})$$

For a 21 T external magnetic field (corresponding to 900 MHz ^1H Larmor frequency) and a temperature of 300 K, the polarization difference of the protons in a protein sample is only 0.014%. Since any observed signal arises from transitions between the two states, and the population difference between the states is intrinsically small, the sensitivity of NMR experiments is also inherently low. From Eq. 9 it follows that the polarization difference between the states can be increased by using higher magnetic fields or lowering the temperature. The sensitivity enhancements achieved this way, however, are very small compared to the enhancements possible due to dynamic nuclear polarization.^{54-60,62} In the proton case, the theoretical enhancement due to DNP is equal to $\gamma_e/\gamma_H = 660$ where γ_e and γ_H denote the electron and proton gyromagnetic ratios, respectively. Achieving this enhancement then can potentially lead to a 660^2 factor of acquisition time savings.

1.3.2. The chemical shift interaction

The chemical shift Hamiltonian is described in the following equation

$$H_{CS} = \gamma \hbar (\mathbf{I} \cdot \boldsymbol{\sigma} \cdot \mathbf{B}_0). \quad (\text{Eq. 10})$$

Here, $\boldsymbol{\sigma}$ is the chemical shielding tensor, and it describes the perturbation of the nuclear spin caused by the surrounding electrons. As the external magnetic field orients the nuclear spins,

it also determines the strength and direction of the electron shielding around them, thus giving rise to an orientational, or anisotropic, contribution. The size of this contribution is on the order of 1 – 100 kHz, depending on the nucleus, and can lead to broad spectral features (known as “powder patterns”) for static powder samples. The chemical shift anisotropy can be averaged with the use of magic angle spinning, and MAS NMR spectra usually contain relatively sharp peaks with chemical shifts corresponding to the isotropic value. In some cases, when the chemical shift anisotropy is particularly large, e.g. carbonyl nuclei, and the MAS frequency is not fast enough, artifacts known as “spinning side-bands” may be observed in the spectra. It is important to remember, however, that the chemical shift anisotropy encodes spatial structural information that can be used in protein structure calculation and refinement.^{66,67}

1.3.3. The scalar interaction

The scalar or J-coupling interaction between two nuclear spins i and j arises from interactions mediated through the bonding electrons and has the following form

$$H_J = \gamma_i \gamma_j (\mathbf{I}_i \cdot \mathbf{J} \cdot \mathbf{I}_j). \quad (\text{Eq. 11})$$

Where \mathbf{J} is the scalar tensor. This interaction is typically small (10 – 100 Hz) and is hard to measure in rotating solids. Therefore, the effective scalar coupling reduces to

$$H_J = J (\mathbf{I}_i \cdot \mathbf{I}_j). \quad (\text{Eq. 12})$$

where J is the isotropic value. Since the size of the ^{13}C - ^{13}C J-couplings is on the order of the typical ^{13}C line-widths observed in protein spectra, these interactions can be a serious source of line broadening. Labeling schemes that reduce the number of directly bonded ^{13}C atoms in proteins and therefore lead to improved line width and experimental performance will be discussed later in this thesis.

1.3.4. The dipolar interaction

The classical energy describing the interaction between two magnetic dipoles μ_1 and μ_2 connected by a distance vector r is given by the following expression

$$E = \frac{\mu_0}{4\pi} \left\{ \frac{\boldsymbol{\mu}_1 \cdot \boldsymbol{\mu}_2}{r^3} - 3 \frac{(\boldsymbol{\mu}_1 \cdot \mathbf{r})(\boldsymbol{\mu}_2 \cdot \mathbf{r})}{r^5} \right\}. \quad (\text{Eq. 13})$$

Quantum mechanically, the magnetic moment operator $\boldsymbol{\mu}$ for a spin I is described by the equation

$$\boldsymbol{\mu}_i = \gamma \hbar \mathbf{I}_i. \quad (\text{Eq. 14})$$

Therefore, the dipolar Hamiltonian for the interaction of two nuclear spins I and S can be written in the following way

$$H_D = \left(\frac{\mu_0}{4\pi} \right) \gamma_I \gamma_S \hbar \left(\frac{\mathbf{I} \cdot \mathbf{S}}{r^3} - 3 \frac{(\mathbf{I} \cdot \mathbf{r})(\mathbf{S} \cdot \mathbf{r})}{r^5} \right). \quad (\text{Eq. 15})$$

In Cartesian representation this expression can be rewritten in the more familiar form

$$H_D = \gamma_I \gamma_S (\mathbf{I} \cdot \mathbf{D} \cdot \mathbf{S}). \quad (\text{Eq. 16})$$

where \mathbf{D} is the dipolar tensor. Unlike the chemical shift tensor, the dipolar tensor does not contain an isotropic component, and it can be averaged to zero by molecular motion. e.g. in solution NMR.

It is more convenient, however, to use spherical coordinates and to rewrite the Hamiltonian in Eq. 15 in the following way

$$H_D = \omega_D (A + B + C + D + E + F), \quad (\text{Eq. 17})$$

where

$$\begin{aligned}
\omega_D &= \left(\frac{\mu_0}{4\pi} \right) \frac{\gamma_I \gamma_S \hbar}{r^3} & (\text{Eq. 18}) \\
A &= I_z S_z (3 \cos^2 \theta - 1) \\
B &= -\frac{1}{4} [I^+ S^- + I^- S^+] (3 \cos^2 \theta - 1) \\
C &= \frac{3}{2} [I_z S^+ + I^+ S_z] \sin \theta \cos \theta e^{-i\phi} \\
D &= \frac{3}{2} [I_z S^- + I^- S_z] \sin \theta \cos \theta e^{-i\phi} \\
E &= \frac{3}{4} I^+ S^+ \sin^2 \theta e^{-2i\phi} \\
F &= \frac{3}{4} I^- S^- \sin^2 \theta e^{+2i\phi}
\end{aligned}$$

The polar angles θ and ϕ specify the orientation of the I - S nuclear vector r with respect to the external magnetic field B_0 , while ω_D describes the relationship between distance and experimentally determined dipolar coupling. I^+ , I^- , S^+ and S^- are the raising and lowering operators for spins I and S , respectively.

In order to understand the effect of the dipolar Hamiltonian, H_D needs to be transformed to a frame, rotating at the Larmor frequency of the observed spin, as this is the frame from which spins are observed during an NMR experiment. Furthermore, the properties of the resulting Hamiltonian depend on whether I and S are the same type of nucleus or not. In the *homonuclear* case, e.g. when I and S represent two ^{13}C nuclei or two ^1H nuclei, the first order average dipolar Hamiltonian in the rotating frame contains contribution from the A and B terms defined in Eq. 18, and adopts the following form

$$H_D^{\text{hom}} = -\omega_D \frac{1}{2} (3 \cos^2 \theta - 1) [3I_z S_z - \mathbf{I} \cdot \mathbf{S}]. \quad (\text{Eq. 19})$$

This Hamiltonian is an example of a homogenous interaction, and is therefore not averaged out under MAS, unless the MAS frequency is much larger than the size of the interaction. For example, the protons in a protein sample represent a strongly coupled dipolar bath, with interactions on the order of 20 – 50 kHz.⁶¹ Therefore, at moderate MAS frequencies, these interactions dominate the ^1H line width in the spectra, and high resolution ^1H NMR spectroscopy of fully protonated solid samples is not possible under these conditions. Much

better ^1H line widths can be obtained in perdeuterated protein samples, where the proton concentration is reduced and the network of strongly coupled spins is diluted to a great extent.⁶⁸

The first-order average *heteronuclear* dipolar Hamiltonian in the rotating frame is

$$H_D^{heter} = -\omega_D (3\cos^2\theta - 1) I_z S_z. \quad (\text{Eq. 20})$$

This Hamiltonian is truncated even further than the homonuclear one, and does not contain a contribution from the B term up to first order. It represents an inhomogeneous interaction and behaves in a similar way as the chemical shift.

1.3.5. The radio-frequency Hamiltonian

The general form of the RF Hamiltonian is

$$H_{RF} = -\gamma\hbar\mathbf{I} \cdot \mathbf{B}_1. \quad (\text{Eq. 21})$$

where \mathbf{B}_1 describes the irradiation field of strength B_1 and frequency ω . In an NMR experiment, the RF field usually oscillates with time t in a direction, perpendicular to the direction of the external magnetic field, and Eq. 21 can be rewritten as

$$H_{RF} = -2\gamma\hbar B_1 (\cos\omega t) I_x. \quad (\text{Eq. 22})$$

Since $I_x = \frac{I^+ + I^-}{2}$ where I^+ and I^- are the raising and lowering operators, this Hamiltonian can induce transitions between the energy levels of the spin system.

1.3.6. The effect of MAS

The main sources of line broadening in biomolecular MAS NMR spectroscopy are the chemical shift anisotropy and the heteronuclear dipolar interactions. In liquids, these Hamiltonian terms are averaged out by molecular motions either to their isotropic value (chemical shift) or to zero (dipolar coupling). Since both of these Hamiltonians contain a $3\cos^2\theta - 1$ dependence, they can also be averaged out to the first-order by choosing an appropriate value for θ that makes the above expression equal to zero. This value for θ is 54.7° , which represents the magic angle.⁶⁹ When the MAS frequency ω_r is much larger than

the chemical shift anisotropy, the broad powder pattern collapses into a sharp isotropic peak. In the case when ω_r is on the order of the chemical shift anisotropy interaction, spinning side-bands separated by ω_r appear in the spectra. The spinning side-bands can be used to obtain the chemical shift tensor elements, and they therefore carry important structural information.⁶⁶ However, their appearance can also complicate the interpretation of the spectra and in protein MAS NMR spectroscopy ω_r is usually selected in such a way, so that the spinning side-bands fall into an empty region of the spectrum.

Since MAS averages out the dipolar Hamiltonian, the distance information encoded in the dipolar couplings is lost, and the relevant terms of the Hamiltonian need to be re-introduced using pulses of RF irradiation. There are many pulse sequences that can be used to achieve that and some of them will be discussed throughout the thesis (e.g. see Section 1.4, Chapters 4 and 8). In some cases, however, the elimination of dipolar couplings can be beneficial, as is the case for the ^{13}C - ^1H couplings that cause significant line broadening in the spectra. As they are averaged only incompletely by MAS (the strong ^1H - ^1H couplings introduce a homogeneous component to the heteronuclear coupling), proton decoupling is usually used during the acquisition period of the pulse sequences.^{70,71}

1.4. Protein Structure Determination with MAS NMR Spectroscopy

1.4.1. Resonance assignments

The structure determination process in MAS NMR consists of three steps: resonance assignments, measurement of distance constraints, and structure calculation. Resonance assignments are usually performed with 2D and 3D experiments, which correlate the chemical shifts of several spins via coherence transfers. Typical 2D correlation experiments are shown in Figure 1.1. They usually start with a cross-polarization (CP) step, where the higher polarization of the abundant high γ proton nuclei is transferred to the observed low γ nuclei, e.g. ^{13}C and ^{15}N .⁷² After CP, the ^{13}C coherence, for example, is allowed to evolve during a variable time t_1 (Figure 1.1a). During the subsequent mixing step, coherence transfer is induced by applying a suitable pulse sequence, and the resulting FID is detected during time t_2 . ^1H - ^{13}C (or ^1H - ^{15}N) interactions are usually eliminated by two pulse phase modulation

(TPPM) decoupling during the evolution and detection periods, and sometimes during mixing.^{70,71}

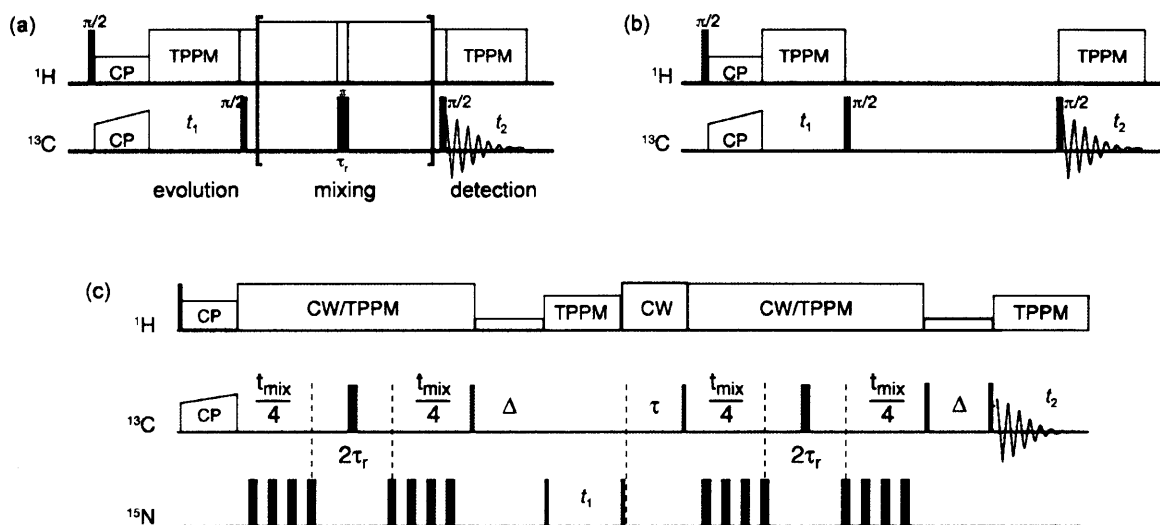


Figure 1.1. 2D dipolar correlation experiments: (a) RFDR,⁵ (b) PDS,⁷³ (c) ZF-TEDOR.¹³ (a) and (b) are examples of ¹³C-¹³C correlation experiments, while (c) presents a ¹⁵N-¹³C experiment.

The spin-spin couplings responsible for polarization transfer can either be the J couplings or the dipolar couplings. In MAS NMR most methods rely on the dipolar couplings, which are usually two orders of magnitude larger than the J couplings. The coherence transfers can be further divided into homonuclear (¹³C-¹³C) and heteronuclear (direct ¹⁵N-¹³C) transfers. The homonuclear experiments can be used to identify amino acid spin systems, while the heteronuclear experiments are used to establish the connectivity pattern in the protein sequence. Useful correlations include the N(CO)CA (Figure 1.2a) experiment, in which polarization is transferred from the amide ¹⁵N to the ¹³C α of the preceding residue; and the N(CA)CB (Figure 1.2b) experiment, which allows the transfer of polarization to the side chains of the amino acid through the directly bonded ¹³C α . 3D experiments might be necessary in some cases in order to improve the resolution of the spectra.

These correlation schemes can employ a variety of experiments for the mixing step. This includes radio frequency-driven dipolar recoupling (RFDR)⁵ (Figure 1.1a), proton driven spin diffusion (PDS)⁷³ (Figure 1.1b), transferred echo double resonance (TEDOR) (Figure 1.1c),¹³ SPECIFIC CP,¹¹ etc. After assignment the resonances can be used for prediction of

the secondary structure of the protein with the help of the chemical shift index and the TALOS software.^{74,75}

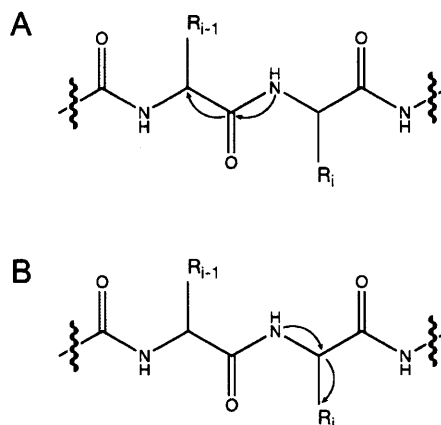


Figure 1.2. (a) N(CO)CA and (b) N(CA)CB correlations. The direction of the polarization transfer is shown with arrows.

1.4.2. Distance measurements

The distance constraints obtained by MAS NMR can be quantitative or semi-quantitative. Experiments like PDSO (Figure 1.1b) and its variant DARR,¹² are usually quite efficient in recoupling distant ^{13}C spins, but the transfer is hard to quantify since the polarization can be relayed from one ^{13}C spin to another, and multiple pathways might exist for recoupling of the two spins of interest. Therefore, the distance constraints obtained with this experiment are used much like the NOE constraints in solution NMR, i.e. they are separated in distance bins based on the mixing time when they appear.^{17,76} While based on a completely different transfer mechanism, the proton assisted recoupling (PAR) sequence can be used in a similar way for structure determination.⁷⁷ This experiment relies on the third spin assisted recoupling mechanism (TSAR), which involves second-order terms of the form $C_1^\pm C_2^\mp H_z$ to recouple distant ^{13}C spins. Distances of up to 7 Å have been detected, however, the transfer efficiency has a strong geometric dependence on the orientation of the ^{13}C , ^{13}C , ^1H spin system. The

heteronuclear version of this experiment is called proton assisted insensitive nuclei cross polarization (PAIN CP).^{78,79}

A number of experiments exist that can be used in quantitative measurements in selectively labeled samples. For example, the double quantum experiment dipolar recoupling windowless sequence (DQ DRAWS)^{80,81} is well suited to measure backbone to backbone distances in amyloid fibril samples with a selective ¹³C label placed at a single carbonyl site (See Chapter 4). The distance between a lone ¹⁵N-¹³C pair can be measured for example by using an experiment called rotational echo double resonance (REDOR).⁴

The simultaneous measurement of ¹³C-¹³C distances in uniformly labeled samples can be complicated due to a phenomenon called dipolar truncation.⁸² In these samples, each nucleus is dipolar coupled to a network of other labeled nuclei, and the strong one- and two-bond couplings can obscure the weak multi-bond interactions. In order to overcome this problem it is necessary to reduce the size of the effective spin system, e.g. by using a selective or narrowband pulse to isolate the spins of interest. For example, the band selective RFDR experiment (BASE RFDR) can be used to obtain long-range correlations between aliphatic carbons much more efficiently.⁸³ A heteronuclear experiment that can be used to obtain quantitative distances between ¹⁵N and ¹³C nuclei in uniformly labeled protein samples is ZF TEDOR.¹³ Some of the problems with using uniformly labeled samples can be alleviated by employing the alternating labeling scheme instead as discussed throughout the chapters.¹⁵⁻¹⁷

1.5. Thesis outline

The work presented in this thesis focuses on the MAS NMR structural investigation of two amyloid fibril systems – the first one formed by TTR(105-115), the 11-residue fragment of the disease-related protein transthyretin; the second one formed by the 99-residue protein β_2 -microglobulin (β_2m), implicated in dialysis-related amyloidosis. The TTR(105-115) case exemplifies our efforts to characterize the hierarchy of structures present in the fibril, including the organization of the β -strands into β -sheets, the β -sheet interface, and the protofilament-to-protofilament interactions that hold the fibrils together. Our efforts were guided with information obtained from cryo-electron microscopy, atomic force microscopy and STEM measurements, and resulted in the very first atomic resolution structure of a complete amyloid fibril. The second case describes our efforts to extend this work to the

protein β_2m , a process complicated not only by the much larger size of the protein involved but also by the high degree of dynamics exhibited in the fibrils. Nevertheless, we were able to characterize the secondary, tertiary and quaternary interactions in the β_2m fibrils and to compare at molecular level β_2m fibrils formed under different conditions. Wherever possible, we have used dynamic nuclear polarization (DNP), in order to speed up the data acquisition time and the signal-to-noise ratios in the MAS NMR correlation experiments. The presentation of these results is divided in the following way.

Section I focuses on the application of DNP in the MAS NMR studies of amyloid fibrils and starts with a background chapter (Chapter 2) on DNP theory, implementation and instrumentation. Understanding the DNP polarization mechanisms, in particular the solid-effect, the cross-effect and thermal mixing, and the choice of polarizing agent are essential in optimizing the achieved enhancements in the spectra, while reliable instrumentation is vital in the reproducible performance of the MAS NMR experiments under DNP. Chapter 3 presents enhancements, relaxation data and comparison between room temperature and low temperature experimental data for a variety of amyloid systems, including TTR(105-115), β_2m , GNNQQNY, and PI3 SH3 fibrils, emphasizing the gains in time and the much larger number of structural constraints that can be obtained with DNP. It also compares the DNP enhancements and low temperature behavior of the GNNQQNY peptide in two different forms, crystalline and amyloid fibrils. While some residues in the GNNQQNY crystals exhibit much larger line widths and chemical shift changes in the DNP experiments performed at low temperature, the amyloid fibrils preserve their structure and integrity and have relatively well-resolved spectra, thus making them very good candidates for structural studies employing DNP.

Section II is dedicated to the structural investigation of the TTR(105-115) amyloid fibrils, with Chapter 4 presenting the suite of MAS NMR experiments and labeling schemes that were used to unravel the structural organization of the fibrils.

Section III presents our progress on the structural characterization of β_2m amyloid fibrils and starts with analysis of the secondary structure of the fibril morphology formed at low pH and low salt concentration (Chapter 5). Chapter 6 presents an efficient method to determine the tertiary structure of the fibrils, and Chapter 7 describes the experiments and labeling schemes that we have employed in order to characterize the quaternary interactions in the

fibrils. Chapter 8 then presents a molecular level structural comparison of the fibrils formed at pH 2.5 and low ionic strength, the fibrils formed at pH 3.6 and high ionic strength, and the fibrils formed by a truncation variant of the protein implicated in disease and formed under physiological conditions.

References:

- (1) Andrew, E. R.; Bradbury, A.; Eades, R. G. *Nature* **1958**, *182*, 1659-1659.
- (2) Lowe, I. J. *Phys. Rev. Lett.* **1959**, *2*, 285-287.
- (3) Griffin, R. *Nat. Struct. Mol. Biol.* **1998**.
- (4) Gullion, T.; Schaefer, J. J. *J. Magn. Reson.* **1989**, *81*, 196-200.
- (5) Bennett, A. E.; Ok, J. H.; Griffin, R. G.; Vega, S. J. *Chem. Phys.* **1992**, *96*, 8624-8627.
- (6) Hing, A. W.; Vega, S.; Schaefer, J. J. *J. Magn. Reson.* **1992**, *96*, 205-209.
- (7) Baldus, M.; Meier, B. H. J. *J. Magn. Reson. A* **1996**, *121*, 65-69.
- (8) Verel, R.; Baldus, M.; Nijman, M.; van Os, J. W. M.; Meier, B. H. *Chem. Phys. Lett.* **1997**, *280*, 31-39.
- (9) Feng, X.; Eden, M.; Brinkmann, A.; Luthman, H.; Eriksson, L.; Graslund, A.; Antzutkin, O. N.; Levitt, M. H. *J. Am. Chem. Soc.* **1997**, *119*, 12006-12007.
- (10) Costa, P. R.; Gross, J. D.; Hong, M.; Griffin, R. G. *Chem. Phys. Lett.* **1997**, *280*, 95-103.
- (11) Baldus, M.; Petkova, A. T.; Herzfeld, J.; Griffin, R. G. *Mol. Phys.* **1998**, *95*, 1197-1207.
- (12) Takegoshi, K.; Nakamura, S.; Terao, T. *Chem. Phys. Lett.* **2001**, *344*, 631-637.
- (13) Jaroniec, C. P.; Filip, C.; Griffin, R. G. *J. Am. Chem. Soc.* **2002**, *124*, 10728-10742.
- (14) Rienstra, C. M.; Hohwy, M.; Mueller, L. J.; Jaroniec, C. P.; Reif, B.; Griffin, R. G. *J. Am. Chem. Soc.* **2002**, *124*, 11908-11922.
- (15) LeMaster, D. M.; Kushlan, D. M. *J. Am. Chem. Soc.* **1996**, *118*, 9255-9264.
- (16) Hong, M. *J. Magn. Reson.* **1999**, *139*, 389-401.
- (17) Castellani, F.; van Rossum, B.; Diehl, A.; Schubert, M.; Rehbein, K.; Oschkinat, H. *Nature* **2002**, *420*, 98-102.
- (18) Huber, M.; Hiller, S.; Schanda, P.; Ernst, M.; Bockmann, A.; Verel, R.; Meier, B. H. *Chemphyschem* **2011**, *12*, 915-918.

- (19) Rosay, M.; Tometich, L.; Pawsey, S.; Bader, R.; Schauwecker, R.; Blank, M.; Borchard, P. M.; Cauffman, S. R.; Felch, K. L.; Weber, R. T.; Temkin, R. J.; Griffin, R. G.; Maas, W. E. *Phys. Chem. Chem. Phys.* **2010**, *12*, 5850-5860.
- (20) Chiti, F.; Dobson, C. M. *Annu. Rev. Biochem.* **2006**, *75*, 333-366.
- (21) Dobson, C. M. *Nature* **2003**, *426*, 884-890.
- (22) Fowler, D. M.; Koulov, A. V.; Balch, W. E.; Kelly, J. W. *TRENDS Biochem. Sci.* **2007**, *32*, 217-224.
- (23) Sipe, J. D.; Cohen, A. S. *J. Struct. Biol.* **2000**, *130*, 88-98.
- (24) Rambaran, R. N.; Serpell, L. C. *Prion* **2008**, *2*, 112-117.
- (25) Cohen, A. S.; Calkins, E. *Nature* **1959**, *183*, 1202-1203.
- (26) Eanes, E. D.; Glenner, G. G. *J. Histochem. Cytochem.* **1968**, *16*, 673-&.
- (27) Marsh, R. E.; Corey, R. B.; Pauling, L. *Biochim. Biophys. Acta* **1955**, *16*, 1-34.
- (28) Sunde, M.; Serpell, L. C.; Bartlam, M.; Fraser, P. E.; Pepys, M. B.; Blake, C. C. F. *J. Mol. Biol.* **1997**, *273*, 729-739.
- (29) Prusiner, S. B. *Science* **1982**, *216*, 136-144.
- (30) Gujjarro, J. I.; Sunde, M.; Jones, J. A.; Campbell, I. D.; Dobson, C. M. *Proc. Natl. Acad. Sci. U. S. A.* **1998**, *95*, 4224-4228.
- (31) Chapman, M. R.; Robinson, L. S.; Pinkner, J. S.; Roth, R.; Heuser, J.; Hammar, M.; Normark, S.; Hultgren, S. J. *Science* **2002**, *295*, 851-855.
- (32) Barnhart, M. M.; Chapman, M. R. *Annu. Rev. Microbiol.* **2006**, *60*, 131-147.
- (33) Uptain, S. M.; Lindquist, S. *Annu. Rev. Microbiol.* **2002**, *56*, 703-741.
- (34) King, C. Y.; Tittmann, P.; Gross, H.; Gebert, R.; Aebi, M.; Wuthrich, K. *Proc. Natl. Acad. Sci. U. S. A.* **1997**, *94*, 6618-6622.
- (35) Tessier, P. M.; Lindquist, S. *Nature* **2007**, *447*, 556-+.
- (36) Tessier, P. M.; Lindquist, S. *Nat. Struct. Mol. Biol.* **2009**, *16*, 598-605.
- (37) Spencer, R. G. S.; Halverson, K. J.; Auger, M.; McDermott, A. E.; Griffin, R. G.; Lansbury, P. T. *Biochemistry* **1991**, *30*, 10382-10387.
- (38) Lansbury, P. T.; Costa, P. R.; Griffiths, J. M.; Simon, E. J.; Auger, M.; Halverson, K. J.; Kocisko, D. A.; Hendsch, Z. S.; Ashburn, T. T.; Spencer, R. G. S.; Tidor, B.; Griffin, R. G. *Nat. Struct. Biol.* **1995**, *2*, 990-998.

- (39) Costa, P. R.; Kocisko, D. A.; Sun, B. Q.; Lansbury, P. T.; Griffin, R. G. *J. Am. Chem. Soc.* **1997**, *119*, 10487-10493.
- (40) Jaroniec, C. P.; MacPhee, C. E.; Bajaj, V. S.; McMahon, M. T.; Dobson, C. M.; Griffin, R. G. *Proc. Natl. Acad. Sci. U.S.A.* **2004**, *101*, 711-716.
- (41) Petkova, A. T.; Ishii, Y.; Balbach, J. J.; Antzutkin, O. N.; Leapman, R. D.; Delaglio, F.; Tycko, R. *Proc. Natl. Acad. Sci. U.S.A.* **2002**, *99*, 16742-16747.
- (42) Paravastu, A. K.; Leapman, R. D.; Yau, W. M.; Tycko, R. *Proc. Natl. Acad. Sci. U. S. A.* **2008**, *105*, 18349-18354.
- (43) Wasmer, C.; Lange, A.; Van Melckebeke, H.; Siemer, A. B.; Riek, R.; Meier, B. H. *Science* **2008**, *319*, 1523-1526.
- (44) Van Melckebeke, H.; Wasmer, C.; Lange, A.; Eiso, A. B.; Loquet, A.; Bockmann, A.; Meier, B. H. *J. Am. Chem. Soc.* **2010**, *132*, 13765-13775.
- (45) Bayro, M. J.; Maly, T.; Birkett, N. R.; MacPhee, C. E.; Dobson, C. M.; Griffin, R. G. *Biochemistry* **2010**, *49*, 7474-7484.
- (46) Bayro, M. J.; Debelouchina, G. T.; Eddy, M. T.; Birkett, N. R.; MacPhee, C. E.; Rosay, M.; Maas, W. E.; Dobson, C. M.; Griffin, R. G. **2011**.
- (47) Iwata, K.; Fujiwara, T.; Matsuki, Y.; Akutsu, H.; Takahashi, S.; Naiki, H.; Goto, Y. *Proc. Natl. Acad. Sci. U.S.A.* **2006**, *103*, 18119-18124.
- (48) Heise, H.; Hoyer, W.; Becker, S.; Andronesi, O. C.; Riedel, D.; Baldus, M. *Proc. Natl. Acad. Sci. U.S.A.* **2005**, *102*, 15871-15876.
- (49) Vilar, M.; Chou, H. T.; Luhrs, T.; Maji, S. K.; Riek-Loher, D.; Verel, R.; Manning, G.; Stahlberg, H.; Riek, R. *Proc. Natl. Acad. Sci. U.S.A.* **2008**, *105*, 8637-8642.
- (50) Comellas, G.; Lemkau, L. R.; Nieuwkoop, A. J.; Kloepper, K. D.; Ladrör, D. T.; Ebisu, R.; Woods, W. S.; Lipton, A. S.; George, J. M.; Rienstra, C. M. *J. Mol. Bio.* **2011**, *In Press, Uncorrected Proof*.
- (51) Helmus, J. J.; Surewicz, K.; Surewicz, W. K.; Jaroniec, C. P. *J. Am. Chem. Soc.* **2010**, *132*, 2393-2403.
- (52) van der Wel, P. C. A.; Lewandowski, J. R.; Griffin, R. G. *J. Am. Chem. Soc.* **2007**, 5117-5130.
- (53) van der Wel, P. C. A.; Lewandoswki, J.; Griffin, R. G. *Biochemistry* **2010**, submitted.

- (54) Abragam, A.; Goldman, M. *Nuclear magnetism: order and disorder*; Clarendon Press: Oxford, 1982.
- (55) Goldman, M. *Spin temperature and nuclear magnetic resonance in solids*; Clarendon Press: Oxford, 1970.
- (56) Jeffries, C. D. *Dynamic Nuclear Orientation*; Interscience: New York, 1963.
- (57) Becerra, L. R.; Gerfen, G. J.; Temkin, R. J.; Singel, D. J.; Griffin, R. G. *Phys. Rev. Lett.* **1993**, *71*, 3561-3564.
- (58) Maly, T.; Debelouchina, G. T.; Bajaj, V. S.; Hu, K.-N.; Joo, C.-G.; Mak-Jurkauskas, M. L.; Sirigiri, J. R.; van der Wel, P. C. A.; Herzfeld, J.; Temkin, R. J.; Griffin, R. G. *J. Chem. Phys.* **2008**, *128*, 052211.
- (59) Hu, K.-N.; Yu, H.-h.; Swager, T. M.; Griffin, R. G. *J. Am. Chem. Soc.* **2004**, *126*, 10844-10845.
- (60) Hu, K. N.; Debelouchina, G. T.; Smith, A. A.; Griffin, R. G. *J. Chem. Phys.* **2011**, *134*.
- (61) Smith, S. O.; Griffin, R. G. *Annu. Rev. Phys. Chem.* **1988**, *39*, 511-535.
- (62) Slichter, C. P. *Principles of Magnetic Resonance - 3rd Ed.*; Springer-Verlag: Berlin, 1996.
- (63) Mehring, M. *Principles of High Resolution NMR in Solids - 2nd Ed.*; Springer-Verlag: Berlin, 1983.
- (64) Duer, M. J. *Introduction to Solid-State NMR Spectroscopy*; Blackwell Publishing: Oxford, 2004.
- (65) Cavanagh, J.; Fairbrother, W.; Palmer, A. G.; Skelton, N. J. *Protein NMR Spectroscopy: Principles and Practice*; Academic Press: New York, 1996.
- (66) Herzfeld, J.; Berger, A. E. *J. Chem. Phys.* **1980**, *73*, 6021-6030.
- (67) Wylie, B. J.; Schwieters, C. D.; Oldfield, E.; Rienstra, C. M. *J. Am. Chem. Soc.* **2009**, *131*, 985-992.
- (68) Linser, R.; Dasari, M.; Hiller, M.; Higman, V.; Fink, U.; del Amo, J. M. L.; Markovic, S.; Handel, L.; Kessler, B.; Schmieder, P.; Oesterhelt, D.; Oschkinat, H.; Reif, B. *Angew. Chem. Int. Ed.*, *50*, 4508-4512.
- (69) Maricq, M. M.; Waugh, J. S. *J. Chem. Phys.* **1979**, *70*, 3300-3316.
- (70) Waugh, J. S. *J. Magn. Reson* **1982**, *50*, 30-49.

- (71) Bennett, A. E.; Rienstra, C. M.; Auger, M.; Lakshmi, K. V.; Griffin, R. G. *J. Chem. Phys.* **1995**, *103*, 6951-6958.
- (72) Pines, A.; Gibby, M. G.; Waugh, J. S. *J. Chem. Phys.* **1972**, *56*, 1776.
- (73) Szeverenyi, N. M.; Sullivan, M. J.; Maciel, G. E. *J. Magn. Reson.* **1982**, *47*, 462-475.
- (74) Cornilescu, G.; Delaglio, F.; Bax, A. *J. Biomol. NMR* **1999**, *13*, 289-302.
- (75) Wishart, D. S.; Sykes, B. D. *J. Biomol. NMR* **1994**, *4*, 171-180.
- (76) Zech, S. G.; Wand, A. J.; McDermott, A. E. *Journal of the American Chemical Society* **2005**, *127*, 8618-8626.
- (77) De Paepe, G.; Lewandowski, J. R.; Loquet, A.; Bockmann, A.; Griffin, R. G. *J. Chem. Phys.* **2008**, *129*.
- (78) Lewandowski, J. R.; De Paepe, G.; Griffin, R. G. *J. Am. Chem. Soc.* **2007**, *129*, 728-729.
- (79) De Paepe, G.; Lewandowski, J. R.; Loquet, A.; Eddy, M.; Megy, S.; Bockmann, A.; Griffin, R. G. *J. Chem. Phys.* **2011**, *134*.
- (80) Karlsson, T.; Popham, J. M.; Long, J. R.; Oyler, N.; Drobny, G. P. *J. Am. Chem. Soc.* **2003**, *125*, 7394-7407.
- (81) Caporini, M. A.; Bajaj, V. S.; Veshtort, M.; Fitzpatrick, A.; MacPhee, C. E.; Vendruscolo, M.; Dobson, C. M.; Griffin, R. G. *J. Phys. Chem. B* **2010**, *114*, 13555-13561.
- (82) Bayro, M. J.; Huber, M.; Ramachandran, R.; Davenport, T. C.; Meier, B. H.; Ernst, M.; Griffin, R. G. *J. Chem. Phys.* **2009**, *130*.
- (83) Bayro, M. J.; Maly, T.; Birkett, N. R.; Dobson, C. M.; Griffin, R. G. *Angew. Chem., Int. Ed.* **2009**, *48*, 5708-5710.

Chapter 2. Dynamic Nuclear Polarization at High Magnetic Fields

Sections 2.1, 2.2 and 2.3 have been adapted from “Dynamic Nuclear Polarization at High Magnetic Fields” by Maly T, Debelouchina GT, Bajaj VS, Hu KN, Joo CG, Mak-Jurkauskas ML, Sirigiri JR, van der Wel PCA, Herzfeld J, Temkin RJ, Griffin RG, published in J. Chem. Phys. 2008, 128, 052211.

Summary

Dynamic nuclear polarization (DNP) is a method that permits NMR signal intensities of solids and liquids to be enhanced significantly, and is therefore potentially an important tool in structural and mechanistic studies of biologically relevant molecules. During a DNP experiment, the large polarization of an exogeneous or endogeneous unpaired electron is transferred to the nuclei of interest by microwave (MW) irradiation of the sample. The maximum theoretical enhancement achievable is given by the gyromagnetic ratios (γ_e / γ_I), being ~ 660 for protons. In the early 1950's, the DNP phenomenon was demonstrated experimentally, and intensively investigated in the following four decades, primarily at low magnetic fields. This chapter focuses on recent developments in the field of DNP with a special emphasis on work done at high magnetic fields (≥ 5 T), the regime where contemporary NMR experiments are performed. After a brief historical survey, we present a review of the classical continuous wave (CW) DNP mechanisms – the solid effect (SE), the cross effect (CE), and thermal mixing (TM). Different polarizing agents and their efficiencies are discussed, and the instrumentation necessary for the implementation of DNP experiments is reviewed.

2.1. Introduction

In 1953 Overhauser proposed that the large Boltzmann polarization of unpaired electrons could be transferred to neighboring nuclei by saturating the corresponding electron paramagnetic resonance (EPR) transition. The result of this process would be an enhancement of the signal intensities of the associated nuclear magnetic resonance (NMR) signals by a factor of $(\gamma_s / \gamma_I) \sim 660$ in the case of protons.¹ The validity of this suggestion was vigorously debated until Carver and Slichter reported an experiment in which they polarized ^7Li and later ^{23}Na and ^1H nuclei,^{2,3} achieving signal enhancements of ~ 100 . This experiment, now known as the Overhauser effect (OE) and widely used in solution NMR experiments for measuring ^1H - ^1H distances, was the first demonstration of dynamic nuclear polarization (DNP).

In the following decade, additional pioneering DNP experiments were performed in both solids and liquids. In 1958 the Solid Effect (SE) was discovered, which required the use of polarizing agents with a homogeneous EPR linewidth (δ) and an inhomogeneous spectral breadth (Δ) smaller than the nuclear Larmor frequency ($\delta, \Delta < \omega_{0I}$).^{4,5} Subsequently Kessenikh et al.,^{6,7} Hwang and Hill,^{8,9} and Wollan¹⁰ reported 9 GHz DNP experiments on systems with inhomogeneously broadened EPR spectra. The polarization mechanism in this case is the cross-effect (CE), which is the dominant continuous wave (CW) mechanism at high magnetic fields. Specifically, the CE is operative when the polarizing agent has an inhomogeneous broadened EPR spectrum whose breadth Δ is larger than the nuclear Larmor frequency ω_{0I} and concurrently the homogeneous linewidth δ remains small ($\Delta > \omega_{0I} > \delta$). The third regime, where the homogeneous EPR linewidth is larger than the nuclear Larmor frequency ($\delta > \omega_{0I}$), is referred to as thermal mixing (TM)¹¹ and requires the existence of a high concentration of paramagnets.

There is currently a renaissance occurring in the development and application of DNP driven by the desire of the spectroscopist to enhance signal intensities in NMR spectra of both solids and liquids. This renaissance began in the 1980's with the appearance of magic angle spinning (MAS) experiments devoted to solids where the necessity of observing low- γ nuclei (^{13}C , ^{15}N , etc.) limits the sensitivity of the experiment. Thus, MAS-DNP methodology was developed to enhance sensitivity in ^{13}C spectra of polymers, carbonaceous and other

materials. These experiments were constrained to low fields (≤ 60 MHz for ^1H) because of the limited frequency range of klystron sources (≤ 40 GHz) used to produce microwaves. At the same time, solid-state NMR was reaping tremendous benefits from the availability of superconducting magnets operating at fields of ≥ 5 T (~ 200 MHz for ^1H), which yields significant improvements in sensitivity and spectral resolution. Thus, today it is not uncommon to record MAS spectra at 16-21 T (700-900 MHz for ^1H). The success of these high-field MAS experiments stimulated interest in developing DNP at high frequencies, and this in turn motivated innovations in a number of required to buoy the experiments to fruition: technological developments in high-frequency microwave (MW) sources, transmission lines and low temperature, multiple resonance MAS NMR probes. In addition, there have been important advances in the design of paramagnetic polarizing agents required for DNP. This in turn has enabled MAS experiments on membrane and amyloid proteins that are either difficult or impossible because of limited signal-to-noise. Therefore, high frequency DNP is yet another example where the development of new instrumentation and methodology enables new areas of scientific inquiry.

In this overview, we focus primarily on the principles and applications of DNP MAS experiments at high magnetic fields and MW frequencies, which we arbitrarily define as ≥ 5 T corresponding to MW irradiation at frequencies ≥ 140 GHz (for $\gamma \sim 2$). For technical reasons discussed below, MW power levels in the range of ~ 10 W are desirable. One MW source that is capable of operating in this frequency regime and producing this level of output power is the gyrotron, a cyclotron resonance maser, and accordingly, we introduced this source into DNP experiments in the early 1990's initially at 140 GHz and more recently at 250 GHz and 460 GHz.¹²⁻¹⁴

The remainder of this overview is organized as follows. In Section 2.2 we discuss CW polarization mechanisms, and in Section 2.3 we describe polarizing agents designed to be used in high field experiments. Section 2.4 is devoted to the most recent developments in MW technology, low temperature probe technology and other instrumentation that enables DNP. We view these instrumental developments as very important since it is presently progress in this area more than anything else that limits progress in applications of DNP.

2.2. Polarizing mechanisms in DNP experiments

To understand the polarization transfer mechanisms operative in a DNP experiment, we consider the general static Hamiltonian for an electron-nuclear system of the form

$$\begin{aligned} H &= H_S + H_I + H_{SI} = \omega_{0S}S_Z - \omega_{0I}I_Z + H_{SI}^{iso} + H_{SI}^{dip} \\ &= \omega_{0S}S_Z - \omega_{0I}I_Z + A(S_ZI_Z + S_YI_Y + S_XI_X) + BS_XI_Z \end{aligned} \quad (1)$$

where ω_{0S} and ω_{0I} are the electron and nuclear Larmor frequencies respectively, S_i and I_i are the electron and nuclear spin operators, H_{SI}^{iso} is the isotropic (Fermi contact) hyperfine interaction between the electron and the nucleus, and H_{SI}^{dip} is the anisotropic dipolar coupling. The hyperfine coupling H_{SI} is given in a basis where the coefficients A and B denote the secular and pseudosecular hyperfine interactions. Note that this convention is the reverse of that commonly employed in ssNMR literature where I is usually ^1H and S is ^{13}C , ^{15}N . The energy levels that result from this Hamiltonian are shown in Figure 2.1 a.

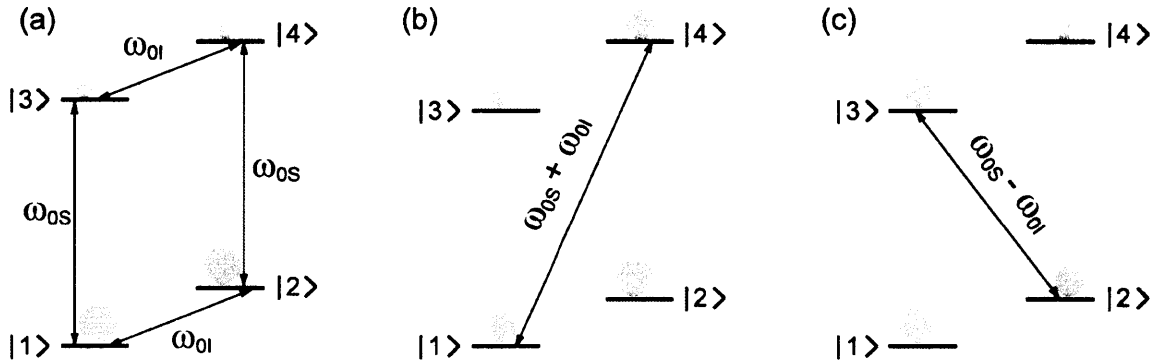


Figure 2.1: Energy level diagrams for the SE. (a) Thermal equilibrium population for a two-level spin system. The spin population is depicted schematically in grey. (b) and (c) Saturation of the forbidden zero-quantum and double-quantum transitions leads to negative enhancement or positive enhancement through the SE.

There are presently three CW DNP mechanisms that have been successfully applied to solids – the SE,^{4,5,15} the CE,^{6,8,9} and TM.¹⁶ Most of the applications of these DNP mechanisms have been performed at low magnetic fields, and the theoretical treatments published in the

literature reflect this fact. In this section we present a brief theoretical overview for each mechanism with an emphasis on high-field theory when available.

2.2.1. The solid effect

The solid effect is a two-spin process, which relies on the mixing of states caused by the nonsecular component B of the hyperfine coupling.¹⁶ The Boltzmann population distribution at thermal equilibrium is shown in Figure 2.1b.

The non-secular term B in the Hamiltonian contains terms of the form $S_z I^+$ and $S_z I^-$ that lead to a mixing of the states of the system. The new mixed states are $|1'\rangle = |1\rangle + q|2\rangle$, $|2'\rangle = |2\rangle - q|1\rangle$, $|3'\rangle = |3\rangle - q|4\rangle$ and $|4'\rangle = |4\rangle + q|3\rangle$. The coefficient q can be calculated by first order perturbation theory and is given by¹¹

$$q = -\frac{3}{4} \frac{\gamma_s \gamma_I}{\omega_{oI}} \frac{1}{r^3} \sin \theta \cos \theta e^{-i\varphi} \quad (2)$$

where r , θ and φ are the polar coordinates describing the electron-nuclear vector. Irradiation at $\omega_{oS} + \omega_{oI}$ or $\omega_{oS} - \omega_{oI}$ leads to zero-quantum (Figure 2.1c) or double-quantum transitions (Figure 2.1d), the probability of which is proportional to $4q^2$.¹⁶ Since q is proportional to ω_{oI} , the transition probability and the enhancement scale with ω_{oI}^{-2} . This field dependence has thus far restricted the utility of the SE in high-field DNP experiments.

Another issue of practical nature which affects the applicability of the SE is the fact that it requires a polarizing agent with a relatively narrow EPR spectrum. In particular, the homogeneous width δ and the inhomogeneous breadth Δ of the EPR spectrum have to be much smaller than ω_{oI} to ensure that only one of the forbidden transitions is excited at a time. Simultaneous irradiation of both transitions leads to partial or complete cancellation of the polarization effect caused by each transition, a situation known as the differential solid effect (DSE).¹⁷

2.2.2. Cross-effect/thermal mixing

The CE was first reported in the 1960s by Kessenikh *et al.*,^{6,7} a few years later by Hwang and Hill^{8,9} and then by Wollan¹⁰. Unlike the SE, this new mechanism was based on allowed transitions and involved the interaction of electron spin packets in an inhomogeneously broadened EPR line. Treatments of a similar effect, called thermal mixing, in a homogeneously broadened EPR line appeared a few years later^{11,18-20}. The intermediate case of an EPR line broadened by both homogeneous and inhomogeneous interactions was treated by Wollan¹⁰. This early theoretical work considers the CE/TM mechanisms at low magnetic field only, and it is only recently that the CE and TM have been used for DNP at high magnetic fields²¹⁻²⁵.

At high magnetic fields, the CE is defined as a three-spin process, which involves the interaction between two dipolar coupled electrons with EPR frequencies ω_{0s1} (electron spin 1) and ω_{0s2} (electron spin 2) that satisfy the relation²⁴

$$\omega_{0s2} - \omega_{s01} = \omega_{0I}. \quad (3)$$

This is the dominant mechanism when the EPR line is inhomogeneously broadened by the g anisotropy and the electrons are weakly coupled via electronic cross relaxation.

The CE requires that the inhomogeneous breadth Δ of the EPR spectrum is larger than the nuclear Larmor frequency ω_{0I} to satisfy the condition that there are two molecular orientations, resulting in two effective EPR resonance frequencies, separated by the correct frequency. At the same time, the homogeneous width must satisfy the condition $\delta < \omega_{0I}$. This condition is achieved when biradicals are used as polarizing agents, where the presence of a dipolar coupling between the two electrons can dramatically improve the efficiency of the DNP effect. In contrast, the TM mechanism involves a *homogeneously* broadened EPR line arising from multiple dipolar-coupled electrons. Here, the condition $\delta > \omega_{0I}$ is satisfied. This condition implies that at high magnetic fields the concentration of the polarizing agent must be high, which could unfortunately compromise the resolution in a MAS NMR experiment.

The thermal equilibrium spin population for a three-spin system is shown in Figure 2.2a. Note that there is no degeneracy present in the general case. However, when the appropriate

polarizing agent is used, i.e. when there are two dipolar coupled electrons separated in frequency by ω_{0l} , levels $|4\rangle$ and $|5\rangle$ or $|6\rangle$ and $|3\rangle$ become equal in energy (Figure 2.2b and c). Irradiation of ω_{0s1} saturates the EPR transitions for one of the two dipolar coupled electrons, and the CE transitions (ω_{CE}) ensure that there is a negative enhancement of the nuclear polarization (Figure 2.2b). Similarly, irradiation of the other EPR transition (ω_{0s2}) leads to positive enhancement (Figure 2.2c).

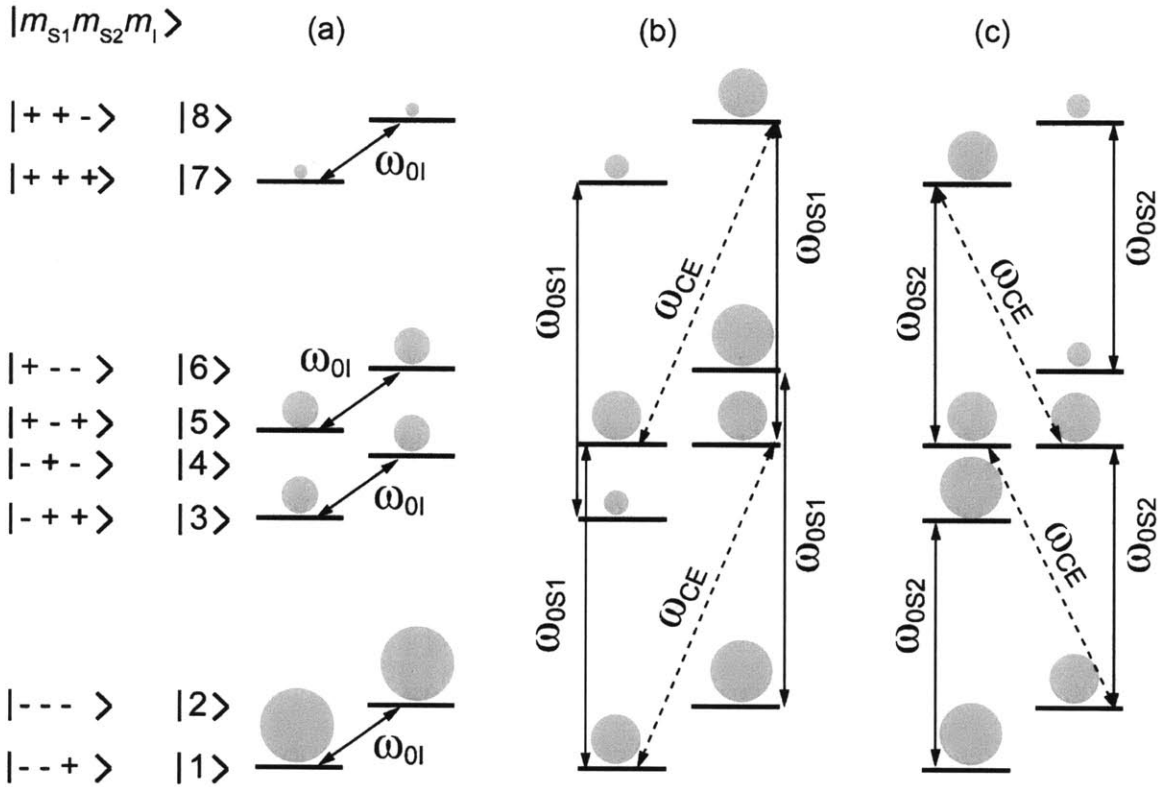


Figure 2.2: Population distribution at thermal equilibrium for a general three-spin system (a). Saturation of the allowed EPR transitions for one of the dipolar coupled electrons (ω_{0s1}) leads to negative enhancement (b). Saturation of the transition corresponding to the second electron (ω_{0s2}) leads to positive enhancement (c).

Since the linewidth of the EPR spectrum scales with the magnetic field, the degeneracy condition becomes harder to satisfy at higher magnetic fields. As a result, enhancements scale

as B_0^{-1} . Despite this unfavorable field dependence, these mechanisms have been used successfully to polarize biological solids at high magnetic fields^{26,27}.

The TM effect is usually treated from a thermodynamic point of view, based on the concept of spin temperature¹⁸. The electron-nuclear spin system can be described as a set of three interacting baths, each characterized by a spin temperature: the electron Zeeman system (EZS), the electron dipolar system (EDS) and the nuclear Zeeman system (NZS).²² Off resonance irradiation of the allowed EPR transition results in a large polarization gradient across the EPR line, which is equivalent to cooling the EDS. This bath is in thermal contact with the NZS, which is also cooled in an energy-conserving three-spin electron-electron-nuclear exchange process, leading to DNP enhancement. The TM process can be direct, i.e. the enhancement is caused by the direct coupling between the NZS and the EDS, or indirect, when both allowed and forbidden transitions are induced¹¹. However, compared to the CE, the TM effect is less efficient and results in smaller enhancements.

2.3. Polarization agents

The mechanism governing the DNP experiment depends strongly on the choice of the polarizing agent, and is influenced by factors such as the width of the EPR spectrum, the radical solubility, the temperature dependence of relaxation times, etc. In addition, the polarizing agent can be either exogeneous (a mono- or biradical or metal ion added to the system) or in principle endogeneous (for example, a stable radical present in a protein). There are many examples of the use of exogeneous radicals as polarizing agents, and, to date, the optimal enhancements in MAS experiments have been achieved with biradicals dispersed in a glassy matrix^{23,25}. In contrast only photo-CIDNP experiments have utilized endogeneous polarizing agents in solids.^{28,29} In solution DNP, the polarizing agent can be dissolved in the solvent,³⁰ attached to a support while the solution flows past it³¹⁻³³, or connected to a bulky particle like Si and suspended in solution.³⁴

Five of the molecules that have been frequently used for polarizing agents in high field DNP experiments are illustrated in Figure 2.3. Two of these, trityl and bis- α,γ -diphenylene- β -phenyl-allyl (BDPA), have either threefold or approximate threefold symmetry, and yield EPR spectra that are relatively narrow. This makes them suitable for SE DNP experiments. TEMPO is a nitroxide based radical, which leads to the TM mechanism at sufficiently high

concentrations, whereas its biradical derivatives, bis-TEMPO-*n*-ethylene oxide (BTnE) and 1-(TEMPO-4-oxy)-3-(TEMPO-4-amino)-propan-2-ol (TOTAPOL) induce CE DNP mechanism.

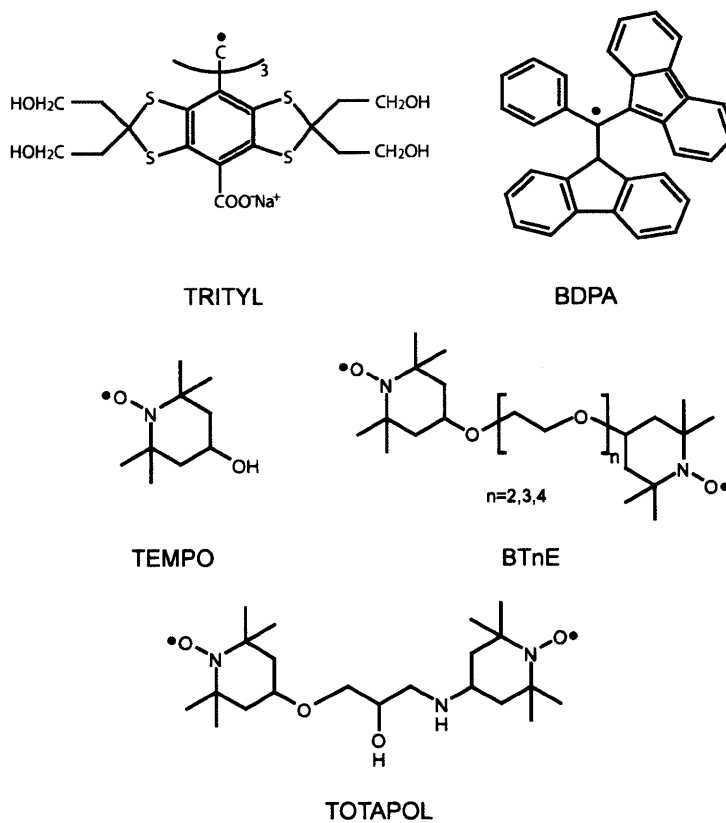


Figure 2.3: Chemical structures of three mono- and two biradical polarizing agents used in high field DNP experiments.

These and similar nitroxide based free radicals/biradicals have been used for both liquid and solid-state bio-DNP since they are stable, unreactive and soluble in a wide variety of solvents. For example TOTAPOL is soluble in glycerol/water solutions and is currently the polarizing agent of choice for experiments involving proteins. In addition to these $g \sim 2$ species very successful DNP experiments have been performed with paramagnetic chromium (V) based compounds, which were used in the preparation of polarized targets for nuclear scattering experiments.³⁵

2.3.1. Polarizing agents for the SE

The resolved SE requires that the homogeneous linewidth δ of the radical is less than the nuclear Larmor frequency ω_{0I} . This requirement ensures that the zero- and double-quantum forbidden transitions are not excited simultaneously and there is no cancellation of the positive and negative enhancement. Currently, only two radicals satisfy this property at high magnetic fields, BDPA³⁶ and trityl.^{37,38} BDPA has an inhomogeneous linewidth of $\Delta \sim 20$ MHz at 211 MHz ¹H Larmor frequency and it was first used to study the SE in a polystyrene matrix.^{11,12,19,39} However, its utility for biological work is greatly limited by its insolubility in aqueous solutions. In contrast, the trityl radical, developed by Nycomed/Amersham was originally designed for low field OE imaging experiments.^{38,40} It is very soluble in aqueous media and because of its symmetry and the absence of large ¹H hyperfine couplings it has a narrow EPR spectrum that supports the SE. Furthermore, trityl has been successfully used together with the HyperSense (Oxford Instruments, Uk) to polarize aqueous solutions.⁴¹

2.3.2. Polarizing agents for TM and CE

The TM and CE mechanisms are the dominant mechanisms when the breadth of the EPR spectrum is large compared to the nuclear Larmor frequency ($\Delta > \omega_{0I}$). If the EPR spectrum is homogeneously broadened, the TM governs the DNP process. The CE, on the other hand, is the dominant mechanism when the EPR spectrum is inhomogeneously broadened. Nitroxide based radicals/biradicals are very suitable for these mechanisms since their EPR linewidth Δ is ~ 600 MHz at a ¹H Larmor frequency of 211 MHz.

Monomeric TEMPO at a high concentrations exhibits partial homogeneous broadening in its EPR spectra²² and DNP is thought to proceed partially through the TM mechanism. The obtained maximum and minimum enhancements are $\sim \pm 50$ at a magnetic field strength of 5 T (140 GHz) using TEMPO concentration of ≥ 40 mM.²⁴ At a magnetic field strength 9 T (250 GHz), the enhancement factor decreases to ~ 20 .⁴² However, above this concentration the electron-nuclear broadening becomes significant and limits the resolution in the spectra.

In contrast, the CE is the dominant mechanism when the intermolecular electron coupling is small and the intramolecular electron-electron dipole coupling is large (~ 22 MHz in the case of TOTAPOL). The biradical polarizing agents shown in Figure 2.3 are typically used in

CE DNP experiments at low concentrations (~10 mM). Thus, the CE operates in the limit $\Delta > \omega_{0I} > \delta$, where strongly coupled electron spin packets are present that effectively communicate with one another and produce larger enhancements than those observed with monoradicals.

The first biradicals used for DNP belonged to the BTnE series and consisted of two TEMPO moieties connected through ethylene glycol linkages.²³ Depending on the length of the tether ($n = 2, 3$ or 4), the electron-electron dipolar coupling increases from ~11 to ~22 MHz, which is a significant improvement over the ~0.3 MHz intermolecular dipolar coupling observed in a 10 mM solution of monomeric TEMPO. As a result, larger enhancements of $\epsilon = 175 \pm 25$ through the CE have been observed for the shortest member of the series ($n = 2$). The use of biradicals with stronger dipolar coupling and exhibiting greater enhancements also means that a lower concentration of the polarizing agent can be used, therefore reducing the residual paramagnetic broadening. Thus, while the enhancement obtained with BT2E increases by a factor of ~4, the overall electron concentration can be reduced by a similar factor from 40 to 10 mM.

Despite its success, the BTnE series is not sufficiently soluble in glycerol/water mixtures, which are the preferred medium for biological samples and they have been succeeded by TOTAPOL²⁵ (see Figure 2.3). This biradical consists of two TEMPO moieties tethered with a three-carbon chain, which leads to an average electron-electron dipolar coupling of ~22 MHz. This radical offers the very important advantage of being soluble in aqueous media, which is achieved by the hydroxyl and secondary amine moieties on the tether and allows for its use in DNP experiments on biological systems.

The TOTAPOL tether, like the BT2E biradical tether, is conformationally flexible, even though the tether in TOTAPOL is shorter and more rigid.⁴³ However, the average orientation of the g -tensors of the two electrons appears to be improved yielding an enhancement extrapolated to infinite power of $e^\infty = 335 \pm 65$ while the corresponding number for BT2E is $e^\infty = 260 \pm 55$.

Finally, we would like to point out a few strategies to further improve polarizing agents available for DNP. The ideal polarizing agent for the CE should have an EPR spectrum consisting of two narrow sharp lines separated by ω_{0I} in order to satisfy the CE matching condition.^{10,24} Although such a polarizing agent has not yet been reported, Hu *et al.* proposed

to approximate this situation by utilizing a narrow line radical (e.g. trityl or BDPA) tethered to a broad line radical (e.g. TEMPO). This idea can be validated with a physical mixture of trityl and TEMPO,²⁴ where the separation between the trityl line and the g_{yy} component of TEMPO is 225 MHz at 5 T, which closely matches the ^1H Larmor frequency of 211 MHz. The observed enhancement is ~ 160 , an improvement of a factor of 4 over the enhancement achieved with TEMPO. Thus biradicals utilizing this approach could offer even larger enhancements than are presently observed.

2.4. Instrumentation

2.4.1 Gyrotrons

The implementation of DNP experiments can be technically challenging as it requires high-power, high-frequency microwave sources, and the ability to perform magic angle spinning at low temperatures (100 K or below). Conventional designs for MAS NMR probe heads for biological applications include a solenoid radio-frequency (RF) coil for delivering ^1H , ^{13}C and ^{15}N pulses, and a stator for distributing the bearing and drive gas for rotor spinning. This complicates the implementation of a microwave cavity into the probe and generally means that the sample resides in a structure with a low Q with respect to the microwave irradiation.⁴⁴ Therefore, in order to be able to excite the necessary electron transitions for DNP, the microwave source has to be able to deliver high power irradiation (10 W or more). In addition, conventional biomolecular NMR experiments are performed at magnetic fields between 5 T and 21 T, thus necessitating the development of high frequency microwave sources (140 GHz and above). A microwave source that can satisfy these requirements is the gyrotron oscillator, a vacuum tube device developed originally for magnetic fusion research applications.⁴⁵

A gyrotron oscillator produces coherent electromagnetic radiation by exploiting a resonance phenomenon between the modes of an interaction structure and an electron beam placed in a magnetic field. The frequency of the emitted radiation is determined by the relativistic electron cyclotron frequency ω_c or its harmonics given by

$$\omega_c = s \frac{eB_0}{\gamma' mc}, \quad (4)$$

where s is an integer determining the harmonics of the operating mode, e is the electron charge, B_0 is the magnetic field, γ' is a relativistic mass factor, m is the electron mass, and c is the speed of light.²⁶ The fact that different harmonics can be used to produce microwave radiation means that magnets with a lower magnetic field can be used to construct the gyrotron, thus reducing the cost, and allowing the possibility of placing the gyrotron in proximity to the NMR magnet.

A gyrotron oscillator contains the following main components: an electron gun, a cavity, a mode converter and a collector.²⁶ The electron gun contains a cathode that emits electrons that are accelerated by an applied voltage of $\sim 10 - 30$ kV. The electrons move through the magnetic field and precess in cyclotron motion. When they enter the cavity, a phenomenon called bunching results in the emission of microwaves. The microwaves are extracted in the mode converter and directed towards the NMR magnet, while the collector gathers the spent electron beam. The dimensions of the cavity can be larger than the operational wavelength, so the power density is not proportional to the frequency, increasing the reliability and the long-term stability of the gyrotron.²⁶ These characteristics are also very important for the successful implementation of DNP experiments for solving complex biological problems.

Today, gyrotron oscillators operating at microwave frequencies of 140, 250, 263, 330, 394 and 460 GHz have been constructed for DNP applications spanning magnetic fields from 5 to 16.5 T.^{13,14,26,46-52} Some of these gyrotrons have been operational for many years,^{12,13} while others have improved designs to provide better stability, higher power and even a frequency tuning capability.^{50,51} These microwave devices have been designed to deliver continuous microwave irradiation, which drives the transitions necessary for the SE and CE polarization mechanisms. In the foreseeable future, more efficient polarization mechanisms based on pulsed DNP schemes might be available for MAS NMR spectroscopy. These experiments will require the use of microwave sources capable of delivering high-power, high-frequency pulses with phase control. A device called a gyroamplifier, capable of amplifying picosecond pulses, has already been constructed for operation at 140 GHz microwave frequency.⁵³

2.4.2. Low temperature MAS NMR probes

The low temperatures required for DNP present certain challenges to the construction of MAS NMR probes. So far, most of the DNP probes use nitrogen gas for cooling and spinning the rotor at 85 – 100 K.^{49,54} Lower temperatures can be achieved by using helium, although the probe construction in this case becomes even more complicated.⁵⁵ At temperatures close to the liquefaction point of nitrogen, the gas is more viscous, and much higher pressures are necessary for spinning. The components of the probe must be able to withstand the higher pressures, to remain mechanically stable at low temperature, and to deliver the cold gas with as little loss in cooling capacity as possible.⁵⁶ This is important since the DNP enhancement has a very steep dependence on the experimental temperature. In addition, the ability to efficiently deliver microwave power to the sample is required, and microwave components such as waveguides, miter bends, and tapers need to be incorporated into the probe without adding to its diameter, and without compromising the RF performance.⁵⁴

Figure 2.4 presents the main components of a DNP MAS NMR probe operating at 211 MHz ¹H Larmor frequency/140 GHz microwave frequency. This design is for a probe inserted from the top of the magnet and is based on published designs by Barnes et al. for a similar probe operating at 380 MHz ¹H Larmor frequency.⁵⁴ The majority of the RF components are placed outside of the magnet in an aluminum box, and the RF is delivered to the sample coil residing in the “sweet spot” of the magnet by a transmission line.⁵⁷ The microwaves (MW) are delivered from the gyrotron to the probe by a MW waveguide,⁵⁸ and then from the top of the probe to the sample by using the inner conductor of the RF transmission line. This arrangement provides more space outside of the transmission line where other components, such as the drive and the bearing lines, can be more easily accommodated. Since the waveguide and the inner conductor have different diameters, a microwave taper must be used at the connection point in order to guide the microwaves efficiently. Part of the taper is built from plastic components like Kel-F that are transparent to the microwaves but provide an electrical break necessary for optimal performance of the RF circuit. In previous designs, a set of mirrors was used instead of the taper, in order to guide the microwaves into the probe.⁵⁴

The vacuum jacketed drive and bearing gas lines deliver cold nitrogen gas to the sample for spinning and cooling, and the used gas leaves the probe through the exhaust pipe. The

probe stator can accommodate a 4 mm rotor, and spinning frequencies of up to 6 KHz have been possible at 90 K. Higher MAS frequencies have been achieved in probes designed for smaller rotors. The probe also contains a sample insert/eject tube that allows the fast exchange of samples without warming and cooling the probe, thus contributing to its long-term stability and reliability.⁵⁴

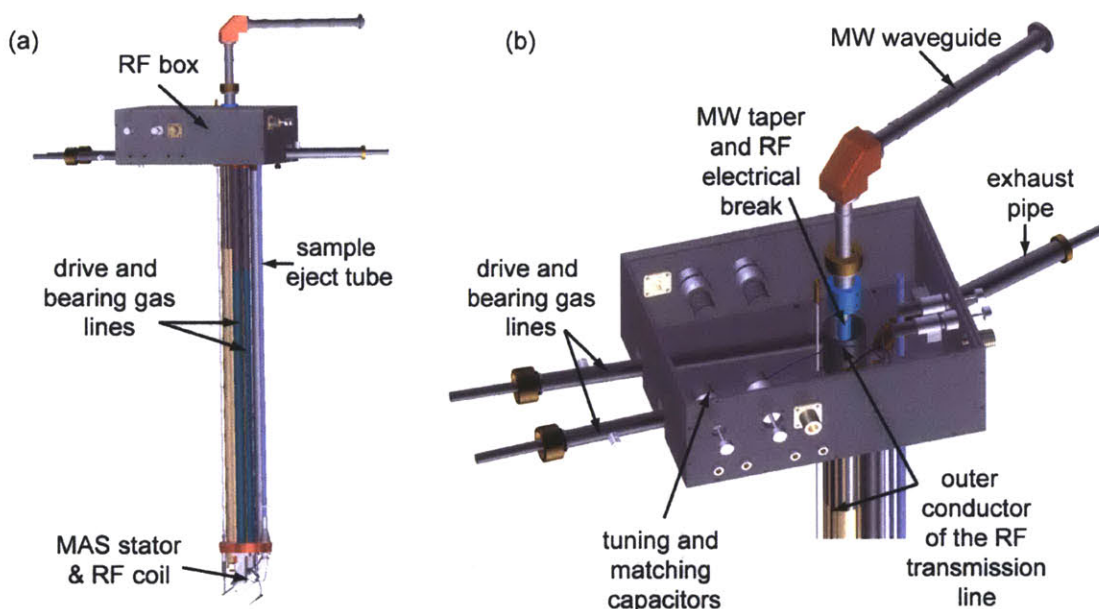


Figure 2.4. The main components of a triple channel MAS NMR probe for DNP experiments, designed for 211 MHz ^1H Larmor frequency and 4 mm sample rotor. (a) Overview of the probe. (b) View from the top showing the microwave taper and other components in the RF aluminum box.

Acknowledgements

I would like to thank Andy Smith, Thorsten Maly and Marvin Bayro for help with the images and text in this chapter, and Kan Nian Hu for help with the DNP theory presented in Section 2.2. We also thank Bjorn Corzilius, Amanda Shing, Jeffrey Bryant, Alexander Barnes, Ron DeRocher, Thorsten Maly, Rebecca Mayrhofer and Paul Waskow for their contributions to the design and implementation of the MAS NMR probe presented in Section 2.4.

References

- (1) Overhauser, A. W. *Physical Review* **1953**, *92*, 411.
- (2) Carver, T. R.; Slichter, C. P. *Physical Review* **1953**, *92*, 212.
- (3) Carver, T. R.; Slichter, C. P. *Physical Review* **1956**, *102*, 975.
- (4) Abragam, A.; Proctor, W., G. *C. R. Acad. Sci.* **1958**, *246*, 2253.
- (5) Erb, E.; Motchane, J., L.; Uebersfeld, J. *C. R. Acad. Sci.* **1958**, *246*, 2121.
- (6) Kessenikh, A., V.; Lushchikov, V., I.; Manenkov, A., A.; Taran, Y., V. *Soviet Physics - Solid State* **1963**, *5*, 321-329.
- (7) Kessenikh, A., V.; Manenkov, A., A.; Pyatnitskii, G., I. *Soviet Physics - Solid State* **1964**, *6*, 641-643.
- (8) Hwang, C., F.; Hill, D., A. *Physical Review Letters* **1967**, *19*, 1011.
- (9) Hwang, C., F.; Hill, D., A. *Physical Review Letters* **1967**, *18*, 110.
- (10) Wollan, D., S. *Phys. Rev. B* **1976**, *13*, 3671.
- (11) Wind, R. A.; Duijvestijn, M. J.; van, d. L., C.; Manenschijn, A.; Vriend, J. *Prog. NMR* **1985**, *17*, 33-67.
- (12) Becerra, L.; Gerfen, G.; Temkin, R.; Singel, D.; Griffin, R. *Phys. Rev. Lett.* **1993**, *71*, 3561-3564.
- (13) Bajaj, V.; Farrar, C.; Hornstein, M.; Mastovsky, I.; Viereg, J.; Bryant, J.; Elena, B.; Kreischer, K.; Temkin, R.; Griffin, R. *J. Magn. Res.* **2003**, *160*, 85-90.
- (14) Hornstein, M. K.; Bajaj, V. S.; Griffin, R. G.; Kreischer, K. E.; Mastovsky, I.; Shapiro, M. A.; Sirigiri, J. R.; Temkin, R. *J. IEEE T. Elec. Dev.* **2005**, *52*, 798-807.
- (15) Jeffries, C., D. *Physical Review* **1957**, *106*, 164.
- (16) Abragam, A.; Goldman, M. *Rep. Prog. Phys.* **1978**, *41*, 395-467.
- (17) Henstra, A.; Dirksen, P.; Wenckebach, W. T. *Phys. Lett. A* **1988**, *134*, 134-136.
- (18) Goldman, M. *Spin temperature and nuclear magnetic resonance in solids*; Clarendon Press: Oxford, 1970; Vol. International series of monographs on physics.
- (19) Duijvestijn, M., J.; Wind, R., A.; Smidt, J. *Physica B+C* **1986**, *138*, 147-170.
- (20) Wenckebach, W., Th; Swanenburg, T., J. B.; Poulis, N., J. *Phys. Rep.* **1974**, *14*, 181-255.
- (21) Hall, D.; Maus, D.; Gerfen, G.; Inati, S.; Becerra, L.; Dahlquist, F.; Griffin, R. *Science* **1997**, *276*, 930-2.

- (22) Farrar, C. T.; Hall, D. A.; Gerfen, G. J.; Inati, S. J.; Griffin, R. G. *J. Chem. Phys.* **2001**, *114*, 4922-4933.
- (23) Hu, K.; Yu, H.; Swager, T.; Griffin, R. *J. Am. Chem. Soc.* **2004**, *126*, 10844-5.
- (24) Hu, K.; Bajaj, V.; Rosay, M.; Griffin, R. *J. Chem. Phys.* **2007**, *126*, 044512.
- (25) Song, C.; Hu, K.; Joo, C.; Swager, T.; Griffin, R. *J. Am. Chem. Soc.* **2006**, *128*, 11385-90.
- (26) Bajaj, V. S.; Hornstein, M. K.; Kreischer, K. E.; Sirigiri, J. R.; Woskov, P. P.; Mak-Jurkauskas, M. L.; Herzfeld, J.; Temkin, R. J.; Griffin, R. G. *J. Magn. Reson.* **2007**, *190*, 86-114.
- (27) van der Wel, P.; Hu, K.; Lewandowski, J.; Griffin, R. *J. Am. Chem. Soc.* **2006**, *128*, 10840-6.
- (28) Diller, A.; Roy, E.; Gast, P.; van Gorkom, H.; de Groot, H.; Glaubitz, C.; Jeschke, G.; Matysik, J.; Alia, A. *Proc. Nat. Acad. Sci. USA* **2007**, *104*, 12767-71.
- (29) Prakash, S.; Alia, A.; Gast, P.; de Groot, H.; Jeschke, G.; Matysik, J. *Biochemistry* **2007**, *46*, 8953-60.
- (30) Loening, N.; Rosay, M.; Weis, V.; Griffin, R. *J. Am. Chem. Soc.* **2002**, *124*, 8808-9.
- (31) Dorn, H. C.; Wang, J.; Allen, L.; Sweeney, D.; Glass, T. E. *J. Magn. Reson.* **1988**, *79*, 404-412.
- (32) Dorn, H. C.; Gitti, R.; Tsai, K. H.; Glass, T. E. *Chem. Phys. Lett.* **1989**, *155*, 227-232.
- (33) McCarney, E.; Armstrong, B.; Lingwood, M.; Han, S. *Proc. Nat. Acad. Sci. USA* **2007**, *104*, 1754-9.
- (34) Dorn, H. C.; Gu, J.; Bethune, D. S.; Johnson, R. D.; Yannoni, C. S. *Chem. Phys. Lett.* **1993**, *203*, 549-554.
- (35) Crabb, D., G.; Meyer, W. *Annu. Rev. Nuc. Part. Sci.* **1997**, *47*, 67-109.
- (36) Koelsch, C. F. *J. Am. Chem. Soc.* **1957**, *79*, 4439-4441.
- (37) Ardenkjaer-Larsen, J.; Laursen, I.; Leunbach, I.; Ehnholm, G.; Wistrand, L.; Petersson, J.; Golman, K. *J. Magn. Reson.* **1998**, *133*, 1-12.
- (38) Reddy, T.; Iwama, T.; Halpern, H.; Rawal, V. *J. Org. Chem.* **2002**, *67*, 4635-9.
- (39) Afeworki, M.; McKay, R. A.; Schaefer, J. *Macromol.* **1992**, *25*, 4084-4091.
- (40) Anderson, S.; Golman, K.; Rise, F.; Wikstrom, H.; Wistrand, L.-G. 1996; Vol. US 5,530,140.

- (41) Ardenkjær-Larsen, J.; Fridlund, B.; Gram, A.; Hansson, G.; Hansson, L.; Lerche, M.; Servin, R.; Thaning, M.; Golman, K. *Proc. Nat. Acad. Sci. USA* **2003**, *100*, 10158-63.
- (42) Bajaj, V.; Farrar, C.; Hornstein, M.; Mastovsky, I.; Viereg, J.; Bryant, J.; Elena, B.; Kreischer, K.; Temkin, R.; Griffin, R. *J. Magn. Reson.* **2003**, *160*, 85-90.
- (43) Hu, K. N.; Song, C.; Yu, H.; Swager, T. M.; Griffin, R. G. *J. Chem. Phys.* **2008**, *128*, 052302.
- (44) Nanni, E. A.; Barnes, A. B.; Matsuki, Y.; Woskov, P. P.; Corzilius, B.; Griffin, R. G.; Temkin, R. J. *J. Magn. Res.* **2011**, *210*, 16-23.
- (45) Felch, K. L.; Danly, B. G.; Jory, H. R.; Kreischer, K. E.; Lawson, W.; Levush, B.; Temkin, R. J. *Proceedings of the IEEE* **1999**, *87*, 752-781.
- (46) Becerra, L. R.; Gerfen, G. J.; Bellew, B. F.; Bryant, J. A.; Hall, D. A.; Inati, S. J.; Weber, R. T.; Un, S.; Prisner, T. F.; McDermott, A. E.; Fishbein, K. W.; Kreischer, K.; Temkin, R. J.; Singel, D. J.; Griffin, R. G. *J. Magn. Res.* **1995**, *A117*, 28-40.
- (47) Joye, C.; Griffin, R.; Hornstein, M.; Hu, K.; Kreischer, K.; Rosay, M.; Shapiro, M.; Sirigiri, J.; Temkin, R.; Woskov, P. *IEEE T. Plasma Sci.* **2006**, *34*, 518-523.
- (48) Hornstein, M.; Bajaj, V.; Griffin, R.; Temkin, R. *IEEE T. Plasma Sci.* **2006**, *34*, 524-533.
- (49) Rosay, M.; Tometich, L.; Pawsey, S.; Bader, R.; Schauwecker, R.; Blank, M.; Borchard, P. M.; Cauffman, S. R.; Felch, K. L.; Weber, R. T.; Temkin, R. J.; Griffin, R. G.; Maas, W. E. *Phys. Chem. Chem. Phys.* **2010**, *12*, 5850-5860.
- (50) Torrezan, A. C.; Han, S. T.; Shapiro, M. A.; Sirigiri, J. R.; Temkin, R. J.; *Ieee 2008 33rd International Conference on Infrared, Millimeter and Terahertz Waves, Vols 1 and 2* **2008**, 612-613.
- (51) Torrezan, A. C.; Han, S. T.; Mastovsky, I.; Shapiro, M. A.; Sirigiri, J. R.; Temkin, R. J.; Barnes, A. B.; Griffin, R. G. *IEEE T. Plasma Sci.* **2010**, *38*, 1150-1159.
- (52) Matsuki, Y.; Takahashi, H.; Ueda, K.; Idehara, T.; Ogawa, I.; Toda, M.; Akutsu, H.; Fujiwara, T. *Phys. Chem. Chem. Phys.* **2010**, *12*, 5799-5803.
- (53) Kim, H. J.; Nanni, E. A.; Shapiro, M. A.; Sirigiri, J. R.; Woskov, P. P.; Temkin, R. J. *Phys. Rev. Lett.* **2010**, *105*.
- (54) Barnes, A. B.; Mak-Jurkauskas, M. L.; Matsuki, Y.; Bajaj, V. S.; van der Wel, P. C. A.; DeRoche, R.; Bryant, J.; Sirigiri, J. R.; Temkin, R. J.; Lugtenburg, J.; Herzfeld, J.; Griffin, R. G. *J. Magn. Reson.* **2009**, *198*, 261.

- (55) Thurber, K. R.; Tycko, R. *J. Magn. Res.* **2008**, *195*, 179-186.
- (56) Allen, P. J.; Creuzet, F.; De, G., H. J. M.; Griffin, R. G. *Journal of Magnetic Resonance* **1991**, *92*, 614-617.
- (57) *Probes for Special Purposes*; McKay, R. A.; Grant, D. M.; Harris, R. K., Eds.; John Wiley: Chichester ; New York, 1996; Vol. 6.
- (58) Woskov, P. P.; Bajaj, V. S.; Hornstein, M. K.; Temkin, R. J.; Griffin, R. G. *IEEE T. Microw. Theory* **2005**, *53*, 1863-1869.

Chapter 3. Dynamic Nuclear Polarization Studies of Amyloid Fibrils

Section 3.5 was adapted from “Dynamic nuclear polarization-enhanced solid-state NMR spectroscopy of GNNQQNY nanocrystals and amyloid fibrils” by Debelouchina GT, Bayro MJ,* van der Wel PCA, Caporini MA, Barnes AB, Rosay M, Maas WE, Griffin RG, published in Phys. Chem. Chem. Phys. 2010, 12, 5911.*

Summary

Dynamic nuclear polarization (DNP) has shown great promise in increasing the sensitivity of solid-state NMR experiments. It utilizes the inherently larger polarization of electrons that are introduced in the sample in the form of a biradical, typically TOTAPOL. The biradical's EPR spectrum is irradiated with microwaves at cryogenic temperatures and the electron polarization is transferred to the ^1H nuclei via the cross effect mechanism. Here, we present DNP studies performed at 100 K and 9.4 T of four amyloid fibril systems formed by the peptide GNNQQNY, the transthyretin (TTR) segment spanning residues 105-115, the 86-residue SH3 domain from PI3 kinase (PI3 SH3), and the 99-residue disease-related protein β_2 -microglobulin ($\beta_2\text{m}$). We compare the DNP enhancements and relaxation behavior of these systems, and discuss the effects of radical and temperature on the spectral resolution and the efficiency of recoupling experiments and ^1H - ^{13}C cross polarization. We also present DNP-enhanced MAS NMR data collected on nanocrystals formed by the GNNQQNY peptide and contrast their low temperature behavior to that observed for the GNNQQNY amyloid fibrils.

3.1. Introduction

Magic angle spinning NMR (MAS NMR) is particularly well suited for the structural studies of insoluble biological systems such as amyloid fibrils and membrane proteins in their native lipid environment. The sensitivity of the MAS NMR experiments can be greatly improved by the use of dynamic nuclear polarization (DNP)¹⁻⁶, a method that allows the transfer of the much larger polarization of an electron spin bath to the nuclei, with predicted theoretical enhancements of 660 and 2640 for proton and carbon nuclei, respectively. These enhancements can lead to extraordinary savings in data acquisition times and the structural studies of biological systems of greater size and complexity can become accessible by MAS NMR.

The preparation of biological samples for DNP studies involves the dispersion of the protein molecule into a matrix containing radicals and cryoprotectant as DNP-enhanced MAS NMR experiments are usually performed at 90 – 100 K and the freezing process is relatively slow.⁷⁻¹¹ So far, TOTAPOL has been the biradical of choice in most biological applications of DNP as it is water soluble and works well with the cross-effect DNP mechanism at higher magnetic fields.¹² With this polarizing agent, enhancements of up to 120 have been observed in peptide crystalline systems at a magnetic field of 5 T.⁹ The improved theoretical understanding of the DNP mechanisms (solid effect, cross effect and thermal mixing) has inspired work on radicals and biradicals with optimized molecular structures and solubility properties, and greater enhancements might be achievable soon in biomolecular DNP applications.¹³⁻¹⁶

The enhancements attained with DNP depend on a great number of experimental factors. The biradical concentration, for example, has to be carefully optimized as it directly influences the observed enhancement but can also compromise the line-widths in the spectra and the transfer efficiency of MAS NMR recoupling experiments. The enhancements are also very sensitive to the relaxation properties of the nuclei and the electrons in the sample, and hence have steep temperature dependence. The solvent/cryoprotectant matrix is usually highly deuterated (94 – 96%) in order to lengthen the proton T_1 time, and the deuteration of the biological molecule of interest might also be desirable for improved polarization transfer.

Here, we present DNP studies of several amyloid fibril systems formed respectively by the Sup35 segment GNNQQNY, the transthyretin (TTR) segment spanning residues 105-115, the

86-residue SH3 domain from PI3 kinase (PI3 SH3), and the 99-residue disease-related protein β_2 -microglobulin (β_2m). We compare the DNP enhancements and relaxation behavior of these systems and discuss the effects of radical, low temperature and molecular motion on the structural information obtainable with DNP-enhanced MAS NMR spectroscopy, with a focus on spectral resolution and experimental efficiency. In addition, we present DNP studies on GNNQQNY nanocrystals and compare their low temperature behavior and interaction with polarizing agent to those of the GNNQQNY amyloid fibrils.

3.2. DNP enhancements of amyloid fibrils

Amyloid fibrils are typically long, unbranched protein filaments containing a high degree of ordered β -sheet structure. While they can be many nm to μm in length, their thickness is usually not more than 10 nm.^{17,18} Therefore, the radical added to a DNP sample would on average be closer to the bulk of the peptide or protein in the fibrils than is the case for the interior of a membrane protein embedded in a lipid environment,^{10,19} or of a crystal with much larger dimensions like those formed by the peptide GNNQQNY.^{9,11} Consequently, the enhancements throughout the fibril and the glassy solvent/cryoprotectant matrix are expected to be more uniform.¹¹

In order to evaluate whether this is the case and what kind of enhancements can be expected from amyloid fibril systems in general, we prepared fibril samples of two peptides (GNNQQNY and TTR(105-115)),^{11,20-24} and two proteins (PI3-SH3 and β_2 -microglobulin).²⁵⁻²⁷ In each of these cases, fibrils were grown following the standard procedure for the peptide or protein in a protonated solvent or buffer (see Materials and Methods), the mature fibrils were pelleted at 250,000g and the pellet was resuspended and washed several times in a solution containing 60% glycerol- d_8 and 40% predominantly deuterated growth buffer with final proton concentration adjusted to 6 – 10 %. 10 mM TOTAPOL was added to each sample, and the fibrils were pelleted again and packed into 3.2 mm Bruker sapphire rotors. All of the experiments were performed in a Bruker 400 MHz DNP setup, equipped with a 263 GHz gyrotron and a low temperature MAS probe, with the temperature controlled to 100 – 103 K, and $\omega_r/2\pi = 9$ kHz.²⁸

The DNP-enhanced ^{13}C CP spectra of the four fibril samples are shown in Figure 3.1, and some additional measured parameters are summarized in Table 3.1. A comparison of the

spectra obtained with and without microwaves at low temperature allows the calculation of the enhancement ϵ due to DNP. In addition, spectra obtained at 100 K versus room temperature (300 K) are already enhanced by a factor of 3 due to the Boltzmann distribution of spin polarization, and a factor of ~ 2 is gained in sensitivity due to the improved performance of the probe at lower temperature. These enhancement factors, however, are not taken into account in the numbers reported further in this chapter.

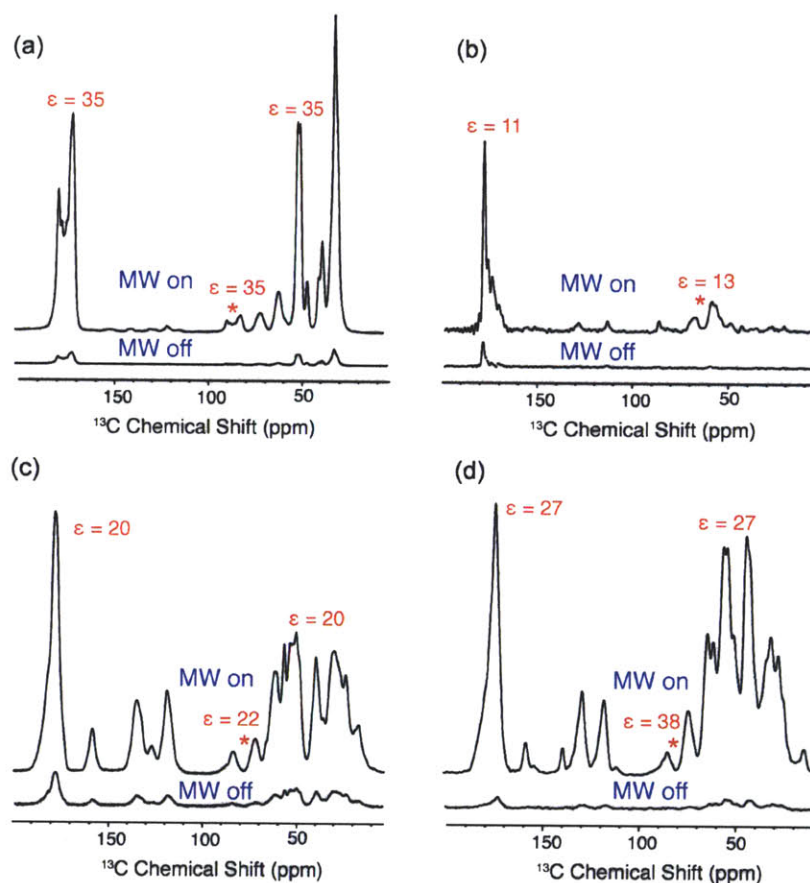


Figure 3.1. ^{13}C CP spectra of four fibril samples recorded with microwaves (MW) on and off at 100 K in order to determine the enhancement due to DNP. (a) GNNQQNY fibril sample, (b) TTR(105-115) sample, (c) $\beta_2\text{m}$ fibril sample, and (d) PI3-SH3 fibril sample. For more details regarding the sample labeling and preparation, see Materials and Methods and Table 1. The asterisks denote the natural abundance glycerol- d_8 signals, and their corresponding DNP enhancements.

Table 3.1. DNP enhancement ϵ and polarization buildup time τ for the fibril signals measured for several different fibril systems and preparations.

Fibril system	Labeling	ϵ_{fibril}	$\epsilon_{\text{glycerol}}$	τ_{buildup} (s)
GNNQQNY	U- ¹³ C, ¹⁵ N gnnQQNy	35	35	5.0
TTR(105-115)	¹⁵ N at Y105, ¹³ C at S115 C'	11	13	1.3
PI3 SH3	100% 2- ¹³ C glycerol, U- ¹⁵ N	28	38	5.5
	50:50 mixture 2- ¹³ C glycerol/U- ¹⁵ N	27	36	3.5
$\beta_2\text{m}$	U- ¹⁵ N, ¹³ C VYAL	20	22	5.5
	100% 2- ¹³ C glycerol, U- ¹⁵ N	32	32	6.5

The observed enhancements for fibril signals are in the range 11 – 35, and 13 – 38 in the case of the natural abundance ¹³C signals of the glycerol that was added as a cryoprotectant to the solvent matrix. As expected, the glycerol enhancements are generally similar to the protein or peptide signals enhancements for three of the fibril samples. The only exception is the PI3-SH3 fibril case, where the preparation of several DNP samples reproducibly showed greater enhancement for the glycerol signals, implying that the radical might not be in direct contact with all of the PI3-SH3 molecules. The cryoEM electron density of these fibrils suggests that they form a tubular structure (~ 80 Å outer diameter),¹⁷ potentially stabilized by water molecules that may be structurally different from the bulk solvent. While the dimensions of the water “gap” (~ 40 Å) can accommodate TOTAPOL molecules (~ 13 Å length), the enhancement profile of the sample suggests that this is probably not the case, and that perhaps only the outer β -sheets of the molecule are in close proximity to the radical. Surprisingly, however, TTR(105-115) also forms fibrils that contain a solvent gap, but the enhancements of the fibril and glycerol signals are comparable. The cryoEM profile of these

fibrils (see Chapter 4) suggests that they are relatively flat, with uniform thickness of ~ 40 Å, smaller than the diameter of the PI3-SH3 fibrils. Therefore, we attribute the different enhancement behavior of this fibril system to the smaller size of the fibrils, and not to the insertion of TOTAPOL in between the protofilaments. β_2m , on the other hand, forms fibrils without a solvent gap but with much more uniform exposure to the bulk solvent,¹⁸ while a resolved cryoEM cross-section profile for the GNNQQNY fibrils is not available at this time. The question of how TOTAPOL (or any other polarizing agent) interacts with the biological system of interest is very important, as it can affect the outcome of a structural measurement in a DNP-enhanced MAS NMR experiment and will be discussed further in the next sections.

The TTR(105-115) fibrils show the lowest DNP enhancement and the shortest polarization buildup time (Table 3.1), implying that the proton T_1 is also shorter than that observed for the other fibril samples.^{12,29} While the enhancement is dependent on a number of experimental variables, in this case we attribute the low value to the suboptimal sample preparation. The sample contains $\sim 8\%$ protons in the buffer, comparable to the concentration in all samples, but they are mostly located on the methyl groups of the acetonitrile component of the fibril formation solution. The rotation of methyl groups, which is not suppressed at 100 K, provides a major source of proton spin-lattice relaxation, a problem that can be alleviated by using deuterated acetonitrile.

The enhancement data presented in this section are our first attempt to compile such information for relatively similar biological samples, and to assess and compare the potential benefits of DNP for the studies of biological systems. In fact, there is still very little such information available in the literature for biological samples in general. It is also important to remember that while the enhancement numbers may seem relatively low, it is the acquisition time savings that determine the benefits due to DNP. Therefore, while the enhancement for the TTR(105-115) sample was only 11, the short T_1 time allowed us to recycle the experiment faster, and great savings in acquisition time were still achieved as discussed below.

3.3. Effects of temperature and TOTAPOL on spectral resolution

The low temperature required for DNP and the addition of polarizing agent can have profound effects on the sample integrity and the resolution and information content in DNP-enhanced correlation spectra. The presence of a paramagnetic species in close proximity to

the observed nuclei can shorten the nuclear T_2 values, and hence lead to line-broadening, and reduced efficiency for dipolar recoupling experiments that involve evolution of transverse magnetization, e.g. ZF-TEDOR,³⁰ DQ-DRAWS,²⁴ etc. In contrast, the reduction of nuclear T_1 values can be sometimes beneficial, as it allows, for example, the faster recycling of the data acquisition. The low temperature behavior of biological samples can be affected by a variety of factors, including but not limited to, changes in the internal dynamics of the peptide backbone and side chains, structural rearrangements due to interactions with the solvent, and freezing out of disordered or heterogeneous regions of the molecule. These factors can lead to significant deviations in the chemical shifts compared to room temperature and cause line-broadening or poor resolution in the DNP-enhanced low temperature spectra. The low temperature, on the other hand, can quench or slow down the rate of dynamic processes that otherwise interfere with cross-polarization, dipolar recoupling or heteronuclear decoupling.^{31,32} Thus, increased intensities for sites that are dynamic at room temperature can be expected at the temperatures necessary for DNP experiments, and better transfer efficiencies might be observed in this case.

In order to separate the effects of temperature and polarizing agent, we prepared some samples without radical and compared the resolution of their 1D spectra to the resolution of samples prepared with 10 mM TOTAPOL. Figures 3.2a and b show such spectra for β_2m amyloid fibrils, both obtained at 100 K. The overall appearance of the two spectra is comparable, although some loss in resolution seems to occur in the aliphatic region of the sample prepared with TOTAPOL. The much longer T_1 in the sample without radical and the lower signal-to-noise, however, prevented us from recording 2D correlation experiments in order to assess the line width differences site-specifically. Overall, however, we can conclude that while the radical has some effect on the line width in the spectra and its effect can be minimized by reducing the electron concentration in the sample, the temperature is the main source of line broadening in β_2m fibril samples. This is most evident by comparing the spectra in Figure 3.2b (100 K, no TOTAPOL) and c (300 K, no TOTAPOL). Control experiments performed at room temperature (data not shown) indicate that the addition of cryoprotectant (glycerol) has no effect on the resolution of β_2m fibrils.

β_2m amyloid fibrils exhibit a high degree of dynamics at room temperature, resulting in the weak intensity or absence of ~ 20 residues from dipolar spectra recorded at 300 K.²⁶ In

addition, the first 6 residues in the β_2m sequence are highly mobile and can be detected with solution NMR-based through bond experiments.²⁶ The dynamic sites can freeze in different conformations, leading to structural disorder, and hence inhomogeneous line broadening at low temperature. Molecular motion, however, can still contribute to the homogeneous line width in the spectra even at 100 K. For example, methyl group three fold hops can reduce the efficiency of the decoupling or the magic angle spinning resulting in the absence or severe line broadening of methyl peaks at temperatures down to $\sim 90 - 100$ K.^{31,33} Aromatic ring flips can have a similar effect, although their dynamic transitions have usually been observed at higher temperatures and their intensity is generally recovered or even enhances at 100 K.^{31,32,34,35} This behavior is manifested in the spectra presented in Figure 2b and c, where the methyl peaks (around 20 ppm) have a much higher relative intensity at 300 K, while the aromatic peaks are much more intense at 100 K.

Similarly, the presence of 10 mM TOTAPOL has minimal effect on the resolution observed in GNNQQNY amyloid fibril spectra but the change in temperature leads to 40 – 60 Hz increase in the line widths.¹¹ In this case, site-specific resonance assignments were possible at 100 K, and the low temperature chemical shifts were very similar to the ones obtained at 300 K, (< 1 ppm difference for ^{13}C sites). This significant finding indicates that despite the increase in line widths, the fibrils preserve their structure and integrity at the low temperatures required for DNP. Similar experiments are under way for the PI3-SH3 and TTR(105-115) fibrils.

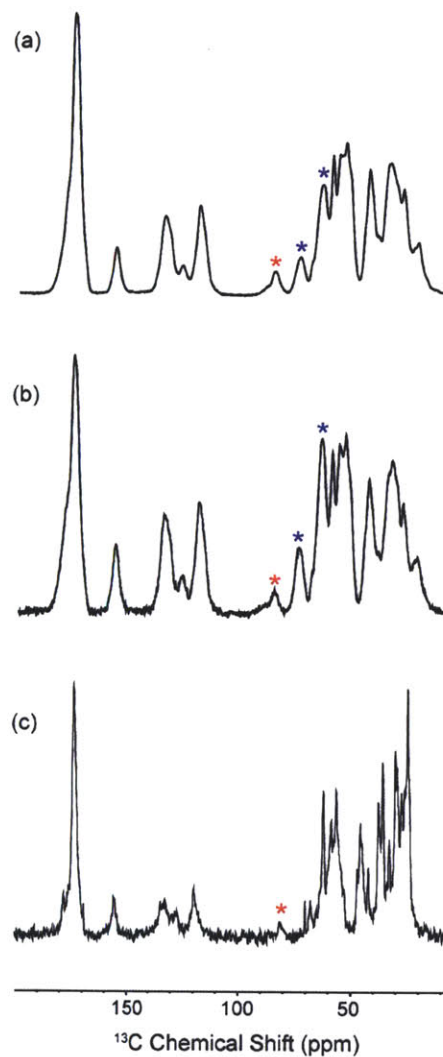


Figure 3.2. Low temperature ^{13}C CP spectra of $\beta_2\text{m}$ fibril samples prepared with (a) 10 mM TOTAPOL, glycerol- d_8 /deuterated buffer matrix diluted with 5% protons, and (b) no TOTAPOL, glycerol- d_5 /protonated buffer matrix. The spectrum in (a) was obtained with a recycle delay of 6.5 s, and 16 scans, while the spectrum in (b) was recorded with a recycle delay of 30 s, and 64 scans. (c) ^{13}C CP spectrum obtained at 300 K and 500 MHz ^1H Larmor frequency with a $\beta_2\text{m}$ fibril sample prepared without TOTAPOL, and without glycerol, in 100% protonated pH 2.5 buffer. 128 scans with a recycle delay of 3 s were recorded. The red asterisks denote spinning side bands, while the blue asterisks denote signals arising from the natural abundance glycerol signals. The intensity in spectra (b) and (c) were normalized to the intensity in spectrum (a), so that the resolution of the three spectra could be compared.

3.4. Effects of temperature and TOTAPOL on experimental efficiency

3.4.1. ^1H - ^{13}C cross polarization

Table 3.2 presents the values necessary for optimal cross polarization (CP) transfer in the DNP samples, and T_2' values wherever available. The $\text{C}\alpha$ sites (and the aliphatic sites in general) reach maximum intensity with shorter cross-polarization times as they have directly bonded ^1H atoms, while the CO maximum usually occurs later as the polarization transfer is less direct. At room temperature, in samples prepared without TOTAPOL, similar behavior is observed except that maximum intensity is reached with slightly longer cross polarization times (~ 200 - $500 \mu\text{s}$ for the aliphatic sites, $1.5 - 2.0 \text{ ms}$ for the carbonyl sites).

The sample prepared without polarizing agent is of particular interest, as it allows us to distinguish the effects of electron-nuclear relaxation and temperature. Importantly, the $\text{C}\alpha$ sites reach maximum intensity around $75 \mu\text{s}$, on the same time scale as the rest of the samples prepared with 10 mM TOTAPOL. The faster buildup of ^{13}C intensity is therefore most likely a manifestation of the reduced interference of molecular dynamics at 100 K with the ^1H - ^{13}C cross polarization transfer. The CO sites reach their maximum at 0.8 ms , accelerated compared to room temperature, and surprisingly, faster than for the samples containing radical. We attribute this difference to the much higher protonation levels of the glycerol/buffer mixture used in the preparation of the sample without TOTAPOL. The most important difference between this sample and the ones containing radical, however, is the observation that while the $\text{C}\alpha$ intensity reaches its maximum on the same time scale, it remains constant up to 1 ms , similar to the behavior of fibril samples without polarizing agent at room temperature. The $\text{C}\alpha$ intensity for samples prepared with TOTAPOL and 100 K , on the other hand, starts to decrease after $200 - 500 \mu\text{s}$, much earlier than the optimal time for the CO sites. Thus, the cross polarization time chosen for such a sample at the end is suboptimal for both the aliphatic and carbonyl sites. This behavior is most likely due to the presence of electron-nuclear relaxation, which can decrease the $T_{1\rho o}$ value that governs the spin relaxation during the CP spin locking pulse.

Table 3.2. Cross-polarization times necessary to obtain maximum signal intensity for the Ca sites (Ca max), the CO sites (CO max), and the value chosen to perform the CP experiments (CP opt). If measured, T_2' for the samples are also reported.

Fibril system	Labeling	Ca max	CO max	CP opt	T_2'
GNNQQNY	U- ¹³ C, ¹⁵ N gnnQQNy	0.075 ms	2.0 ms	1.2 ms	12 ms ^(a)
TTR(105-115)	¹⁵ N at Y105, ¹³ C at S115 C'	-	1.5 ms	1.5 ms	12 ms
PI3 SH3	100% 2- ¹³ C glycerol, U- ¹⁵ N	0.080 ms	1.5 ms	0.8 ms	-
	50:50 mixture 2- ¹³ C glycerol/U- ¹⁵ N	0.090 ms	1.4 ms	0.8 ms	11 ms
β_2m	U- ¹⁵ N, ¹³ C VYAL	0.075 ms	2.0 ms	1.2 ms	-
	U- ¹⁵ N, ¹³ C VYAL, no TOTAPOL ^(b)	0.075 ms	0.8 ms	0.8 ms	-
	100% 2- ¹³ C glycerol, U- ¹⁵ N	0.075 ms	1.5 ms	1.0 ms	-

(a) Selective pulse on the carbonyl peaks was applied. Without this pulse, the measured value was 5 ms.

(b) All other listed samples contain 10 mM TOTAPOL.

3.4.2. Transverse relaxation

Whenever possible, T_2' values were measured using a spin echo pulse sequence. This pulse sequence also leads to evolution of the ¹³C-¹³C J-couplings, which can interfere with the measurement. Therefore, in the case of the GNNQQNY fibrils, where uniform ¹³C labeling was used, a selective pulse was applied on the carbonyl region of the spectrum, thus refocusing the scalar coupling contribution of the directly bonded Ca atoms. The selective pulse was not necessary for the TTR(105-115) fibrils where only the S115 CO atoms was ¹³C labeled, or for the PI3-SH3 sample where the 2-¹³C glycerol labeling minimized the possibility for directly bonded ¹³C labeled CO and Ca sites. In all three cases, the carbonyl T_2'

values were 11-12 ms, relatively short compared to the room temperature values of 18-20 ms. This is most likely due the presence of electrons in the sample, and it is therefore a parameter that can be experimentally controlled by optimizing the biradical concentration. The reduced T_2' value has a significant effect on dipolar recoupling experiments that contain echo periods (e.g. ZF-TEDOR)^{30,36}, and whose efficiency might be reduced at mixing times longer than 10 ms.¹¹

3.5. Comparison of GNNQQNY crystals and amyloid fibrils

3.5.1. DNP of GNNQqny monoclinic crystals

A typical DNP-enhanced 1D ^{13}C CP spectrum of the GNNQqny crystals is presented in Figure 3.3 and compared to a spectrum obtained without simultaneous microwave irradiation. The enhancement due to DNP varies for the different components of the sample, i.e. the enhancement for the two glycerol peaks at ~ 70 ppm is ~ 40 , while the enhancement observed for the signals arising from the peptide is ~ 20 . The explanation for this behavior is that TOTAPOL remains outside the crystals and the polarization has to cross the barrier between the glassy solvent and the crystal interior.⁹ This is also manifested by the slower rate of polarization buildup for the peptide residues (10-12 s for the peptide vs 3 s for glycerol).

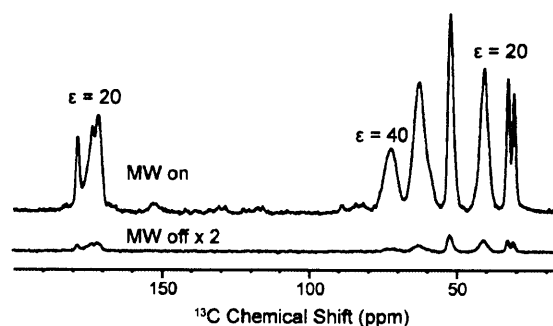


Figure 3.3. ^{13}C CP spectra of $[\text{U-}^{13}\text{C}, ^{15}\text{N GNNQ}]$ QNY monoclinic crystals recorded with (top) and without (bottom) DNP. The enhancement for the signals arising from the crystals is ~ 20 , while the enhancement for the glycerol peaks is ~ 40 . The MW irradiation time is 6 s for both spectra.

The fact that TOTAPOL remains excluded from the crystals offers some significant advantages. First, the concentration of TOTAPOL can be increased quite significantly

without compromising the line width of the spectra. It has been demonstrated that concentrations up to 70 mM in the crystal samples do not lead to significant line broadening at room temperature.⁹ Using higher radical concentration allows for much faster polarization times and scan delays and significantly improves the signal-to-noise ratio per unit time.³⁷ Second, the spectroscopic behavior of the bulk of the peptide molecules can be expected to be only modestly influenced by the presence of radical electrons in the sample, resulting in relaxation parameters that are predominantly governed by temperature and less by the electron-nuclear interaction.

The enhancement due to the cross effect is inversely proportional to the field,³⁸ and therefore the expected enhancement at 9.4 T would be 1.9 times smaller than the enhancement reported at 5 T.⁹ However, the field alone does not explain why the observed enhancement in this study is ~ 20 for the peptide resonances instead of the expected 63. Differences in the experimental conditions, in particular the higher temperature used to record the current data set, are probably significant contributing factors to the lower enhancement. An important observation, however, is that at 100 K, the sensitivity enhancement just due to the temperature effect is ~ 5 (data not shown) as a result of the larger spin polarization and the improved efficiency of the probe at low temperature. Therefore, the overall enhancement compared to 300 K is ~ 100 , resulting in significant gains in the time necessary to record correlation experiments.

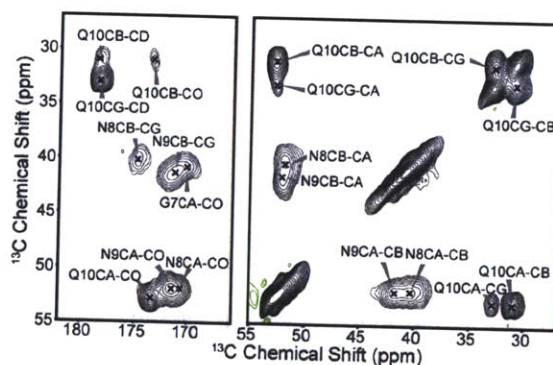


Figure 3.4. DNP-enhanced ^{13}C - ^{13}C PSD correlation spectrum of $[\text{U-}^{13}\text{C}, ^{15}\text{N GNNQ}]\text{QNY}$ monoclinic crystals obtained at 9.4 T, 105 K, $w_r/2p = 9$ kHz, and $t_{\text{mix}} = 5$ ms.

Assignments of the four labeled residues were obtained through a ^{13}C - ^{13}C correlation

experiment recorded with PDSM mixing ($t_{\text{mix}} = 5$ ms) (Figure 3.4) and one- and two-bond ^{15}N - ^{13}C correlation experiments recorded with TEDOR mixing^{30,36} (Figure 3.5). These spectra present improved resolution compared to previously published spectra at 5 T, and despite the heterogeneity and large line widths observed for some sites, the complete low-temperature assignment of all the labeled resonances in the crystals was possible.

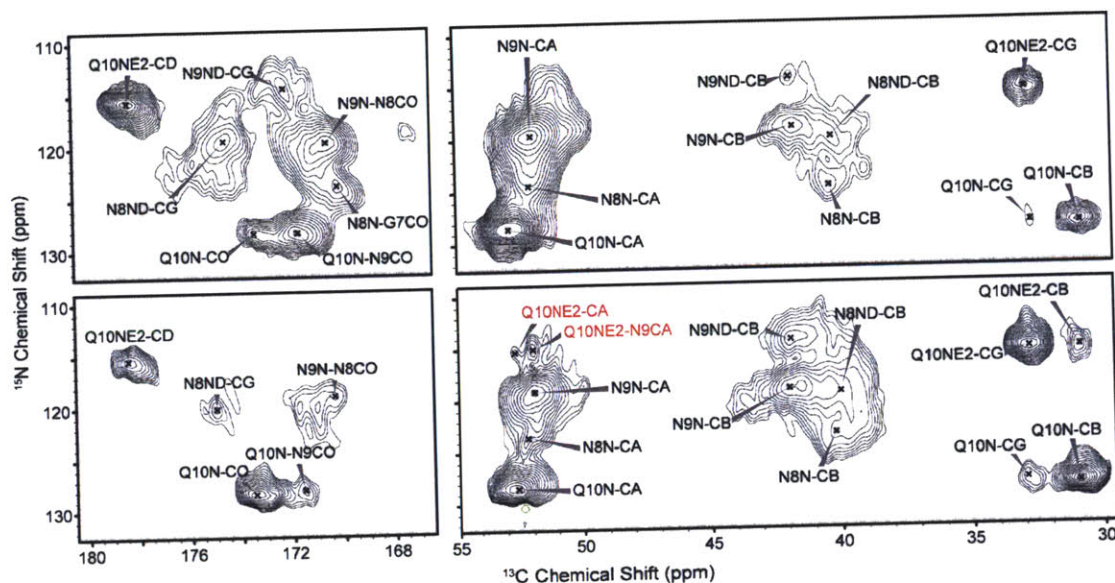


Figure 3.5. DNP-enhanced TEDOR spectra of $[\text{U-}^{13}\text{C}, ^{15}\text{N GNNQ}]\text{QNY}$ monoclinic crystals obtained at 9.4 T, 105 K, $w_r/2p = 9$ kHz, and $t_{\text{mix}} = 1.8$ ms (top), and 3.6 ms (bottom). Two intermolecular contacts are observed at $t_{\text{mix}} = 3.6$ ms.

The TEDOR spectrum of the crystals presented in Figure 5 and recorded with $t_{\text{mix}} = 3.6$ ms is of particular interest as it shows two cross peaks consistent with intermolecular contacts between Q10N ϵ 2 and N9C α and Q10N ϵ 2 and Q10C α respectively (Figure 3.6) with interatomic distances that correspond to ~ 4 Å. In a uniformly labeled sample, the typical one-bond (1.2 Å) transfer efficiency is $\sim 25\%$, while for a concurrent 4 Å distance, the efficiency is reduced to 2%.³⁰ Gln and Asn residues, in particular, contain multiple strong and medium ^{15}N - ^{13}C dipolar couplings that further complicate the transfer between weakly coupled nuclei like the intermolecular contacts shown here. The measurement of such structurally relevant distances is therefore quite difficult and very often also complicated by the presence of dynamics at room temperature. The DNP-enhanced TEDOR spectra, however, demonstrate that such important structural information can be

recorded with sufficient intensity at low temperature in cases where enough resolution is available.

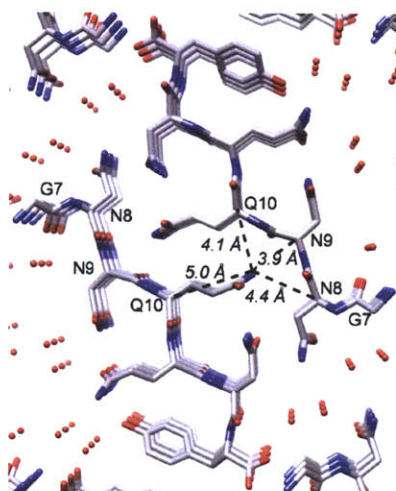


Figure 3.6. Crystal lattice of monoclinic GNNQQNY (PDB ID 1YJP).³⁹ Several possible intra- and intermolecular contacts between Q10 Ne and the Ca atoms of other labeled residues are indicated. The image was produced using the Chimera software.⁴⁰

3.5.2. Temperature dependent structural changes

The experiments described above have allowed us to assign all labeled residues in GNNQqny monoclinic crystals and a significant number of the cross peaks for gnnQQNY fibrils at 100 K. The obtained chemical shifts, together with the line width exhibited in the spectra, provide important information regarding the structural rearrangements and the changes in dynamics the two samples undergo upon freezing. While the change in temperature seems to have little effect on the structural integrity and conformational stability of the fibrils, it affects the residues in the crystals more profoundly.

Comparison of the published room temperature chemical shifts²⁰ (300 K) and the low temperature chemical shifts presented here (100 K) for GNNQqny monoclinic crystals reveals significant structural changes for some of the residues. In particular, the ¹³C chemical shifts for most sites in G7, N8 and N9 differ by more than 1 ppm between 100 K and 300 K, while the difference for the ¹⁵N chemical shifts can be as much as 5 ppm (Figure 3.7). The corresponding differences for Q10, however, are less dramatic. Closer

inspection of the spectra presented in Figure 3.4 and 3.5 also indicates that the cross peaks that have been assigned to the glutamine spin system exhibit narrower line widths ($\sim 1.1 - 1.75$ ppm for ^{13}C resonances and $1.8 - 2.5$ ppm for ^{15}N resonances) and a much lower degree of heterogeneity. In comparison, the line width of the N8CB-CA cross peak in the PDS spectrum (Figure 3.4) is ~ 1.8 ppm in the direct dimension, while the N9N-CA cross peak in Figure 5 is ~ 1.6 ppm for ^{13}C and ~ 3 ppm for ^{15}N .

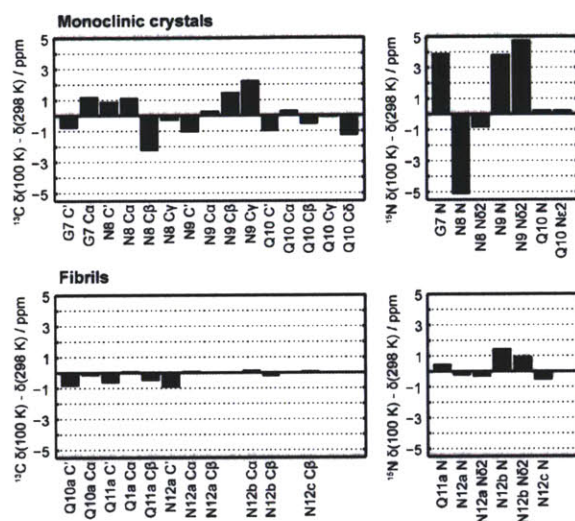


Figure 3.7. Comparison of the ^{13}C and ^{15}N chemical shifts obtained at 100 K with DNP and 298 K without DNP for $[\text{U-}^{13}\text{C}, ^{15}\text{N GNNQ}] \text{QNY}$ monoclinic crystals (top) and $\text{GNN}[\text{U-}^{13}\text{C}, ^{15}\text{N QQN}] \text{Y}$ fibrils (bottom).

Residue Q10 plays an important role in the intermolecular interactions of GNNQNY monoclinic crystals, as it is tightly locked in the dry “steric zipper” that forms between the b-sheets in the crystals (Figure 3.6). The other three residues labeled in this study, however, are in intimate contact with the crystallographic water. Water molecules are found to be an integral part of many protein crystal structures, where they may have a key structural or functional role. Despite their ubiquitous presence, however, there have been few reports documenting their influence on the dynamics of the groups they interact with in protein crystals.⁴¹⁻⁴⁴ At room temperature, these studies are also complicated by the exchange between crystallographic water and the bulk solvent water, as well as chemical exchange between labile protein protons and water molecules in general. Although the

effect of temperature on the dynamic behavior of the crystallographic water molecules is not well understood, it is highly probable that as the sample freezes they undergo structural rearrangements that are translated to the neighboring atoms via non-specific interactions and lead to both the chemical shift displacement and the increase in line width and heterogeneity observed here. The room temperature spectra of the crystals²⁰ show no significant differences in the dynamics of the different residues (as evidenced by their similar cross peak intensities and line width), implying that the freezing out of different conformations accessible at room temperature due to inherent dynamics of the peptide is not likely.

The effect of the freezing of the bulk solvent, on the other hand, is lessened by the glycerol co-solvent, a popular cryoprotectant that was also used for the X-ray crystallography studies of the monoclinic crystals.³⁹ In glycerol-water mixtures, glycerol is thought to disrupt the hydrogen bonding network of the bulk water molecules and to prevent detrimental ice formation upon freezing.^{44,45} The impact of the solvent water molecules on the line width observed in the spectra should also be limited by the high concentration of radical close to the crystal surface that may effectively suppress the broadened signals from the surface exposed peptides.

Remarkably, temperature seems to have less significant impact on the chemical shifts of the gnnQQNy fibrils (Figure 3.7). The changes in the chemical shifts of the assigned residues are <1 ppm for ¹³C, and < 1.5 ppm for ¹⁵N, much smaller than the dramatic chemical shifts differences observed for some sites in the crystals. While the line widths are slightly broader than those observed at room temperature, there are no particular patterns that indicate that certain sites exhibit more line broadening than others at low temperature. This observation, combined with the room temperature control experiments, imply that the effects of lowering the temperature are more uniform and reversible in the fibril sample and much more significant than the effect of the biradical. Future work on cryo-protection might help reduce the line width further at 100 K, which would not only facilitate the assignment process of the spectra, but would also increase T_2 values so that the efficiency of experiments like TEDOR could be improved for the longer distance spin pairs.

3.5. Conclusions

In this chapter, we have shown that DNP enhancements of 10 – 35 can be achieved at 9.4 T in amyloid fibril samples prepared with 10 mM TOTAPOL. While the biradical is relatively close to the peptide or protein molecules in most of the fibril systems, its effect on the spectral resolution is relatively small at this concentration. Most of the line broadening observed in DNP-enhanced MAS NMR spectra seems to be due to the freezing out of disordered or slightly heterogeneous regions at low temperature, although a homogeneous contribution due to molecular motion processes that are still active at 100 K cannot be excluded. Most of the dynamic processes, however, are slowed down at this temperature resulting in faster buildup during ^1H - ^{13}C cross polarization, or in ^{13}C - ^{13}C and ^{15}N - ^{13}C correlation experiments. The presence of 10 mM TOTAPOL (20 mM electrons) in the sample shortens the nuclear $T_{1\rho}$ and T_2' values, causing faster decay of the polarization transfer during CP and experiments like TEDOR. The effect of radical on these parameters can be controlled by optimizing its concentration in the sample.

In addition, we have shown that crystals prepared by the GNNQQNY peptide undergo significant structural changes at low temperature, while the fibrils formed by the same peptide preserve their structural integrity. We attribute these differences to the presence of crystallographic water molecules in the crystals that might undergo a structural transition at low temperature, and affect the structure and resolution of the crystal residues in their proximity.

3.6. Materials and methods

3.6.1. Sample preparation

Monoclinic crystals of 100% [^{13}C , ^{15}N GNNQ]QNY and amyloid fibrils of 100% GNN[^{13}C , ^{15}N QQN]Y peptide (New England Peptide, Gardner, MA) were obtained by following the previously described protocol.^{20,46} The crystals were suspended in 70/23/7% (w/w/w) glycerol- d_8 /D₂O/H₂O matrix containing 35 mM TOTAPOL. The fibrils were placed in 70/23/7% glycerol- d_8 /D₂O/H₂O matrix containing 10 mM TOTAPOL.

TTR(105-115) was synthesized using solid-phase methods and purified by HPLC (New England Peptide, Gardner, MA). The isotopically labeled amino acids for the synthesis were

purchased from Cambridge Isotope Laboratories, Andover, MA. The sample was labeled with ^{15}N at Y105, and ^{13}C at the S115 carbonyl position. Amyloid fibrils were prepared by dissolving ~ 15 mg peptide/mL in a 10% acetonitrile/ H_2O solution, adjusted to pH 2.0 with HCl. The solution was incubated at 37 °C for 2 days, followed by 14 days at 25 °C. The mature fibrils were washed with a solution containing a 60/40% w/w glycerol- d_8 /buffer matrix, where the buffer consisted of a 10/90% v/v protonated acetonitrile/ D_2O mixture with pD adjusted to 2.0 with HCl. This solution also contained 10 mM TOTAPOL.

PI3-SH3 fibrils were grown as described previously²⁵ and two samples were prepared with different labeling. Sample 1 was 100% labeled using 2- ^{13}C glycerol and U- ^{15}N , while Sample 2 was prepared from a 50:50 mixture of monomers where half of the monomers were labeled with 2- ^{13}C glycerol and ^{14}N , and the other half were only uniformly labeled with ^{15}N . The mature fibrils were placed in solution containing a 60/40% w/w glycerol- d_8 /buffer matrix, where the buffer consisted of D_2O mixture with pD adjusted to 2.0 with HCl. This solution also contained 10 mM TOTAPOL.

Long, straight $\beta_2\text{m}$ fibrils were formed at pH 2.5 as described previously.²⁶ Sample 1 was labeled in media containing ^{13}C -labeled glucose and ^{15}N labeled ammonium chloride, with the subsequent addition of natural abundance amino acids except alanine, valine, leucine and tyrosine, producing uniform isotope labeling predominantly at these positions. Solution NMR analysis, however, showed evidence that some label scrambling had occurred. Fibril samples with 10 mM TOTAPOL and no TOTAPOL were prepared with this material. Sample 2 was 100% labeled using 2- ^{13}C glycerol and ^{15}N labeled ammonium chloride. 10 mM TOTAPOL was added to these fibrils as well. $\beta_2\text{m}$ fibrils containing TOTAPOL were pelleted in a solution containing 60/40% w/w glycerol- d_8 /buffer. The buffer component contained 25 mM sodium acetate, 25 mM sodium phosphate, 0.04% (w/v) NaN_3 in D_2O with pD adjusted to 2.5 with HCl. The sample prepared without biradical was suspended in a solution containing 60/40% w/w glycerol- d_5 /protonated buffer.

All fibril samples were pelleted at 265,000g for 1 hr, and transferred to a Bruker 3.2 mm sapphire rotor with a zirconia drive cap (Bruker BioSpin, Billerica, MA).

3.6.2. DNP experiments

The DNP experiments were performed on a Bruker 263 GHz Solids DNP spectrometer,

consisting of a 263 GHz continuous-wave gyrotron source, microwave transmission line, 3.2 mm low temperature MAS probe, gas cooling supply, and 400 MHz AVANCE III wide-bore NMR system.²⁸ The temperature was regulated at 100 – 103 K, and $\omega_r/2\pi = 9$ kHz. 1D ^{13}C experiments were recorded with the parameters summarized in Table 2 with and without continuous microwave irradiation in order to determine the enhancement due to DNP. $2.5 \mu\text{s } ^1\text{H}$, $4.5 \mu\text{s } ^{13}\text{C}$ and $5.0 \mu\text{s } ^{15}\text{N } \pi/2$ pulses were used for the CP experiments and the PDS and TEDOR correlations of GNNQQNY nanocrystals and fibrils. 100 kHz ^1H decoupling was used during the acquisition, evolution and TEDOR mixing periods. The recycle delay was set to 6 s for the crystal sample, and 6.5 s for the fibril sample. Each TEDOR experiment was acquired with 32 scans per t_1 point, 96 t_1 points and dwell time of 111 μs (~5 hr for the crystals and ~5.5 hr for the fibrils). The PDS experiments were acquired with 4 scans per t_1 point, 384 t_1 points, and dwell time of 56 μs (~ 3 hr each).

3.6.3. Room temperature experiments

A ^{13}C CP spectrum of a $\beta_2\text{m}$ fibril sample prepared without TOTAPOL and glycerol was recorded at 500 MHz ^1H Larmor frequency and $\omega_r/2\pi = 10$ kHz. 128 scans and 3 s recycle delay were used. The estimated temperature of the sample is ~ 15 °C.

Acknowledgements

We would like to thank Melanie Rosay and Werner Maas at Bruker BioSpin for giving us time on their 400 MHz DNP spectrometer, where all the DNP data presented in this chapter was recorded. We also thank Shane Pawsey, Jochem Struppe, Leo Tometich, and Eckhard Bez for invaluable assistance during the DNP experiments.

References

- (1) Goldman, M. *Spin temperature and nuclear magnetic resonance in solids*; Clarendon Press: Oxford, 1970.
- (2) Jeffries, C. D. *Dynamic Nuclear Orientation*; Interscience: New York, 1963.

- (3) Abragam, A.; Goldman, M. *Nuclear magnetism: order and disorder*; Clarendon Press: Oxford, 1982.
- (4) Wind, R. A.; Duijvestijn, M. J.; Vanderlugt, C.; Manenschijn, A.; Vriend, J. *Prog. Nucl. Magn. Reson. Spectrosc.* **1985**, *17*, 33-67.
- (5) Becerra, L. R.; Gerfen, G. J.; Temkin, R. J.; Singel, D. J.; Griffin, R. G. *Phys. Rev. Lett.* **1993**, *71*, 3561-3564.
- (6) Maly, T.; Debelouchina, G. T.; Bajaj, V. S.; Hu, K.-N.; Joo, C.-G.; Mak-Jurkauskas, M. L.; Sirigiri, J. R.; van der Wel, P. C. A.; Herzfeld, J.; Temkin, R. J.; Griffin, R. G. *J. Chem. Phys.* **2008**, *128*, 052211.
- (7) Rosay, M.; Zeri, A. C.; Astrof, N. S.; Opella, S. J.; Herzfeld, J.; Griffin, R. G. *J. Am. Chem. Soc.* **2001**, *123*, 1010-1011.
- (8) Rosay, M.; Lansing, J. C.; Haddad, K. C.; Bachovchin, W. W.; Herzfeld, J.; Temkin, R. J.; Griffin, R. G. *J. Am. Chem. Soc.* **2003**, *125*, 13626-13627.
- (9) van der Wel, P. C. A.; Hu, K. N.; Lewandowski, J.; Griffin, R. G. *J. Am. Chem. Soc.* **2006**, *128*, 10840.
- (10) Mak-Jurkauskas, M. L.; Bajaj, V. S.; Hornstein, M. K.; Belenky, M.; Griffin, R. G.; Herzfeld, J. *Proc. Natl. Acad. Sci. U. S. A.* **2008**, *105*, 883.
- (11) Debelouchina, G. T.; Bayro, M. J.; van der Wel, P. C. A.; Caporini, M. A.; Barnes, A. B.; Rosay, M.; Maas, W. E.; Griffin, R. G. *Phys. Chem. Chem. Phys.* **2010**, *12*, 5911-5919.
- (12) Song, C.; Hu, K. N.; Joo, C. G.; Swager, T. M.; Griffin, R. G. *J. Am. Chem. Soc.* **2006**, *128*, 11385.
- (13) Hu, K.-N.; Yu, H.-h.; Swager, T. M.; Griffin, R. G. *J. Am. Chem. Soc.* **2004**, *126*, 10844-10845.
- (14) Matsuki, Y.; Maly, T.; Ouari, O.; Karoui, H.; Le Moigne, F.; Rizzato, E.; Lyubenova, S.; Herzfeld, J.; Prisner, T.; Tordo, P.; Griffin, R. G. *Angew. Chem., Int. Ed.* **2009**, *48*, 4996.
- (15) Dane, E. L.; Maly, T.; Debelouchina, G. T.; Griffin, R. G.; Swager, T. M. *Org. Lett.* **2009**, *11*, 1871-1874.
- (16) Dane, E. L.; Swager, T. M. *J. Org. Chem.* **2010**, *75*, 3533-3536.
- (17) Jimenez, J. L.; Guijarro, J. L.; Orlova, E.; Zurdo, J.; Dobson, C. M.; Sunde, M.; Saibil, H. *R. Embo Journal* **1999**, *18*, 815-821.

- (18) White, H. E.; Hodgkinson, J. L.; Jahn, T. R.; Cohen-Krausz, S.; Gosal, W. S.; Muller, S.; Orlova, E. V.; Radford, S. E.; Saibil, H. R. *J. Mol. Biol.* **2009**, *389*, 48-57.
- (19) Bajaj, V. S.; Mak-Jurkauskas, M. L.; Belenky, M.; Herzfeld, J.; Griffin, R. G. *Proc. Natl. Acad. Sci. U. S. A.* **2009**, *106*, 9244.
- (20) van der Wel, P. C. A.; Lewandowski, J. R.; Griffin, R. G. *J. Am. Chem. Soc.* **2007**, 5117-5130.
- (21) van der Wel, P. C. A.; Lewandoswki, J.; Griffin, R. G. *Biochemistry* **2010**, submitted.
- (22) Jaroniec, C. P.; MacPhee, C. E.; Astrof, N. S.; Dobson, C. M.; Griffin, R. G. *Proc. Natl. Acad. Sci. U.S.A.* **2002**, *99*, 16748-16753.
- (23) Jaroniec, C. P.; MacPhee, C. E.; Bajaj, V. S.; McMahon, M. T.; Dobson, C. M.; Griffin, R. G. *Proc. Natl. Acad. Sci. U.S.A.* **2004**, *101*, 711-716.
- (24) Caporini, M. A.; Bajaj, V. S.; Veshtort, M.; Fitzpatrick, A.; MacPhee, C. E.; Vendruscolo, M.; Dobson, C. M.; Griffin, R. G. *J. Phys. Chem. B* **2010**, *114*, 13555-13561.
- (25) Bayro, M. J.; Maly, T.; Birkett, N. R.; MacPhee, C. E.; Dobson, C. M.; Griffin, R. G. *Biochemistry* **2010**, *49*, 7474-7484.
- (26) Debelouchina, G. T.; Platt, G. W.; Bayro, M. J.; Radford, S. E.; Griffin, R. G. *J. Am. Chem. Soc.* **2010**, *132*, 10414-10423.
- (27) Debelouchina, G. T.; Platt, G. W.; Bayro, M. J.; Radford, S. E.; Griffin, R. G. *J. Am. Chem. Soc.* **2010**, *132*, 17077-17079.
- (28) Rosay, M.; Tometich, L.; Pawsey, S.; Bader, R.; Schauwecker, R.; Blank, M.; Borchard, P. M.; Cauffman, S. R.; Felch, K. L.; Weber, R. T.; Temkin, R. J.; Griffin, R. G.; Maas, W. E. *Phys. Chem. Chem. Phys.* **2010**, *12*, 5850-5860.
- (29) Hu, K. N.; Debelouchina, G. T.; Smith, A. A.; Griffin, R. G. *J. Chem. Phys.* **2011**, *134*.
- (30) Jaroniec, C. P.; Filip, C.; Griffin, R. G. *J. Am. Chem. Soc.* **2002**, *124*, 10728.
- (31) Long, J. R.; Sun, B. Q.; Bowen, A.; Griffin, R. G. *J. Am. Chem. Soc.* **1994**, *116*, 11950-11956.
- (32) Bajaj, V. S.; van der Wel, P. C. A.; Griffin, R. G. *J. Am. Chem. Soc.* **2009**, *131*, 118-128.
- (33) Beshah, K.; Olejniczak, E. T.; Griffin, R. G. *J. Chem. Phys.* **1987**, *86*, 4730-4736.
- (34) Rice, D. M.; Wittebort, R. J.; Griffin, R. G.; Meirovitch, E.; Stimson, E. R.; Meinwald, Y. C.; Freed, J. H.; Scheraga, H. A. *J. Am. Chem. Soc.* **1981**, *103*, 7707-7710.

- (35) Rice, D. M.; Meinwald, Y. C.; Scheraga, H. A.; Griffin, R. G. *J. Am. Chem. Soc.* **1987**, *109*, 1636-1640.
- (36) Hing, A. W.; Vega, S.; Schaefer, J. *J. Magn. Reson.* **1992**, *96*, 205.
- (37) Barnes, A. B.; Corzilius, B.; Mak-Jurkauskas, M. L.; Andreas, L. B.; Bajaj, V. S.; Matsuki, Y.; Belenky, M. L.; Lugtenburg, J.; Sirigiri, J. R.; Temkin, R. J.; Herzfeld, J.; Griffin, R. G. *Phys. Chem. Chem. Phys.* **2010**, *12*, 5861-5867.
- (38) Hu, K. N.; Bajaj, V. S.; Rosay, M.; Griffin, R. G. *J. Chem. Phys.* **2007**, *126*, 044512.
- (39) Nelson, R.; Saway, M. R.; Balbirnie, M.; Madsen, A. O.; Riek, C.; Grothe, R.; Eisenberg, D. *Nature* **2005**, *435*, 773.
- (40) Pettersen, E. F.; Goddard, T. D.; Huang, C. C.; Couch, G. S.; Greenblatt, D. M.; Meng, E. C.; Ferrin, T. E. *J. Comput. Chem.* **2004**, *25*, 1605.
- (41) Gallagher, W.; Tao, F.; Woodward, C. *Biochemistry* **1992**, *31*, 4673.
- (42) Lesage, A.; Bockmann, A. *J. Am. Chem. Soc.* **2003**, *125*, 13336.
- (43) Paulson, E. K.; Morcombe, C. R.; Gaponenko, V.; Dancheck, B.; Byrd, R. A.; Zilm, K. *J. Am. Chem. Soc.* **2003**, *125*, 14222.
- (44) Kempkes, R.; Stofko, E.; Lam, K.; Snell, E. H. *Acta Crystallogr. D* **2008**, *64*, 287.
- (45) Dashnau, J. L.; Nucci, N. V.; Sharp, K. A.; Vanderkooi, J. M. *J. Phys. Chem. B* **2006**, *110*, 13670.
- (46) Balbirnie, M.; Grothe, R.; Eisenberg, D. S. *Proc. Natl. Acad. Sci. U. S. A.* **2001**, *98*, 2375.

Chapter 4. Hierarchical Structure of an Amyloid Fibril Determined by MAS NMR and DNP-Enhanced Distance Measurements

Adapted from a manuscript in preparation with the same title by Debelouchina GT, Bayro MJ, Fitzpatrick AW, Ladizhansky V, Caporini MA, Jaroniec CP, Bajaj VS, Rosay M, MacPhee CE, Maas WE, Dobson CM, Griffin RG; and a manuscript in preparation entitled “An Atomic Resolution Structure of an Amyloid Fibril Reveals Mechanism of Self-Assembly and Origin of Polymorphism” by Fitzpatrick AW, Debelouchina GT, Bayro MJ et al.

Summary

Transthyretin (TTR) is a 55-kDa protein that forms amyloid fibrils *in vivo* in a disease known as senile systemic amyloidosis. The eleven-residue segment spanning residues 105 to 115 can form amyloid fibrils *in vitro* and its structure was the first high-resolution amyloid secondary structure determined by magic angle spinning NMR (MAS NMR). Here, we present MAS NMR experiments and sample labeling schemes designed specifically to probe the higher levels of structural organization in the TTR(105-115) amyloid fibrils, including the β -strand arrangement into β -sheets, the β -sheet interface that defines each protofilament, and the protofilament-protofilament contacts that lead to the formation of the complete fibril. These experiments were guided from structural information obtained with other methods such as cryo-electron microscopy and atomic force microscopy, and whenever possible, we used dynamic nuclear polarization (DNP) to speed up the NMR acquisition times and improve the signal-to-noise of the acquired data. We evaluate the performance and the information content of the presented experiments and show evidence for the inherent structural complexity characterizing the fibril organization.

4.1. Introduction

The deposition of amyloid and amyloid-like fibrils in tissues and cells is the characteristic feature of at least 30 different human pathologies.¹ In addition, functional amyloid has been identified in several species, including humans.^{1,2} On the other hand, many proteins and peptides can form amyloid-like fibrils *in vitro*,³ although sometimes non-native conditions like low pH, high salt concentration or the addition of metal ions are required. While the proteins responsible for amyloid are very diverse in their sequences and native structures, the resulting fibrils share several physicochemical characteristics: they are rich in β -sheet structure; they bind the dye Congo red, resulting in a green birefringence under polarized light; and they give a distinctive X-ray diffraction pattern called “cross- β ”.^{4,5} This pattern consists of two reflections, one indicative of a 4.7 Å separation between the β strands along the fibril axis, and a second one corresponding to a 8-11 Å distance, which results from the sheet-to-sheet separation perpendicular to the fibril axis.

The atomic resolution structure of amyloid fibrils, however, remained elusive for a long time due to their insolubility and non-crystalline nature, which hampered the use of standard structural techniques like solution NMR and X-ray crystallography. Therefore, magic angle spinning NMR (MAS NMR) became the structural method of choice as it only requires the presence of microscopic order in the sample and it relies on dipolar couplings to obtain structural information in solid samples. The development and use of protein MAS NMR spectroscopy, together with complementary techniques such as cryo-electron microscopy (cryoEM), atomic force microscopy (AFM), scanning transmission electron microscopy (STEM), etc., has led to great progress in understanding amyloid fibril structure and the underlying forces that lead to protein aggregation. Up to today, progress has been made in the structural studies of the amyloid fibrils formed by many peptides and proteins, including A β ,^{6,7} Het-s,⁸ α -synuclein,^{9,10} β_2 -microglobulin,^{11,12} the SH3 domain of PI3 kinase,^{13,14} the human prion protein,¹⁵ etc.

In this chapter, we present the suite of MAS NMR experiments and labeling schemes that has allowed us to unravel the structural hierarchy present in the fibrils formed by a small segment of the amyloidogenic, disease-related protein transthyretin^{16,17} (TTR). The secondary structure of the amyloid form of this peptide, TTR(105-115), was one of the very first structures of biologically relevant molecules determined *de novo* by MAS NMR (Figure

4.1).^{18,19} The peptide in the fibril form adopts an extended β -strand conformation with the absence of significant dynamics along the backbone. Overall, 76 structurally relevant constraints (7 per residue) were reported, including 41 backbone dihedral angle restraints and 35 ^{15}N - ^{13}C distances that revealed the precise conformation of the majority of the side chains. The work relied on the use of three U- ^{15}N , ^{13}C samples where only four residues were labeled sequentially at a time (YTIAALLSPYS, YTIAALLSPYS, YTIAALLSPYS). This allowed the unambiguous assignment of the chemical shifts (with the exception of the Tyr rings), and facilitated the measurement of the ϕ and ψ backbone torsion angles through 3D dipolar-chemical shift correlation experiments.²⁰⁻²³

Here, we extend this work to present experiments specifically designed to probe the different levels of fibril organization with the goal of obtaining a complete atomic resolution structure of the entire fibril. Using the definitions of amyloid structural hierarchy by Petkova et al.,⁶ we aim to understand how the TTR(105-115) monomers stack to form the β -sheets of the fibrils (tertiary structure), and how the resulting β -sheets are arranged with respect to each other (quaternary structure). Furthermore, we show experiments that reveal the protofilament-to-*protofilament* interactions in the fibrils, which to our knowledge is the first time this has been possible by MAS NMR. The process has been guided by information obtained from other methods like cryoEM, AFM and STEM, which have allowed us to formulate and test hypotheses regarding the structural organization of the fibrils.²⁴ In addition, we have greatly benefited from the advances in dynamic nuclear polarization (DNP), a method that significantly improves the sensitivity of MAS NMR experiments and can lead to unprecedented savings in data acquisition time.²⁵⁻³¹

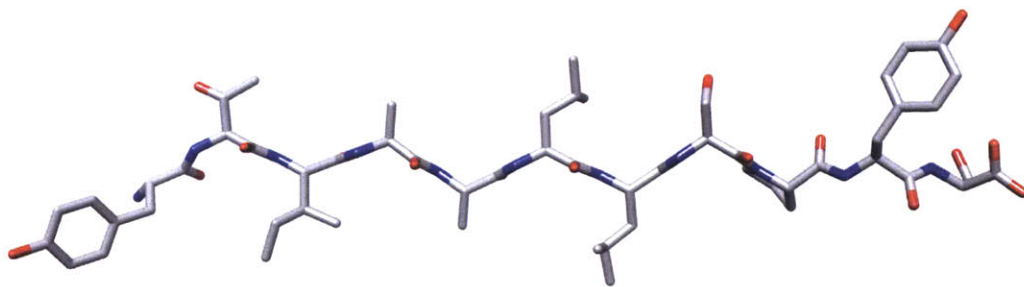


Figure 4.1. High-resolution structure of the TTR(105-115) monomer in amyloid fibrils (PDB ID: 1RVS).

4.2. Results and Discussion

4.2.1. Intra-sheet arrangement

Once the secondary structure of the monomer in the fibrils is known, the next step of the structure determination process generally involves establishing the organization of the known β -strands into β -sheets. The parallel, in-register arrangement is quite common among amyloid fibrils formed by large peptides (larger than 20 residues)³²⁻³⁴ and proteins,^{12,13} although the more complicated arrangement where one molecule forms two loops of a β -helix, and thus participates with two β -strands in a parallel β -sheet, has also been described.⁸ In the case of small amyloidogenic peptides, both parallel and anti-parallel arrangements have been observed in crystals,³⁵ with the possibility that the strands are in-register or out-of-register with an arbitrary residue offset (Figure 4.2a).

Several approaches exist for unraveling the intrasheet arrangement of β -strands in amyloid fibrils. In longer peptides and proteins, a common method involves preparing fibril samples from a 50/50 mixture of exclusively ^{13}C and exclusively ^{15}N labeled monomers and examining the nature of the intermolecular correlations in the ^{15}N - ^{13}C spectra.^{12,13,34,36} It has recently been shown, however, that information regarding the intrasheet organization is also available from long-mixing 2D ^{13}C - ^{13}C correlations of samples prepared with 2- ^{13}C glycerol as the carbon source.¹³ In shorter peptides, where many possibilities exist for the supramolecular arrangement of the peptides in the fibril,³⁷ this problem can be simplified by the use of specific labeling, and symmetry based³⁸ or double quantum pulse sequences^{39,40} have been used to obtain the corresponding distances.

In TTR(105-115), eight different samples were prepared where each sample was labeled at the carbonyl position only for residues I107-P113, and S115.^{24,41} The possible intrasheet distances for the $^{13}\text{C}_1$ S115 sample are illustrated in Figure 4.2a. In the parallel, in-register case, the labeled atoms form an infinite chain where all the atoms have identical chemical shifts and are separated by 4.7 Å. When the two strands in the β -sheet are one residue out-of-register, a “zig-zag” pattern emerges with expected average distances of ~ 5.5 Å. In the anti-parallel case, the expected distances may be too long to measure by dipolar NMR techniques. Double-quantum filtered DRAWS (DQF-DRAWS) is particularly well suited to differentiate

between these possibilities, as it can yield very precise distances for spins with degenerate chemical shifts and large chemical shift anisotropies.^{40,41}

The 1D DQF-DRAWS buildup curve for the $^{13}\text{C}_1$ S115 sample is shown in Figure 4.2b, with a maximum DQ efficiency of $\sim 8\%$, occurring at approximately 12 ms of mixing time. The experimental data was fit with the program SPINEVOLUTION,⁴² using a four spin model with a boundary condition to account for the infinite chain of nuclear spins, and a relaxation parameter that models the effects of incoherent relaxation and experimental imperfections.⁴¹ The extracted intermolecular distance for the $^{13}\text{C}_1$ S115 labeled sample is $4.26 \pm 0.03 \text{ \AA}$, and the distances for the other seven samples are in the range $4.31 - 4.52 \text{ \AA}$.²⁴ These distances are consistent with a parallel, in-register arrangement of the β -strands in the fibrils.

The buildup curve shown in Figure 4.2b was acquired using dynamic nuclear polarization (DNP), a method that can significantly enhance the sensitivity of NMR spectra and lead to unprecedented savings in acquisition time.²⁵⁻²⁸ This technique utilizes the inherently larger polarization of electrons, which is transferred to the nuclei via a microwave-driven process performed at low temperatures (90 K). The electrons are introduced in the sample in the form of a biradical, typically TOTAPOL,⁴³ and glycerol is added for cryoprotection. The significant signal enhancements demonstrated in MAS DNP experiments have been utilized in the study of a variety of biological systems, including membrane proteins,^{30,44,45} nanocrystals^{29,31} and, more recently, amyloid fibrils.^{13,31} In particular, studies of the fibrils formed by the GNNQQNY peptide³¹ demonstrated that the sample integrity and structure is preserved in the DNP samples and that the low temperature suppresses dynamic processes that can interfere with the recoupling experiment of choice, in this case ZF-TEDOR.⁴⁶ Subsequently, DNP-enhanced ZF-TEDOR was used to show that the fibrils formed by the SH3 domain of PI3 kinase form parallel, in-register β -sheets.¹³ The enhancement factor of ~ 30 , and the diminished influence of dynamics on the dipolar transfer, particularly for the side-chains, allowed the collection of a much greater set of intermolecular structural constraints in a fraction of the conventional experimental time.

In the case of TTR(105-115) fibrils reported here, DNP enhancement of ~ 10 was observed in a fibril sample prepared with 10 mM TOTAPOL⁴³ in a 60/40% w/w glycerol- d_8 /buffer matrix, where the buffer consisted of a 10/90% v/v acetonitrile/ D_2O mixture with pD adjusted

to 2.0 with HCl. The polarization buildup time was 1.3 s, which is equivalent to the ^1H T_1 relaxation⁴³, and allowed us to record experiments with a 2.0 s scan delay. Both the enhancement factor and the buildup time in this fibril system are lower than the numbers reported for the GNNQQNY fibrils ($\epsilon = 35$, buildup time 5 s)³¹ and PI3 SH3 fibrils ($\epsilon = 30$),¹³ obtained using an identical DNP setup and TOTAPOL concentration. These differences can be due to a variety of factors: the buffer composition and pH can affect the stability of the TOTAPOL radical, while the ^1H T_1 relaxation rates, and hence the enhancement, are very sensitive to overall protonation levels in the sample and slight differences in the effective temperature during the experiment. In the TTR(105-115) case, in particular, the presence of multiple methyl groups in the peptide itself and in the acetonitrile used in the buffer matrix, might provide an additional relaxation sink. Nevertheless, the relatively short T_1 time in the TTR(105-115) sample allowed us to record the DQF-DRAWS experiment depicted in Figure 2b in approximately 1.5 hr. The equivalent experiment recorded at room temperature without DNP required 3.5 days of acquisition time, with a fit distance of $4.29 \pm 0.05 \text{ \AA}$.²⁴

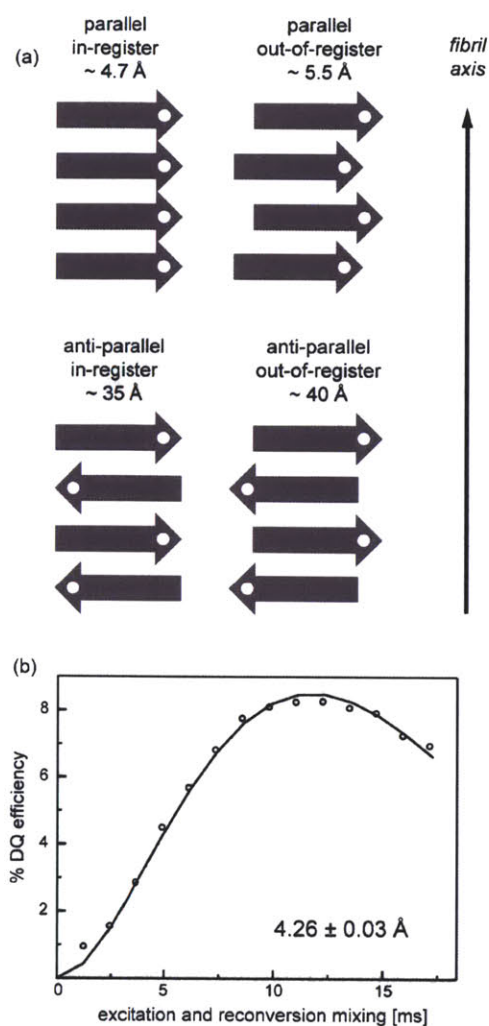


Figure 4.2. (a) Several possible arrangements of the β -strands within each sheet, along with the expected distances between the labeled atoms (white circles). (b) DNP-enhanced DQ-DRAWS experiment obtained at 400 MHz of a sample labeled with ^{13}C at S115 carbonyl position. The fit distance is $4.26 \pm 0.03 \text{ \AA}$, consistent with a parallel, in-register intra-sheet arrangement.

4.2.2. Inter-sheet contacts

Much of what is known regarding the inter-sheet interface in amyloid fibrils, particularly those formed by small peptides, has been revealed by the X-ray structures of crystals formed by amyloidogenic peptides.^{35,37} In such crystals, the inter-sheet interface is free of water molecules, and the sidechains of the adjacent sheets are tightly interdigitated, forming the so-

called steric zipper. A wet interface then may exist on the outside surfaces of the β -sheets for some peptides. Based on the crystal structures of thirteen different peptides, eight possible different classes of steric zippers were proposed, some of them yet to be observed experimentally. While this information has been extremely valuable in understanding the interactions that stabilize amyloid structures, it is only part of the story for some peptides. For example, GNNQQNY, a short segment from the yeast prion protein Sup35, can form both crystals and fibrils, and MAS NMR spectra of both forms revealed one and three sets of chemical shifts respectively.^{47,48} Similar structural complexity has been observed for the fibrils formed by the peptide SNNFGAILSS, related to type 2 diabetes.⁴⁹ Therefore, probing the exact nature of the inter-sheet interface can be rather complicated even for small peptides, but can reveal additional details regarding the structural stability of amyloid fibrils.

In order to tackle this problem for TTR(105-115), we prepared two specifically labeled samples, YTIAALLSPYS and YTIAALLSPYS that allowed us to characterize the inter-sheet contacts throughout the length of the peptide. Figure 4.3 shows a PDS⁵⁰ spectrum recorded with the YTIAALLSPYS sample. Even with the relatively short mixing time ($\tau_{\text{mix}} = 100$ ms), there are many cross-peaks (labeled in red) in the spectrum that correspond to correlations between residues in the opposite ends of the molecule, e.g. P113C β – A108C β and S112C α – I107C δ . Since the peptide molecules are organized in a parallel, in-register manner within the sheet, such correlations can only arise if the two sheets are arranged in an anti-parallel fashion. This is also confirmed in a ¹⁵N-¹³C correlation spectrum recorded with PAIN-CP mixing^{51,52} (Figure 4.4), where three inter-sheet backbone-to-sidechain correlations are observed, as well as one backbone-to-backbone correlation (S112N-A108C α).

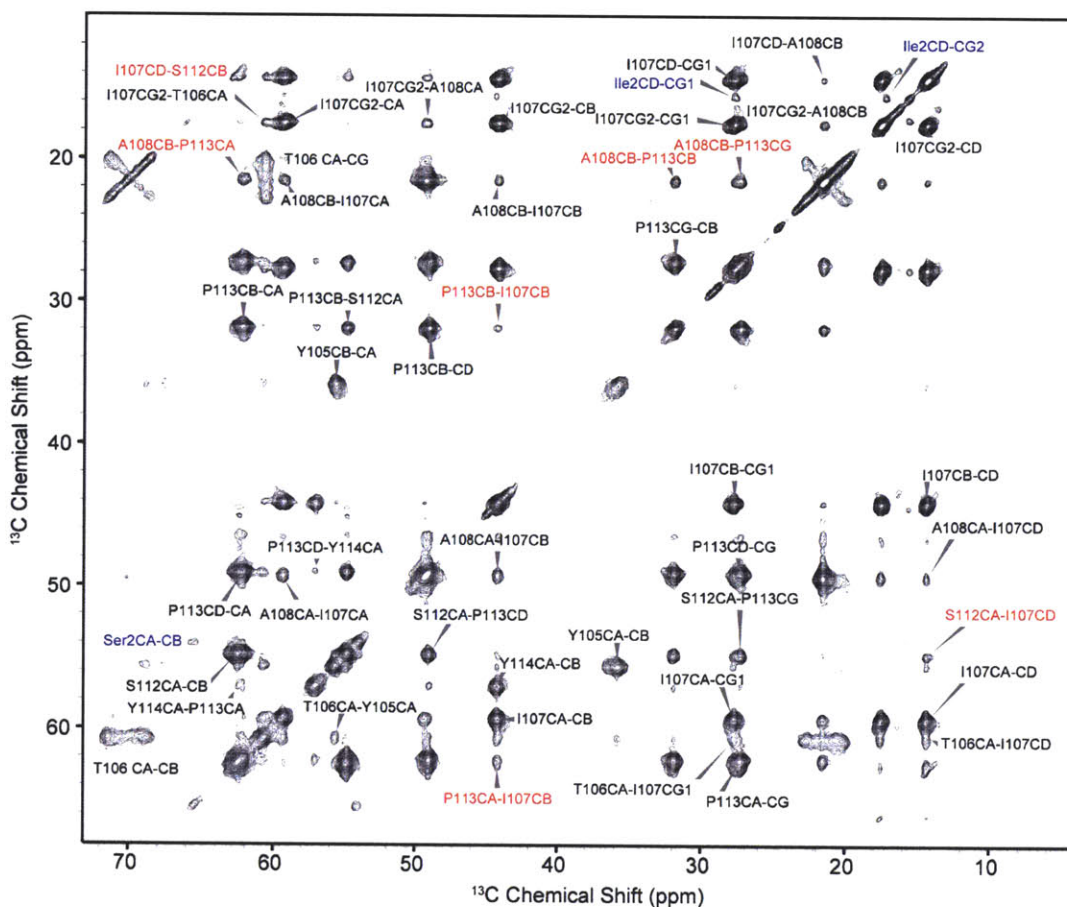


Figure 4.3. ^{13}C - ^{13}C correlation experiment used in unraveling the inter-sheet interface in the TTR(105-115) fibrils. The spectrum was obtained at 900 MHz, $\omega_r/2\pi=11.0$ kHz and 100 ms PSD mixing with a ^{13}C , ^{15}N YTIAALLSPYS labeled TTR(105-115) fibril sample. The blue labels correspond to multiplicity observed for the Ile and Ser spin systems. The observed inter-sheet correlations are labeled in red.

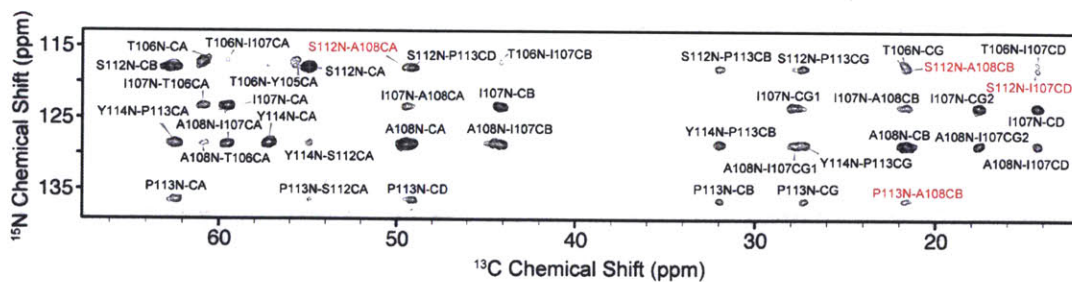


Figure 4.4. ^{15}N - ^{13}C correlation experiment used in defining the inter-sheet organization of the TTR(105-115) fibrils. The spectrum was obtained with PAIN-CP mixing ($\tau_{\text{mix}} = 10$ ms) with a ^{13}C , ^{15}N YTIAALLSPYS labeled TTR(105-115) fibril sample. Inter-sheet correlations are labeled in red.

While the PDS and PAIN-CP data give a very clear qualitative picture of the sheet-to-sheet interface in the fibrils, these experiments are hard to quantify. In the PDS case, for example, multiple spin diffusion pathways and relay transfer can complicate the distance interpretation. The PAIN-CP mechanism, on the other hand, relies on a cross-term between ^1H - ^{15}N and ^1H - ^{13}C dipolar couplings and the intensity of the transfer has a strong geometric dependence on the position of the ^1H spin.⁵² Therefore, the observed contacts in these type of spectra are usually separated in distance bins based on the mixing time when they are first observed. These rather broad distance classes are then used in the structure calculation, much like the NOE constraints used in solution NMR.

In order to complement the constraints from the PDS and PAIN-CP spectra, we performed 3D ZF-TEDOR experiments^{46,53} that allowed us to obtain accurate inter-sheet distances for P113N-A108C β , S112N-A108C β , and S112N-I107C δ 1. The experiments consisted of recording 2D ^{15}N - ^{13}C correlations at different mixing times, then extracting the intensity of the cross-peaks of interest and comparing the experimental and simulated build-up curves (Figure 4.5). For comparison, Figure 4.5 also contains simulations of several known intra-molecular distances¹⁹ in the TTR(105-115) molecule, which served as a calibration of the simulation procedure. In particular, the TEDOR transfer dynamics between distal ^{15}N - ^{13}C pairs is influenced by the proximity of other ^{15}N atoms to the ^{13}C carbon of interest. If such ^{15}N atoms are present nearby, the transfer from the distal ^{15}N atom can still be observed as a crosspeak in the 2D spectrum, however, it occurs on an accelerated time scale compared to the transfer for a lone ^{15}N - ^{13}C of an equivalent distance. For example, the I107N-A108C β distance ($4.8 \pm 0.4 \text{ \AA}$) is longer than the I107N-C δ 1 distance ($4.3 \pm 0.5 \text{ \AA}$) but the two curves have very different maxima (9 ms vs 12 ms). The transfer dynamics in the first case is accelerated due to the presence of A108N, which is only 2.4 \AA away from the C β atom. In order to reflect the properties of the spin systems in relation to TEDOR transfer, we included the contribution of the proximal A108N atom in the simulations of the buildup curves involving A108C β (Figure 4.5a). Alternatively, only one ^{15}N atom was sufficient to describe the TEDOR transfer when fitting the I107N - C δ 1 and S112N - I107C δ 1 distances (Figure 4.5b).

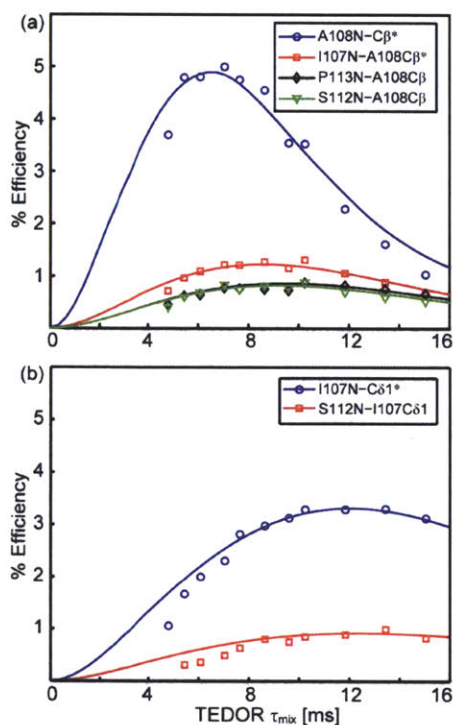


Figure 4.5. Experimental and simulated TEDOR buildup curves obtained from the cross-peak intensities in 2D ZF-TEDOR experiments recorded as a function of mixing time for (a) correlations to A108C β , and (b) correlations to I107C δ 1. The fitted distances are: 2.4 ± 0.2 Å for A108N-C β *, 4.8 ± 0.4 Å for I107N-A108C β *, 5.4 ± 0.5 Å for S112N-A108C β , 6.0 ± 0.4 Å for P113N-A108C β ; 4.3 ± 0.5 Å for I107N-C δ 1*, and 5.8 ± 0.5 Å for S112N-I107C δ 1. The intra-molecular distances marked with asterisks are known and were used as a calibration of the simulation procedure.

The distance constraints obtained from the YTIAALLSPYS sample were complemented with distances measured with a sample uniformly ^{15}N and ^{13}C labeled in the center of the peptide, i.e. YTIAAALLSPYS. Using the TEDOR experiment described above, cross-peaks between A109N and L111C δ 1 and C δ 2 were observed with fitted distances of 4.4 ± 0.5 Å and 4.6 ± 0.5 Å respectively (Figure 5.6a). With this sample it was also possible to measure some long-distance ^{13}C - ^{13}C constraints that complemented the inter-sheet ^{15}N - ^{13}C distances acquired with TEDOR. Obtaining accurate long-range ^{13}C - ^{13}C distances in uniformly labeled samples can be quite challenging due to a phenomenon known as dipolar truncation.⁵⁴ In this case, the strong one- and two-bond ^{13}C - ^{13}C couplings dominate the polarization transfer and the transfer to more distant carbon atoms is attenuated or eliminated. Experiments like PDS D ⁵⁰ and PAR⁵⁵ are less sensitive to these effects since they rely on higher order

mechanisms. However, as discussed above, they yield ambiguous distance restraints due to the complexity of the polarization transfer.

To obtain accurate ^{13}C - ^{13}C distances in the YTIAALLSPYS labeled peptide, we used the rotational resonance in the tilted frame width experiment⁵⁶ (R2TRW) to reintroduce the $^{13}\text{C}' - ^{13}\text{C}_{\gamma,\delta}$ dipolar interactions without reintroducing the strong $^{13}\text{C}' - ^{13}\text{C}\alpha$ or $^{13}\text{C}' - ^{13}\text{C}\beta$ couplings, thus avoiding dipolar truncation. The experiment starts with ^1H - ^{15}N cross-polarization,⁵⁷ t_1 evolution of the ^{15}N dimension, and selective transfer of polarization from ^{15}N to the labeled carbonyls in the sample via SPECIFIC CP.⁵⁸ The inclusion of a ^{15}N dimension during these steps provides better resolution for the carbonyl region in the spectra. During the constant time mixing period that follows, polarization is transferred from the carbonyl atoms to the side-chains via a combination of carefully selected spinning frequency and rf field strength. The spinning frequency ω_r is selected such that $2 \times \omega_r$ is slightly larger than the chemical shift difference in kHz between the carbonyls and the side-chain atoms of interest. The rf field strength applied during the mixing period is varied, adding a 3rd dimension to the experiment. Figure 4.6b depicts two ^{15}N - ^{13}C correlations recorded with two different rf field strengths during mixing, showing some intra-molecular cross-peaks between the leucine carbonyls and side-chain atoms, as well as inter-molecular cross-peaks between A108C' and L111C δ 1 and C δ 2. The intensities of these cross-peaks were fit using a two spin model as described in Ref. 42 and the extracted distances for A108C' - L111C δ 1 and A108C' - L111C δ 2 were $4.78 \pm 0.48 \text{ \AA}$.

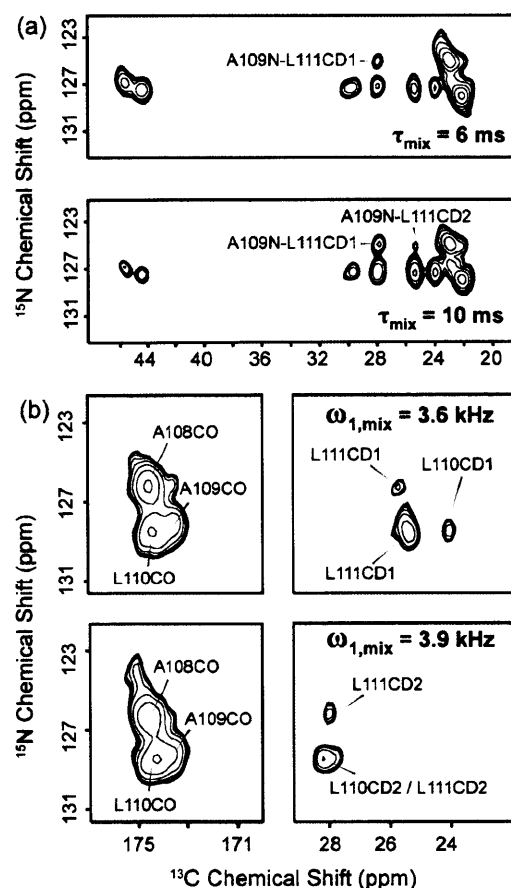


Figure 4.6. Two-dimensional ^{15}N - ^{13}C correlation spectra recorded at 500 MHz ^1H Larmor frequency with a YTIAALLSPYS labeled sample using (a) TEDOR mixing, and (b) a rotational resonance in the tilted frame width (R2TRW) experiment. Both spectra were recorded at 10.1 kHz spinning rate and with carrier frequency set at 65 ppm. R2TRW mixing was 25 ms with TPPM decoupling of 83 kHz during mixing. Examples of two ^{13}C recoupling fields used during the mixing period of the R2TRW experiment are given in (b).

The six intermolecular TEDOR and R2TRW distances obtained in the two specifically labeled samples were used for the structure calculation of the β -sheet fibril interface presented in Figure 4.7. While these contacts are not that numerous, they place important constraints on the proximity of the two the β -strands and the resulting structure can be used as a calibration for the semi-quantitative constraints obtained by the PAIN-CP and PDSO experiments. For example, the PAIN-CP spectrum presented in Figure 5.4 contains a cross-peak between S112N and A108C α , which corresponds to a backbone-to-backbone inter-sheet contact of ~ 7 Å. While such a distance is relatively long, it has been shown before in model protein systems that the TSAR mechanism can yield cross-peaks for similar ^{15}N - ^{13}C distances under favorable

spin geometry.⁵² Several even shorter distance backbone-to-backbone correlations involving A108N might also be present in the PAIN-CP spectrum but they could not be assigned unambiguously due to the very similar chemical shifts of Y114N and A108N. It is important to note that the N-C α regions of the long-mixing TEDOR experiments obtained for the TTR(105-115) samples contain fewer cross-peaks in general and such backbone-to-backbone inter-sheet correlations could not be obtained quantitatively.

In order for all of the observed contacts to be fulfilled (both quantitative and semi-quantitative), the two sheets not only have to be arranged in an anti-parallel manner with respect to each other, but also a C2 symmetry with respect to an axis parallel to the peptide molecules has to be imposed. These requirements give rise to a rather unexpected feature of the inter-sheet interface, namely that the side-chains are arranged in an odd-even-odd-even manner. This means that each side chain should reside in two different environments: in one of the β -sheets it is exposed to water, while in the other β -sheet it is locked in a dry steric zipper. The spectra, on the other hand, contain only one major set of cross-peaks. This apparent inconsistency will be discussed further in the following sections.

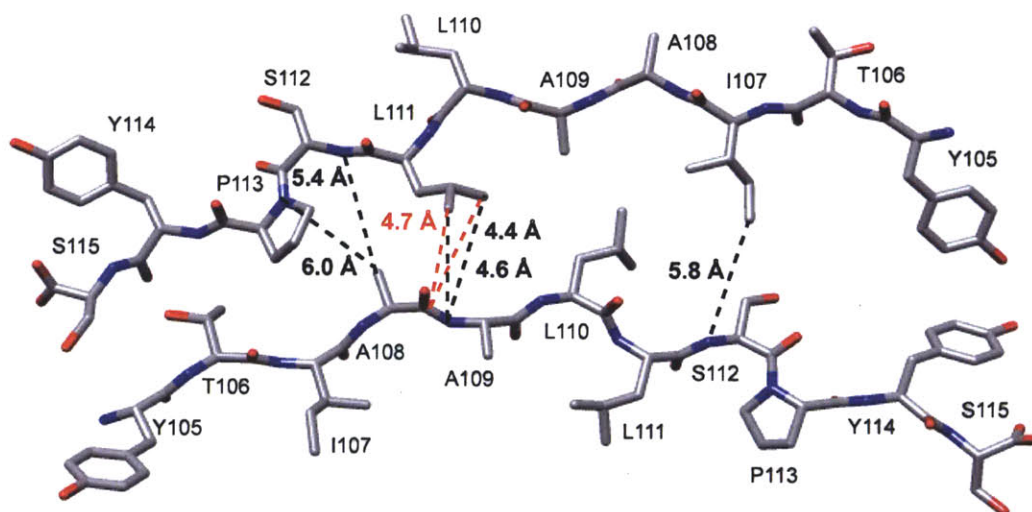


Figure 4.7. Summary of the observed quantitative contacts that constrain the odd-even-odd-even anti-parallel β -sheet interface. Contacts in black were observed in TEDOR spectra, while the distances labeled in red were measured using an R2TRW experiment.

4.2.3. Protofilament arrangement

One of the most challenging aspects of studying the structure of amyloid fibrils is identifying the nature of the contacts between the protofilaments. In the easiest case, the mass-per-length ratio and cryoEM would indicate that the fibril consists only of one protofilament, e.g. Het-s fibrils formed at neutral pH.^{59,60} In other cases, e.g. β_2 -microglobulin fibrils formed at pH 2.5, several different interfaces can be seen in the cryoEM density profile.⁶¹ While obtaining distance constraints specific to the protofibril interface might be possible with MAS NMR, a good hypothesis based on other methods is essential in doing so unambiguously.

The cryo-electron microscopy of TTR(105-115) fibrils identified three classes of fibrils, with cross-sectional widths of 80 Å, 120 Å and 160 Å respectively. The building block of the fibrils, as identified by NMR, consists of two β -sheets, arranged in an anti-parallel fashion, with an overall length of ~ 40 Å (Figure 4.7). This constitutes one protofilament in the fibrils and based on the cryoEM cross-sections, there appear to be fibrils that consist of two, three or four laterally arranged protofilaments. Since the fibrils are organized by stacking the building blocks laterally with respect to each other, one can then expect that the interactions between the protofilaments are interactions between the termini of the peptides (Figure 5.8a,b). In this case, there are two possible arrangements: the C-terminus of a peptide from one protofilament faces the N-terminus of a peptide from the adjacent protofilament (“head-to-tail” arrangement), or the two peptides from adjacent protofilaments interact with their C-termini (“head-to-head” arrangement). These possibilities can be distinguished by placing a ^{15}N label on the N-terminus (Y105N), and a ^{13}C label on the C-terminus (S115C') of the peptide and obtaining the distance between the labels.

Figure 4.8c shows a DNP-enhanced REDOR dephasing curve obtained for the S115 carbonyl peak. Fitting of the experimental data revealed that S115 C' is 3.5 Å away from the only labeled nitrogen atom in the sample, i.e. Y105N. This observation is only consistent with the “head-to-tail” arrangement depicted in Figure 4.8a. Again, this experiment benefitted greatly from DNP, which allowed us to record the data (S and S_0 data points) in ~ 5 hours, while obtaining a similar curve at room temperature took more than 24 hours.

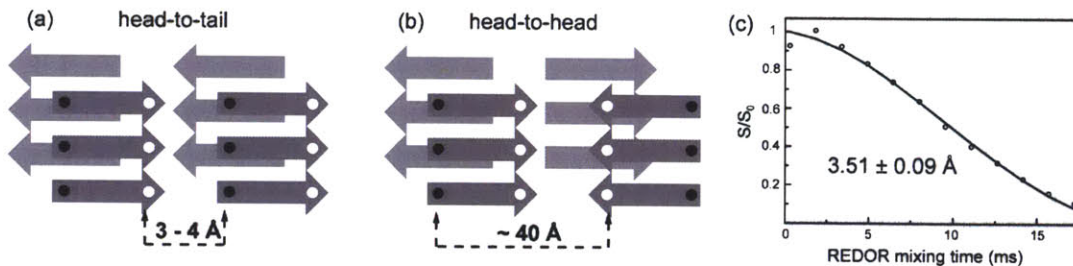


Figure 4.8. Two possible protofilament arrangements are (a) the head-to-tail, and (b) the head-to-head arrangements. The black circles correspond to a ^{15}N label in the N-terminus of the peptide, while the white circles represent the ^{13}C labeled carbonyl atom of the C-terminus. The expected ^{15}N - ^{13}C distances in each case are given on the bottom. (c) A 1D DNP-enhanced ^{15}N - ^{13}C experiment utilizing REDOR mixing was used to measure the distance between the two labels. The fit distance is $3.51 \pm 0.09 \text{ \AA}$, consistent with a head-to-tail protofilament organization.

4.3.4. Evidence for structural complexity in the spectra

The DNP-enhanced REDOR experiment described above unambiguously shows the existence of the “head-to-tail” arrangement in the TTR(105-115) fibrils. Even in the simplest case, however, where the fibril consists of only two protofilaments (Figure 4.8a), there are two different environments for the termini of the peptide. The C-terminus of one peptide interacts with the N-terminus of a second peptide to form the protofilament-to-Protofilament interface (“buried ends”), while the other ends of the two peptides face the solvent (“free ends”). In addition, since each protofilament consists of two β -sheets with side-chains arranged in an “odd-even-odd-even” manner, the termini of the two β -sheets are not equivalent, and one can anticipate a separate peak for each of them. Therefore, overall four peaks are expected for the terminal residues. Since the termini are respectively ^{15}N and ^{13}C labeled, this structural complexity should manifest itself as additional peaks in 1D ^{15}N and ^{13}C spectra. These spectra are shown in Figure 5.9a,b where peak multiplicity is indeed observed. The ^{13}C spectrum contains four peaks in the carbonyl region with integrated area ratios of 2.5 : 1.0 : 0.7 : 0.7 and ^{13}C chemical shifts of 181.9, 180.6, 177.4 and 175.1 ppm, while the ^{15}N spectrum contains two rather broad peaks with ^{15}N chemical shifts of 39.8 and 38.3 ppm (integrated area ratios of 3.0 : 1.0). This peak multiplicity has been observed reproducibly in different sample preparations of TTR(105-115) fibrils.

As expected, only some of the ^{13}C peaks in Figure 4.9a dephase under REDOR mixing (namely, the peaks with chemical shifts of 181.9 and 180.6 ppm) as they correspond to

carbonyl atoms that are relatively close to a nitrogen atom (3.5 Å), and thus participate in the protofilament interface. The other two peaks do not dephase, as presumed for carbonyl atoms facing the solvent (data not shown). The peaks corresponding to “buried” ends are expected to have higher intensities and integrated areas since there are, on average, more “buried” than “free” ends in the fibrils, however, since the distribution of the different fibril types in the sample is unknown, at this point we cannot provide quantitative analysis.

In order to complement the REDOR data, we also recorded a 2D ^{15}N - ^{13}C TEDOR correlation spectrum ($\tau_{\text{mix}} = 8.5$ ms) that qualitatively shows the same behavior (Figure 4.9c). However, the second dimension allows us to observe that the two major ^{13}C peaks are correlated to two different ^{15}N atoms with chemical shifts that are only 0.2 ppm apart. i.e. there are two slightly different protofilament interfaces. These chemically inequivalent nitrogen environments cannot be distinguished in the 1D spectrum in Figure 5.9b and fall under the intensity of the major ^{15}N peak in the spectrum but their presence is manifested in the relatively large line width of this peak (1 ppm or 50 Hz). Since the minor peak in the 1D spectrum presents similar line width (1.2 ppm or 60 Hz), it possibly contains the contributions of the two expected “free” ^{15}N labeled termini.

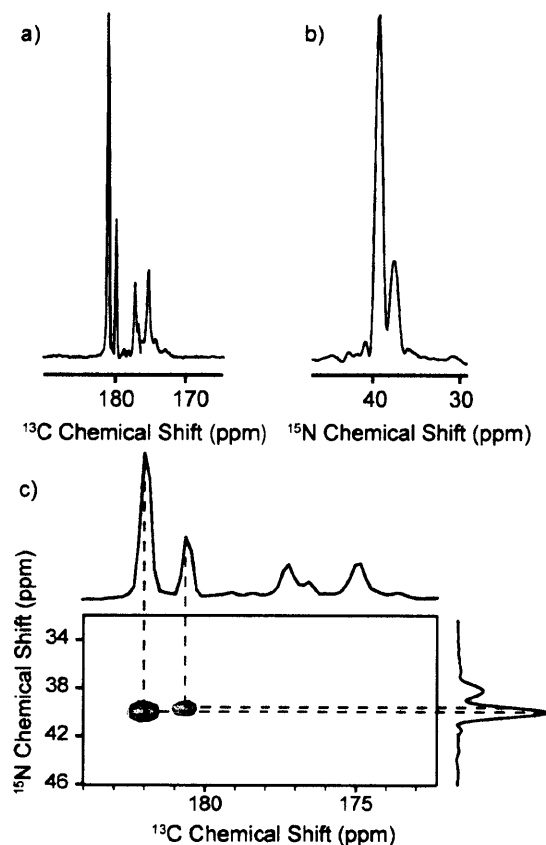


Figure 4.9. Degeneracy in TTR(105-115) fibril spectra: a) ^{13}C MAS CP and b) ^{15}N MAS CP spectra of a sample labeled with ^{15}N at the Y105 position and with ^{13}C at the carbonyl S115 position. c) TEDOR spectrum obtained with $\tau_{\text{mix}} = 8.5$ ms. The ^{13}C chemical shifts of the two cross-peaks match the chemical shifts of the two major peaks in the 1D spectrum, while the ^{15}N chemical shifts average of the cross-peaks matches the chemical shift of the major ^{15}N peak.

The chemical shifts of the peaks observed in the ^{13}C and ^{15}N spectra also merit some discussion. Both peaks in the ^{15}N spectra have upfield chemical shifts, consistent with terminal amino groups. The chemical shifts of the “buried” ^{13}C ends are also indicative of carboxylic groups at the end of the peptide, while the chemical shifts of the “free” ends are more upfield and therefore more similar to the chemical shifts of internal carbonyl carbons. Since their intensity is well above the natural abundance signals, they do arise from the only labeled S115 C' atom in the sample, and they must report on a different hydrogen bonding environment for the “free” ends in the fibrils. In principle, the “free” ends are exposed to the solvent water molecules, and their hydrogen bonding interactions, if any, might be more labile. The “buried” ends, on the other hand, form hydrogen bonds with each other, and these

hydrogen bonds must be stable enough to hold the protofilaments together on a much longer time scale.

The presence of multiple peaks for Y105 N and S115 C' is expected considering the structure of the TTR(105-115) fibrils presented above, however, peak doubling for the non-terminal residues as a result of the “odd-even-odd-even” interface is generally not observed in the spectra. How can we rationalize this apparent discrepancy?

Perhaps the most plausible and in some ways counterintuitive explanation is that these two environments are actually not that different from each other, particularly for the backbone atoms. The termini of the peptides are very sensitive reporters of the chemical environment, as slight differences in hydrogen bonding would result in relatively large changes in the chemical shifts. Even in the termini, however, these differences are only obvious for the carbonyl atom of the S115 residue. While we can detect the four different conformations for this residue, in the 1D spectrum of the N-terminus only the difference between the “free” and “buried” ends can be distinguished. The TEDOR experiment in Figure 4.9c is rather unusual since it correlates the two specifically labeled termini and the ^{13}C dimension has sufficient resolution to also resolve the chemical shift difference of 0.2 ppm in the ^{15}N dimension. In a typical one-bond TEDOR experiment with uniformly labeled residues (e.g. see Y105 N α correlation in Figure 4.10), where even the “free” and the “buried” ends have very similar C α chemical shifts, resolving the differences between the two β -sheet environments in the protofilament would be very challenging.

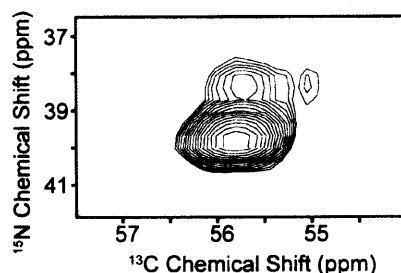


Figure 4.10. One-bond NCA correlation spectrum of a TTR(105-115) sample, uniformly ^{13}C , ^{15}N labeled at YTIAALLSPYS. Only the region corresponding to the N-terminal Y105N-C α cross-peaks is shown. At least two different conformations of the N-terminal residue are observed, with ^{15}N chemical shifts of 39.8 and 38.3 ppm. The spectrum was recorded with TEDOR mixing ($\tau_{\text{mix}} = 1.8$ ms).

The side-chain atoms of some residues might be more sensitive to their environment (dry steric zipper vs solvent) and this might explain the additional cross-peaks observed for Ile and Ser in the PDS spectrum in Figure 5.3. These cross-peaks, however, are rather weak and the difference in intensity between the major and minor form could be due to a higher degree of dynamics for the side-chains that are facing the solvent and not locked in a steric zipper. These dynamic processes could be interfering with the cross-polarization transfer or the decoupling used during the experiments, thus resulting in lower intensity for the corresponding cross-peaks. These peaks, however, could also appear as a result of conformational exchange and at this point we do not have enough evidence to distinguish between these possibilities.

4.2.5. Combining MAS NMR, cryoEM, AFM and STEM to obtain the full structure of the fibril

The MAS NMR experiments presented above detail the atomic resolution structure of the TTR(105-115) fibrils on a 1 – 7 Å length scale. The measured distances in this range provide structural constraints (summarized in Appendix I) that define the intra-sheet organization, the inter-sheet interface, and the protofilament-to-protofilament arrangement. However, the fibrils are also characterized by distances on longer length scales as observed by cryoEM and AFM.²⁴ The three different fibril classes detected by these methods have widths of 80 Å, 120 Å and 160 Å respectively, and thickness of ~ 40 Å. Each fibril is many nm long, with a helical twist along its length and a pitch of 995 Å, 818 Å, and 972 Å depending on the fibril class. Furthermore, scanning tunneling electron microscopy (STEM) measurements then reveal that each fibril class contains 8, 12 and 16 peptide molecules per cross-section, organized respectively in 4, 6 and 8 protofilaments as described above.²⁴

In addition to the longer length scales that cryoEM provides access to, this method also presents some important pieces of structural information inaccessible by MAS NMR. The electron density profile of the cross-sections of each fibril class reveals two layers of electron density, consistent with the presence of peptide molecules, sandwiching a layer that contains solvent molecules.²⁴ Each peptide layer is ~ 14 Å thick and therefore contains two peptide molecules (i.e. one protofilament), while the solvent layer in the middle spans ~ 11 Å. The thickness of the fibrils and the layers within each cross-section do not vary among the three fibril classes. At this point it is not clear whether the solvent layer in the middle consists of

water molecules, or acetonitrile molecules (see sample preparation), and MAS NMR experiments to resolve this issue are currently under way. Similar solvent gaps have been observed in the cryoEM electron density maps of other amyloid fibrils (e.g. PI3-SH3 fibrils),⁶² and the crystals of amyloidogenic peptides like GNNQQNY contain water channels of ~ 8 Å thickness,³⁷ thus implying that solvent molecules can have a very important structural role in mediating the stability of fibril structures.

In order to obtain the structure of the complete fibril for each class, the structure calculated with MAS NMR constraints was fit into the electron density profiles obtained with cryoEM (Figure 4.11). The correlation coefficients of the fit were 0.90, 0.93 and 0.95 for each class, respectively, demonstrating the remarkable agreement between the two methods.²⁴

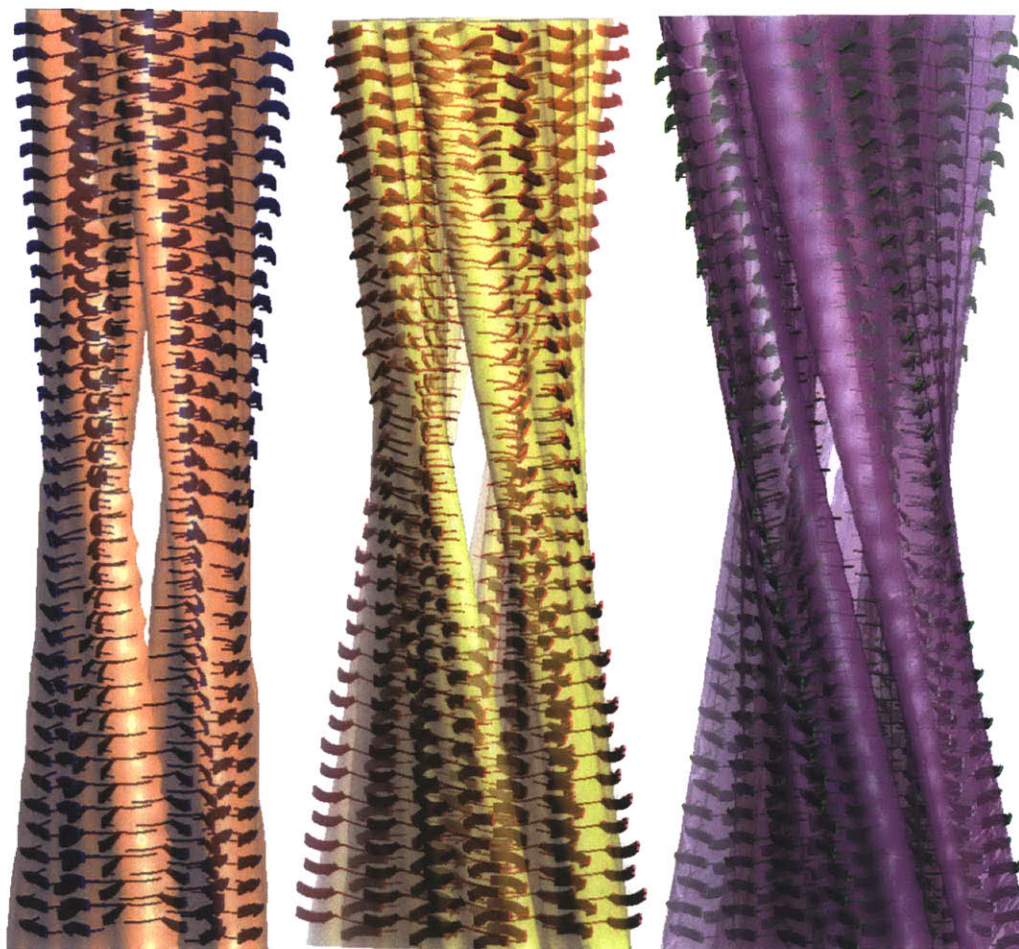


Figure 4.11. Atomic resolution structures of the three different TTR(105-115) fibril classes as determined by MAS NMR, cryoEM, AFM and STEM.

4.3. Conclusions

In summary, we have presented MAS NMR experiments and labeling schemes that have allowed us to characterize systematically the different levels of structural organization present in the amyloid fibril formed by the TTR(105-115) peptide segment. DNP-enhanced DQ-DRAWS and REDOR experiments performed at 400 MHz ^1H Larmor frequency with specifically labeled samples allowed us to obtain high-quality data regarding the β -strand and protofilament interactions in the fibrils in a fraction of the conventional experimental time. High-field, room temperature experiments performed at 500, 750 and 900 MHz ^1H Larmor frequency, on the other hand, were essential in assigning unambiguously and quantifying the long-range interactions that define the unusual “odd-even-odd-even” β -sheet interface in the fibrils. The high resolution presented by these experiments was also a key in identifying different conformations of the termini of the peptide, consistent with the proposed fibril structure. The differences in the chemical shifts for some of these conformations were very small and only detected under very special circumstances, implying that structural complexity can be hidden within the line-width of the peaks, even for fibril preparations that yield one major set of cross-peaks in the spectra.

The structure determination process described here was guided by information obtained by other methods, including cryo-EM, AFM, STEM and X-ray diffraction that probe length scales larger than those accessible by NMR. This allowed us to formulate and test different hypothesis and to ultimately observe interactions that make possible the remarkable stability of amyloid fibrils. The powerful combination of MAS NMR (with sensitivity enhancement provided from DNP) and such methods will in no doubt lead to great future advances in biochemistry and structural biology.

4.4. Methods

4.4.1. Sample Preparation

TTR(105-115) was synthesized using solid-phase methods and purified by HPLC (CS Bio, Menlo Park, CA and New England Peptide, Gardner, MA). The isotopically labeled amino acids for the synthesis were purchased from Cambridge Isotope Laboratories, Andover, MA. The following labeling schemes were used: uniformly ^{15}N , ^{13}C YTIAALLSPYS; uniformly ^{15}N , ^{13}C YTIAALLSPYS; and a sample labeled with ^{15}N at Y105, and ^{13}C at the S115

carbonyl position. Amyloid fibrils were prepared by dissolving ~ 15 mg peptide/mL in a 10% acetonitrile/H₂O solution, adjusted to pH 2.0 with HCl. The solution was incubated at 37 °C for 2 days, followed by 14 days at 25 °C. The mature fibrils were characterized by TEM, and centrifuged down at 320,000 × *g* for 2 hr. The resulting pellet was transferred either into a 4 mm zirconia rotor (20 mg fibrils, Varian-Agilent Technologies, Santa Clara, CA) or a 3.2 mm rotor (15 mg of fibrils, Bruker BioSpin, Billerica, MA).

4.4.2. DNP Experiments

The sample for the DNP experiments was prepared by washing the mature fibrils with a solution containing a 60/40% w/w glycerol-d₈/buffer matrix, where the buffer consisted of a 10/90% v/v acetonitrile/D₂O mixture with pD adjusted to 2.0 with HCl. This solution also contained 10 mM TOTAPOL.⁴³ The sample was pelleted at 320,000 × *g* for 2 hr, and packed into a 3.2 mm sapphire rotor (Bruker BioSpin, Billerica, MA). The DNP experiments were performed on a Bruker 263 GHz Solids DNP spectrometer, consisting of a 263 GHz continuous-wave gyrotron source, microwave transmission line, 3.2 mm low temperature MAS probe, gas cooling supply, and 400 MHz AVANCE III wide-bore NMR system.⁶³ The DNP-enhanced DQ-DRAWS and REDOR experiments were performed at 100 K, $\omega_r/2\pi = 6.5$ kHz and 3 s scan delay. 55.5 kHz ¹³C pulses and 40 kHz ¹⁵N pulsed were applied during the mixing periods of the experiments respectively. 100 kHz TPPM⁶⁴ ¹H decoupling was used during acquisition and REDOR, while 100 kHz continuous-wave ¹H decoupling was applied during the DQ-DRAWS mixing period. The DNP-enhanced DQ-DRAWS experiment was recorded with 128 scans per mixing time, 14 mixing times, and overall acquisition time of ~ 1.5 hr. The DNP-enhanced REDOR was recorded with 256 scans per mixing time, 12 mixing times and *S* and *S*₀ experiments were necessary. The overall time of this experiment was ~ 5 hr.

4.4.3. Room Temperature MAS NMR Experiments

2D PDS and PAIN-CP experiments were performed on a Bruker spectrometer operating at 900 MHz ¹H Larmor frequency, equipped with a triple-channel 3.2 mm E-free MAS probe (Bruker BioSpin, Billerica, MA). The sample used for these experiments was U-¹³C, ¹⁵N

labeled at 7 residues (YTIAALLSPYS). The PDSM experiments were performed at 11 kHz MAS, and 83 kHz TPPM decoupling during acquisition. 32 scans were recorded per t_1 point (892 t_1 points, 11.5 ms t_1 evolution and 24 ms t_2 evolution). The PAIN-CP experiments were performed at 20 kHz MAS, while matching ~ 50 kHz ^1H B_1 field, ~ 50 kHz ^{13}C B_1 field, and ~ 35 kHz ^{15}N B_1 field during mixing. 64 scans per t_1 point, and 192 t_1 points were recorded, with 9.6 ms t_1 evolution, 18.4 ms t_2 evolution, and a scan delay of 2.7 s. In these experiments, the center frequency was set to 40 ppm for ^{13}C , and 126 ppm for ^{15}N . ZF-TEDOR experiments were performed using the same sample on a custom-built spectrometer (courtesy of D. J. Ruben, Francis Bitter Magnet Laboratory, Massachusetts Institute of Technology, Cambridge, MA) operating at 750 MHz ^1H Larmor frequency, and utilizing a triple-channel 3.2 mm Bruker E-free MAS probe (Bruker BioSpin, Billerica, MA). 40 kHz ^{15}N pulses, 83 kHz ^{13}C pulses, and 91 kHz ^1H TPPM decoupling during mixing and acquisition were used in this case, while $\omega_r/2\pi = 12.5$ kHz. 128 scans per t_1 point, and 256 t_1 points were collected, with 10.2 ms t_1 acquisition, and 24 ms t_2 acquisition, and 2.7 s scan delay.

The experiments on the YTIAALLSPYS sample were performed on a custom-built 500 MHz spectrometer (courtesy of D. J. Ruben, Francis Bitter Magnet Laboratory, Massachusetts Institute of Technology, Cambridge, MA) equipped with a 4 mm triple channel Varian-Chemagnetix probe. ZF-TEDOR experiments were performed with 83 kHz ^1H TPPM decoupling, 83 kHz ^{13}C pulses and 50 kHz ^{15}N pulses during mixing. R2TRW experiments were performed as described in Ref. 42, with 25 ms mixing, 83 kHz TPPM decoupling, and a carrier frequency set at 65 ppm. The spinning frequency was set to 10.1 kHz.

The temperature of the cooling gas in each case was set to 2 °C, while we estimate that the actual sample temperature was 10 – 15 °C, depending on $\omega_r/2\pi$ and rf-induced heating. Spectra were processed and analyzed using the programs NMRPipe⁶⁵ and Sparky⁶⁶. Indirect external referencing to DSS was done based on adamantane ^{13}C chemical shifts.⁶⁷

4.4.4. Data Fitting

Distances were extracted from buildup curves (DQ-DRAWS, TEDOR) and dephasing curves (REDOR) using the SPINEVOLUTION simulation program.⁴² The DQ-DRAWS data was fit as described previously in Ref. 19, while a detailed description of the simulation of REDOR spectra with SPINEVOLUTION is given in Ref. 21. In all cases, the error in the

reported distances was based on the 95% confidence interval derived from the elements of the covariance matrix of the fit. TEDOR simulations were performed in the following way: The Ala108 spin system was approximated by a ^{15}N atom and two ^{13}C atoms, corresponding to $\text{C}\alpha$ and $\text{C}\beta$, with $J_{\text{C}\alpha\text{-C}\beta} = 20$ Hz also included in the simulation. For the simulation of longer distances, a second ^{15}N atom was included in the spin system, corresponding to Ile107N, Ser112N or P113N. In this case, the distance between Ala108C β and the distant ^{15}N , in addition to a relaxation parameter, were used as fit parameters in the simulation. The presence of the proximal ^{15}N (2.4 Å) was necessary in the simulation as it influences the long-distance TEDOR transfer dynamics quite significantly. The Ile107 spin system was approximated by a ^{15}N atom and four ^{13}C atoms (corresponding to $\text{C}\beta$, $\text{C}\gamma 2$, $\text{C}\gamma 1$, and $\text{C}\delta 1$). The J-coupling between $\text{C}\delta 1$ and $\text{C}\gamma 2$ was set to 20 Hz and was included in the simulation. Since there are no ^{15}N atoms within 4 Å from Ile107 $\text{C}\delta 1$, only one ^{15}N atom was sufficient to describe the TEDOR transfer when fitting the I107N – $\text{C}\delta 1$ and S112N-I107C $\delta 1$ distances.

References

- (1) Chiti, F.; Dobson, C. M. *Annu. Rev. Biochem.* **2006**, *75*, 333-366.
- (2) Fowler, D. M.; Koulov, A. V.; Balch, W. E.; Kelly, J. W. *TRENDS Biochem. Sci.* **2007**, *32*, 217-224.
- (3) Dobson, C. M. *Nature* **2003**, *426*, 884-890.
- (4) Nilsson, M. R. *Methods* **2004**, *34*, 151-160.
- (5) Sunde, M.; Serpell, L. C.; Bartlam, M.; Fraser, P. E.; Pepys, M. B.; Blake, C. C. F. *J. Mol. Biol.* **1997**, *273*, 729-739.
- (6) Petkova, A. T.; Yau, W. M.; Tycko, R. *Biochemistry* **2006**, *45*, 498-512.
- (7) Paravastu, A. K.; Leapman, R. D.; Yau, W. M.; Tycko, R. *Proc. Natl. Acad. Sci. U. S. A.* **2008**, *105*, 18349-18354.
- (8) Wasmer, C.; Lange, A.; Van Melckebeke, H.; Siemer, A. B.; Riek, R.; Meier, B. H. *Science* **2008**, *319*, 1523-1526.
- (9) Heise, H.; Hoyer, W.; Becker, S.; Andronesi, O. C.; Riedel, D.; Baldus, M. *Proc. Natl. Acad. Sci. U.S.A.* **2005**, *102*, 15871-15876.

- (10) Vilar, M.; Chou, H. T.; Luhrs, T.; Maji, S. K.; Riek-Loher, D.; Verel, R.; Manning, G.; Stahlberg, H.; Riek, R. *Proc. Natl. Acad. Sci. U.S.A.* **2008**, *105*, 8637-8642.
- (11) Debelouchina, G. T.; Platt, G. W.; Bayro, M. J.; Radford, S. E.; Griffin, R. G. *J. Am. Chem. Soc.* **2010**, *132*, 10414-10423.
- (12) Debelouchina, G. T.; Platt, G. W.; Bayro, M. J.; Radford, S. E.; Griffin, R. G. *J. Am. Chem. Soc.* **2010**, *132*, 17077-17079.
- (13) Bayro, M. J.; Debelouchina, G. T.; Eddy, M. T.; Birkett, N. R.; MacPhee, C. E.; Rosay, M.; Maas, W. E.; Dobson, C. M.; Griffin, R. G. **2011**.
- (14) Bayro, M. J.; Maly, T.; Birkett, N. R.; MacPhee, C. E.; Dobson, C. M.; Griffin, R. G. *Biochemistry* **2010**, *49*, 7474-7484.
- (15) Helmus, J. J.; Surewicz, K.; Nadaud, P. S.; Surewicz, W. K.; Jaroniec, C. P. *Proc. Natl. Acad. Sci. U.S.A.* **2008**, *105*, 6284-6289.
- (16) Blake, C. C. F.; Geisow, M. J.; Oatley, S. J.; Rerat, B.; Rerat, C. *J. Mol. Biol.* **1978**, *121*, 339-356.
- (17) Gustavsson, A.; Engstrom, U.; Westermark, P. *Biochem. Biophys. Res. Commun.* **1991**, *175*, 1159-1164.
- (18) Jaroniec, C. P.; MacPhee, C. E.; Astrof, N. S.; Dobson, C. M.; Griffin, R. G. *Proc. Natl. Acad. Sci. U.S.A.* **2002**, *99*, 16748-16753.
- (19) Jaroniec, C. P.; MacPhee, C. E.; Bajaj, V. S.; McMahon, M. T.; Dobson, C. M.; Griffin, R. G. *Proc. Natl. Acad. Sci. U.S.A.* **2004**, *101*, 711-716.
- (20) Hong, M.; Gross, J. D.; Griffin, R. G. *J. Phys. Chem. B* **1997**, *101*, 5869-5874.
- (21) Costa, P. R.; Gross, J. D.; Hong, M.; Griffin, R. G. *Chem. Phys. Lett.* **1997**, *280*, 95-103.
- (22) Feng, X.; Eden, M.; Brinkmann, A.; Luthman, H.; Eriksson, L.; Graslund, A.; Antzutkin, O. N.; Levitt, M. H. *J. Am. Chem. Soc.* **1997**, *119*, 12006-12007.
- (23) Rienstra, C. M.; Hohwy, M.; Mueller, L. J.; Jaroniec, C. P.; Reif, B.; Griffin, R. G. *J. Am. Chem. Soc.* **2002**, *124*, 11908-11922.
- (24) Fitzpatrick, A. et al., in preparation.
- (25) Becerra, L. R.; Gerfen, G. J.; Temkin, R. J.; Singel, D. J.; Griffin, R. G. *Phys. Rev. Lett.* **1993**, *71*, 3561-3564.
- (26) Hall, D. A.; Maus, D. C.; Gerfen, G. J.; Inati, S. J.; Becerra, L. R.; Dahlquist, F. W.; Griffin, R. G. *Science* **1997**, *276*, 930-932.

- (27) Maly, T.; Debelouchina, G. T.; Bajaj, V. S.; Hu, K.-N.; Joo, C.-G.; Mak-Jurkauskas, M. L.; Sirigiri, J. R.; van der Wel, P. C. A.; Herzfeld, J.; Temkin, R. J.; Griffin, R. G. *J. Chem. Phys.* **2008**, *128*, 052211.
- (28) Goldman, M. *Spin temperature and nuclear magnetic resonance in solids*; Clarendon Press: Oxford, 1970.
- (29) van der Wel, P. C. A.; Hu, K. N.; Lewandowski, J.; Griffin, R. G. *J. Am. Chem. Soc.* **2006**, *128*, 10840.
- (30) Mak-Jurkauskas, M. L.; Bajaj, V. S.; Hornstein, M. K.; Belenky, M.; Griffin, R. G.; Herzfeld, J. *Proc. Natl. Acad. Sci. U. S. A.* **2008**, *105*, 883.
- (31) Debelouchina, G. T.; Bayro, M. J.; van der Wel, P. C. A.; Caporini, M. A.; Barnes, A. B.; Rosay, M.; Maas, W. E.; Griffin, R. G. *Phys. Chem. Chem. Phys.* **2010**, *12*, 5911-5919.
- (32) Petkova, A. T.; Ishii, Y.; Balbach, J. J.; Antzutkin, O. N.; Leapman, R. D.; Delaglio, F.; Tycko, R. *Proc. Natl. Acad. Sci. U.S.A.* **2002**, *99*, 16742-16747.
- (33) Luca, S.; Yau, W. M.; Leapman, R.; Tycko, R. *Biochemistry* **2007**, *46*, 13505-13522.
- (34) Iwata, K.; Fujiwara, T.; Matsuki, Y.; Akutsu, H.; Takahashi, S.; Naiki, H.; Goto, Y. *Proc. Natl. Acad. Sci. U.S.A.* **2006**, *103*, 18119-18124.
- (35) Sawaya, M. R.; Sambashivan, S.; Nelson, R.; Ivanova, M. I.; Sievers, S. A.; Apostol, M. I.; Thompson, M. J.; Balbirnie, M.; Wiltzius, J. J. W.; McFarlane, H. T.; Madsen, A. O.; Riek, C.; Eisenberg, D. *Nature* **2007**, *447*, 453.
- (36) Van Melckebeke, H.; Wasmer, C.; Lange, A.; Eiso, A. B.; Loquet, A.; Bockmann, A.; Meier, B. H. *J. Am. Chem. Soc.* **2010**, *132*, 13765-13775.
- (37) Nelson, R.; Sawaya, M. R.; Balbirnie, M.; Madsen, A. O.; Riek, C.; Grothe, R.; Eisenberg, D. *Nature* **2005**, *435*, 773.
- (38) Tycko, R. *J. Chem. Phys.* **2007**, *126*, 9.
- (39) Benzinger, T. L. S.; Gregory, D. M.; Burkoth, T. S.; Miller-Auer, H.; Lynn, D. G.; Botto, R. E.; Meredith, S. C. *Proc. Natl. Acad. Sci. U.S.A.* **1998**, *95*, 13407-13412.
- (40) Karlsson, T.; Popham, J. M.; Long, J. R.; Oyler, N.; Drobny, G. P. *J. Am. Chem. Soc.* **2003**, *125*, 7394-7407.
- (41) Caporini, M. A.; Bajaj, V. S.; Veshtort, M.; Fitzpatrick, A.; MacPhee, C. E.; Vendruscolo, M.; Dobson, C. M.; Griffin, R. G. *J. Phys. Chem. B* **2010**, *114*, 13555-13561.

- (42) Veshtort, M.; Griffin, R. G. *J. Magn. Reson.* **2006**, *178*, 248-282.
- (43) Song, C.; Hu, K. N.; Joo, C. G.; Swager, T. M.; Griffin, R. G. *J. Am. Chem. Soc.* **2006**, *128*, 11385.
- (44) Bajaj, V. S.; Mak-Jurkauskas, M. L.; Belenky, M.; Herzfeld, J.; Griffin, R. G. *Proc. Natl. Acad. Sci. U. S. A.* **2009**, *106*, 9244.
- (45) Goncalves, J. A.; Ahuja, S.; Erfani, S.; Eilers, M.; Smith, S. O. *Prog. Nucl. Magn. Reson. Spectrosc.* **2010**, *57*, 159-180.
- (46) Jaroniec, C. P.; Filip, C.; Griffin, R. G. *J. Am. Chem. Soc.* **2002**, *124*, 10728-10742.
- (47) van der Wel, P. C. A.; Lewandowski, J. R.; Griffin, R. G. *J. Am. Chem. Soc.* **2007**, 5117-5130.
- (48) van der Wel, P. C. A.; Lewandoswki, J.; Griffin, R. G. *Biochemistry* **2010**, submitted.
- (49) Nielsen, J. T.; Bjerring, M.; Jeppesen, M. D.; Pedersen, R. O.; Pedersen, J. M.; Hein, K. L.; Vosegaard, T.; Skrydstrup, T.; Otzen, D. E.; Nielsen, N. C. *Angew. Chem.-Int. Edit.* **2009**, *48*, 2118-2121.
- (50) Szeverenyi, N. M.; Sullivan, M. J.; Maciel, G. E. *J. Magn. Reson.* **1982**, *47*, 462-475.
- (51) Lewandowski, J. R.; De Paepe, G.; Griffin, R. G. *J. Am. Chem. Soc.* **2007**, *129*, 728-729.
- (52) De Paepe, G.; Lewandowski, J. R.; Loquet, A.; Eddy, M.; Megy, S.; Bockmann, A.; Griffin, R. G. *J. Chem. Phys.* **2011**, *134*.
- (53) Nieuwkoop, A. J.; Wylie, B. J.; Franks, W. T.; Shah, G. J.; Rienstra, C. M. *J. Chem. Phys.* **2009**, *131*, 8.
- (54) Bayro, M. J.; Huber, M.; Ramachandran, R.; Davenport, T. C.; Meier, B. H.; Ernst, M.; Griffin, R. G. *J. Chem. Phys.* **2009**, *130*.
- (55) De Paepe, G.; Lewandowski, J. R.; Loquet, A.; Bockmann, A.; Griffin, R. G. *J. Chem. Phys.* **2008**, *129*.
- (56) Ladizhansky, V.; Griffin, R. G. *J. Am. Chem. Soc.* **2004**, *126*, 948-958.
- (57) Pines, A.; Gibby, M. G.; Waugh, J. S. *J. Chem. Phys.* **1972**, *56*, 1776.
- (58) Baldus, M.; Petkova, A. T.; Herzfeld, J.; Griffin, R. G. *Mol. Phys.* **1998**, *95*, 1197-1207.
- (59) Sen, A.; Baxa, U.; Simon, M. N.; Wall, J. S.; Sabate, R.; Saupe, S. J.; Steven, A. C. *J. Biol. Chem.* **2007**, *282*, 5545-5550.
- (60) Mizuno, N.; Baxa, U.; Steven, A. C. *Proc. Natl. Acad. Sci. U. S. A.* **2011**, *108*, 3252-3257.

- (61) White, H. E.; Hodgkinson, J. L.; Jahn, T. R.; Cohen-Krausz, S.; Gosal, W. S.; Muller, S.; Orlova, E. V.; Radford, S. E.; Saibil, H. R. *J. Mol. Biol.* **2009**, *389*, 48-57.
- (62) Jimenez, J. L.; Guijarro, J. L.; Orlova, E.; Zurdo, J.; Dobson, C. M.; Sunde, M.; Saibil, H. R. *Embo Journal* **1999**, *18*, 815-821.
- (63) Rosay, M.; Tometich, L.; Pawsey, S.; Bader, R.; Schauwecker, R.; Blank, M.; Borchard, P. M.; Cauffman, S. R.; Felch, K. L.; Weber, R. T.; Temkin, R. J.; Griffin, R. G.; Maas, W. E. *Phys. Chem. Chem. Phys.* **2010**, *12*, 5850-5860.
- (64) Bennett, A. E.; Rienstra, C. M.; Auger, M.; Lakshmi, K. V.; Griffin, R. G. *J. Chem. Phys.* **1995**, *103*, 6951-6958.
- (65) Delaglio, F.; Grzesiek, S.; Vuister, G. W.; Zhu, G.; Pfeifer, J.; Bax, A. *J. Biomol. NMR* **1995**, *6*, 277-293.
- (66) Goddard, T. D.; Kneller, D. G. *University of California, San Francisco*.
- (67) Morcombe, C. R.; Zilm, K. W. *J. Magn. Reson.* **2003**, *162*, 479-486.

Appendix I

Summary of the structural constraints obtained by MAS NMR for TTR(105-115) amyloid fibrils.

Table A1. Intra-sheet NMR restraints

Residue-Atom	Residue-Atom	Distance (Å)	Method
I107-CO	I107-CO	4.46 +/- 0.12	DQF-DRAWS
A108-CO	A108-CO	4.52 +/- 0.16	DQF-DRAWS
A109-CO	A109-CO	4.41 +/- 0.10	DQF-DRAWS
L110-CO	L110-CO	4.31 +/- 0.22	DQF-DRAWS
L111-CO	L111-CO	4.52 +/- 0.10	DQF-DRAWS
S112-CO	S112-CO	4.45 +/- 0.06	DQF-DRAWS
P113-CO	P113-CO	4.47 +/- 0.08	DQF-DRAWS
S115-CO	S115-CO	4.29 +/- 0.05	DQF-DRAWS
A109-N	A108-CO	4.40 +/- 0.20	REDOR

Table A2. Inter-sheet NMR restraints

Residue-Atom	Residue-Atom	Distance (Å)	Method
I107-CD1	S112-N	5.8 +/- 0.5	TEDOR
A108-CB	S112-N	5.6 +/- 0.5	TEDOR
A108-CB	P113-N	6.0 +/- 0.5	TEDOR
A109-N	L111-CD1	4.43 +/- 0.5	TEDOR
A109-N	L111-CD2	4.63 +/- 0.5	TEDOR
A108-CO	L111-CD1	4.775 +/- 0.475	R2TR
A108-CO	L111-CD2	4.775 +/- 0.475	R2TR
I107-N	P113-CB	> 6.0	PAIN-CP
I107-CD1	S112-N	5.8 +/- 0.5	PAIN-CP
A108-CB	S112-N	5.6 +/- 0.5	PAIN-CP
A108-CB	P113-N	6.0 +/- 0.5	PAIN-CP
T106-CA	P113-CB	2.5-6.5	PDSD
I107-CA	P113-CA	2.5-6.5	PDSD
I107-CA	P113-CB	2.5-6.5	PDSD
I107-CB	P113-CB	2.5-4.5	PDSD
I107-CB	P113-CD	2.5-6.5	PDSD
I107-CD	S112-CA	2.5-4.5	PDSD
I107-CD	S112-CB	2.5-4.5	PDSD
I107-CD	P113-CB	2.5-6.5	PDSD
I107-CG2	S112-CA	2.5-6.5	PDSD
I107-CG2	S112-CB	2.5-6.5	PDSD
I107-CG2	P113-CA	2.5-8.5	PDSD
I107-CG2	P113-CB	2.5-6.5	PDSD
A108-CB	S112-CA	2.5-6.5	PDSD
A108-CB	P113-CA	2.5-4.5	PDSD
A108-CB	P113-CB	2.5-4.5	PDSD
A108-CB	P113-CG	2.5-4.5	PDSD

Chapter 5. Secondary Structure Analysis of β_2 -Microglobulin Amyloid Fibrils Formed at pH 2.5

Adapted and updated from "Magic Angle Spinning NMR Analysis of β_2 -Microglobulin Fibrils in Two Distinct Morphologies" by Debelouchina GT, Platt GW, Bayro MJ, Radford SE, Griffin RG, published in J. Am. Chem. Soc. 2010, 132, 10414-10423.

Summary

β_2 -Microglobulin (β_2m) is the major structural component of amyloid fibrils deposited in a condition known as dialysis-related amyloidosis. Despite numerous studies that have elucidated important aspects of the fibril formation process *in vitro*, and a magic angle spinning (MAS) NMR study of the fibrils formed by a small peptide fragment, structural details of β_2m fibrils formed by the full-length 99-residue protein are largely unknown. Here, we present a site-specific MAS NMR analysis of long, straight (LS) fibrils formed by the full-length β_2m protein at pH 2.5. High-resolution MAS NMR spectra have allowed us to obtain ^{13}C and ^{15}N resonance assignments for 69 residues of β_2m in LS fibrils, including part of the highly mobile N-terminus. Approximately 25 residues did not yield observable signals. Chemical shift analysis of the sequentially assigned residues indicates that these fibrils contain an extensive β -sheet core organized in a non-native manner, with a *trans*-P32 conformation.

5.1. Introduction

More than twenty-five different proteins are known to form amyloid fibrils that are observed to accumulate in a range of human and animal diseases.¹ Additionally, proteins and peptides that are not involved in disease states can be induced to form amyloid-like fibrils *in vitro*, indicating that formation of these ordered aggregates is potentially a generic attribute of all protein sequences.² These fibrils share common morphological features in that they are long, straight and unbranched, and are formed from multiple protofilaments arranged with a twisted organisation.³ Higher resolution analyses reveal that the fibrils consist of a cross- β architecture, which involves the formation of β -strands oriented perpendicular to the fibril long axis and imparts the characteristic tinctorial properties of all amyloid fibrils, specifically that they bind small fluorescent molecules such as thioflavin-T and Congo Red.⁴⁻⁶ X-ray crystallography has provided insight into the cross- β structural arrangement of crystals formed by short amyloidogenic peptides where the sidechains pack in a tight, self-complementing manner referred to as a “steric zipper”.⁷ Magic angle spinning (MAS) NMR studies on these and other systems have shown, however, that amyloid structures can be much more complex⁸ and that other structural arrangements such as the β -solenoid are also possible.⁹ Indeed, structural models primarily based on MAS NMR data have emerged for a number of different systems including A β (1-40),¹⁰ a 22-residue segment of β_2 -microglobulin,¹¹ amylin,¹² α -synuclein,^{13,14} HET-s(218-289),⁹ etc., and have provided valuable information regarding the common principles and interactions that govern fibril architecture. Our understanding of the structural molecular process of amyloid formation is, however, far from complete and improved knowledge in this area will not only enable design of therapeutic strategies against protein aggregation diseases,¹⁵ but it will also allow for the useful biotechnological properties of protein aggregation to be harnessed.¹⁶

The protein β_2 -microglobulin (β_2m), is the major structural component of amyloid fibrils associated with dialysis-related amyloidosis.¹⁷ The protein is 99 residues in length (with an additional N-terminal Met0 in the recombinant protein), that folds natively into a β -sandwich conformation, where a disulphide bond between C25 and C80 covalently links the sheets.¹⁸ A number of studies have described the formation of amyloid-like fibrils from full-length β_2m *in vitro* under a range of conditions, including the addition of co-solvents and metal ions.¹⁹

Canonical long-straight (LS) amyloid-like fibrils ($\sim 1 \mu\text{m}$ long) have been observed to form *in vitro* from oxidized $\beta_2\text{m}$ under aqueous conditions at both pH 7,^{19,20} where the native globular state is initially populated, and under acidic conditions (pH < 3), where the $\beta_2\text{m}$ polypeptide initially adopts a highly dynamic acid-unfolded state.²¹⁻²³ The presence of an intact disulphide bond is a necessity for formation of these fibrils that, in common with amyloid formed from many different proteins, grow with lag-dependent kinetics, consistent with a nucleated assembly mechanism.

Here, we describe the initial MAS NMR analysis of LS amyloid-like fibrils prepared *in vitro* from the full-length sequence of $\beta_2\text{m}$ and discuss preliminary chemical shift assignments of the $\beta_2\text{m}$ sequence. Our data shed light on the regions of the protein sequence involved in the rigid core of the fibrils and the secondary structure present in these segments when arranged in the fibrillar state.

5.2. Resonance assignment of LS $\beta_2\text{m}$ fibrils

In order to assign sequentially the resonances in the long straight (LS) $\beta_2\text{m}$ fibrils formed at pH 2.5 and low ionic strength we relied on a set of ^{13}C - ^{13}C and ^{15}N - ^{13}C correlation spectra recorded with three differently labeled samples: uniformly ^{13}C , ^{15}N labeled $\beta_2\text{m}$ fibrils (U- $\beta_2\text{m}$), and two samples prepared by growing bacteria in media containing [2- ^{13}C]-glycerol (2- $\beta_2\text{m}$) or [1,3- ^{13}C]-glycerol (1,3- $\beta_2\text{m}$) as the ^{13}C source.³¹⁻³³ Figure 5.1 shows a typical ^{13}C - ^{13}C correlation spectrum of U- $\beta_2\text{m}$ recorded with radio frequency-driven recoupling³⁴⁻³⁶ (RFDR) employing a mixing period $\tau_{\text{mix}} = 1.76$ ms. The resolution of this spectrum (natural line width ~ 0.5 ppm) is comparable to that observed in other amyloid fibril samples previously investigated by MAS NMR, including fibrils formed by TTR(105-115),³⁷ HET-s(218-289),⁹ and PI3-SH3.³⁸ In this spectrum, primarily one-bond correlations are observed, potentially allowing the identification of different spin systems. For example, three Ile residues, one Ala, five Thr, and six Ser residues can be easily identified due to their characteristic chemical shifts.

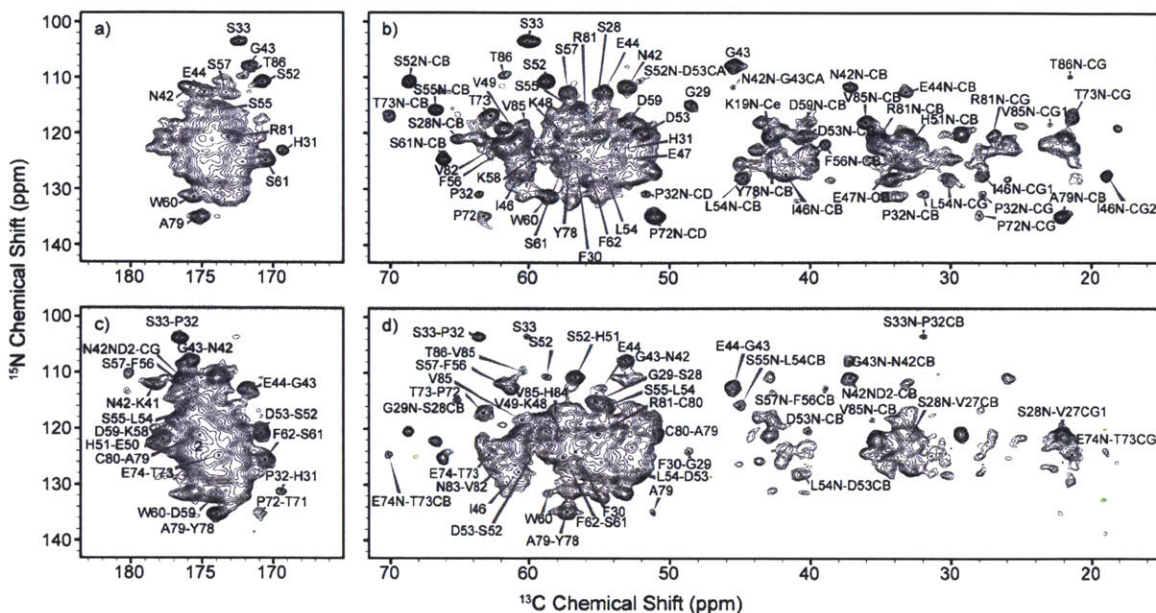


Figure 5.2. a) and b) NCACX and c) and d) NCOX experiments obtained at 700 MHz, $\omega_r/2\pi = 12.5$ kHz with a U- β_2 m fibril sample. 3 ms DCP was employed for ^{15}N - ^{13}C transfer, and RFDR mixing was used for ^{13}C - ^{13}C transfer ($\tau_{\text{mix}} = 3.8$ ms). The labels correspond to a) N-CO, b) N-C α , c) N $_i$ -CO $_{i-1}$, d) N $_i$ -C α_{i-1} and N-C α correlations unless otherwise noted.

The reduced number of labeled spins in these samples further improves the resolution and simplifies the analysis of spectra like the ^{15}N - ^{13}C correlations presented in Figure 5.3. These spectra were recorded using heteronuclear dipolar recoupling *via* TEDOR^{40,41} with $\tau_{\text{mix}} = 1.6$ ms, which is optimal for one-bond polarization transfer, i.e., N $_i$ -CO $_{i-1}$ and N $_i$ -C α_i . The improved line width allows the observation of certain cross-peaks that do not appear or are very weak in spectra recorded with uniformly labeled samples. For example, only two Gly residues are observed in U- β_2 m spectra, while the NCA spectrum of 2- β_2 m contains the three expected Gly cross-peaks. These one-bond ^{15}N - ^{13}C correlations were complemented with medium range TEDOR experiments recorded with the 2- β_2 m and 1,3- β_2 m samples to acquire N $_i$ -C α_{i-1} , N $_i$ -CO $_i$, and N $_i$ -C β_i correlations (Figure 5.4), while medium and long-range ^{13}C - ^{13}C experiments (data not shown) were used to obtain C α_i -C $\alpha_{i\pm 1}$, CO $_i$ -C β_i , CO $_i$ -C γ_i , C α_i -C γ_i , etc, correlations and to complete the sequential assignment of the resonances in LS β_2 m fibrils. A detailed description of our resonance assignment strategy, with particular emphasis on samples prepared with [2- ^{13}C] glycerol, will be given elsewhere.

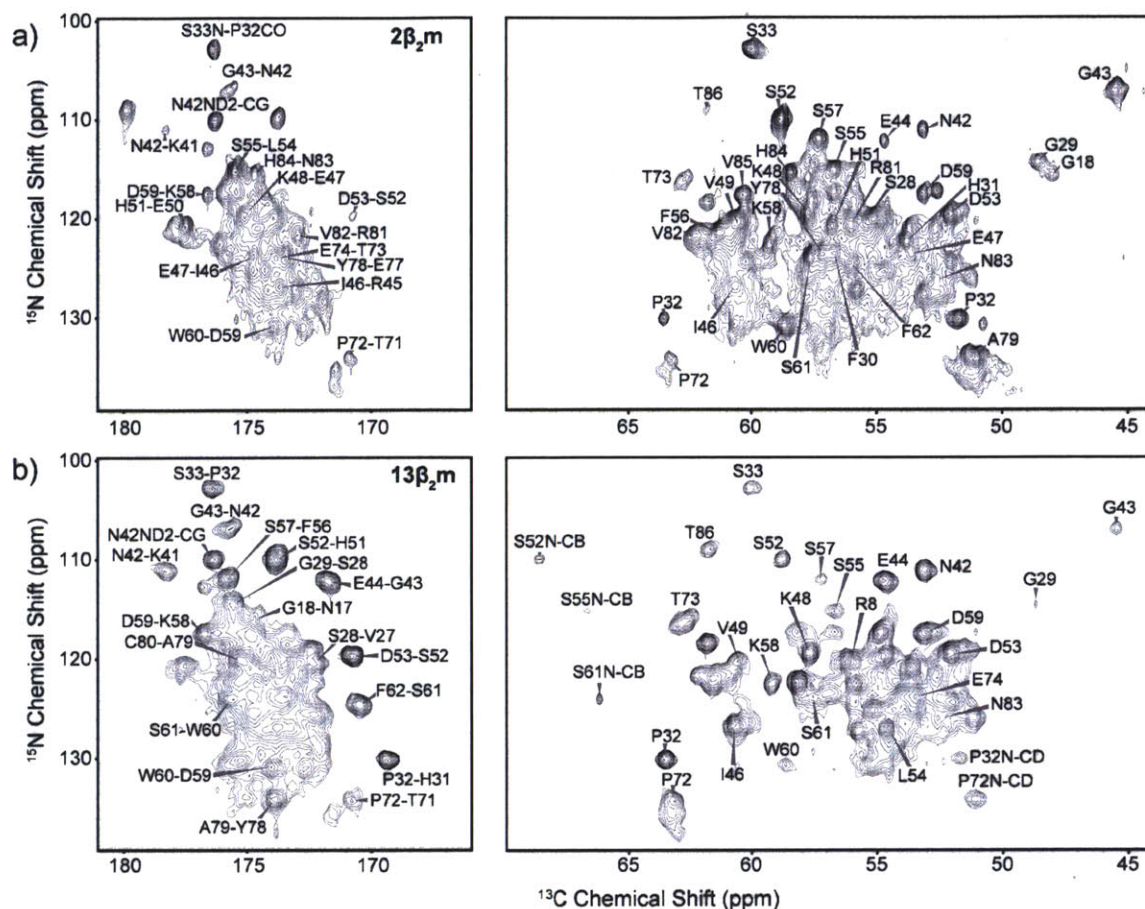


Figure 5.3. ^{15}N - ^{13}C correlation spectra of a) $2\beta_2\text{m}$ LS fibrils, obtained at 700 MHz, $\omega_r/2\pi = 10.0$ kHz, and b) $1,3\beta_2\text{m}$ LS fibrils, obtained at 750 MHz, $\omega_r/2\pi = 12.5$ kHz. Dipolar recoupling was achieved with ZF-TEDOR and $\tau_{\text{mix}} = 1.6$ ms. Unless otherwise noted, the labels refer to $\text{N}_i\text{-CO}_{i-1}$ correlations (left panels) and $\text{N}_i\text{-C}\alpha_i$ correlations (right panels).

originating from either of these three causes or a combination of them, has been observed in multiple amyloid fibril systems including A β ,⁴⁵ α -synuclein,¹³ Het-s(218-289),⁴⁶ and the Y145Stop variant of the human prion protein.^{47,48}

5.3. Dynamics of the N-terminus of LS β_2m fibrils

To investigate the origins of the molecular disorder in the LS fibrils, we performed a MAS INEPT-TOBSY ^{13}C - ^{13}C correlation experiment⁴⁹ and the spectra are presented in Figure 5.6. The INEPT step, commonly used in solution NMR experiments, is efficient only for highly mobile sites when applied to solid samples. These sites usually have vastly attenuated dipolar couplings that do not interfere with the J-coupling mediated polarization transfer during INEPT. The TOBSY (total through-bond correlation spectroscopy) mixing period relies only on the isotropic J-coupling to transfer polarization between the nearby ^{13}C spins. In the LS fibrils, six mobile spin systems can be identified, three of which include the backbone CO atoms. The chemical shifts of these spin systems are consistent with the random coil chemical shift values of Met, Ile, Gln, Arg, Thr and Lys, and, therefore, most likely arise from the first few N-terminal residues (MIQRTPK) of β_2m . The observed flexibility of the N-terminus is consistent with previous studies that indicate a high degree of solvent exposure for the first 20 residues.^{26,50} Consistent with this, dipolar correlation ^{13}C - ^{13}C spectra of a β_2m fibrillar sample that has been partially digested by pepsin, a process that is known to specifically cleave the N-terminal nine residues,^{26,51} have the same number of cross-peaks as the ^{13}C - ^{13}C spectra of undigested fibrils (data not shown). This observation confirms that the N-terminal residues have attenuated effective dipolar couplings and are not expected to appear in experiments based on dipolar mixing.

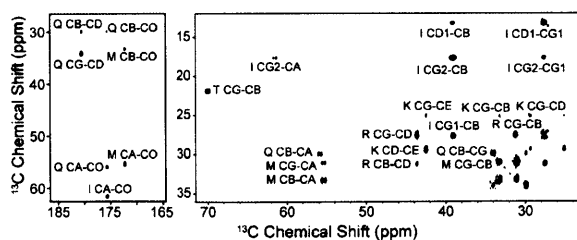


Figure 5.6. ^{13}C - ^{13}C INEPT-TOBSY spectrum obtained at 750 MHz and $\omega_r/2\pi = 16.7$ kHz with a U- β_2m LS fibril sample ($\tau_{mix} = 5.77$ ms).

The dipolar and through-bond correlation experiments have allowed us to obtain spin system assignments for 69 of the 100 residues in LS β_2 m fibrils. This includes 57 sequential assignments from dipolar spectra, 6 additional spin systems that are identified in dipolar spectra but not unambiguously assigned, and 6 mobile residues at the N-terminus. The sequentially assigned regions span residues 17-19, 26-34, 39-65, 70-86 that define the majority of the rigid fibril core. We estimate that the dipolar spectra contain additional cross-peaks consistent with the presence of approximately 5 more residues, which means that approximately 25 residues are not observed in any spectra. For example, while A78 gives well-resolved cross-peaks with sufficient intensity in all spectra, the other alanine residue, A15, is prominently missing. No residues have yet been identified in the region between I7 and E16, and in the C-terminus (L87-M99). No doubling of resonances has been observed, pointing towards the absence of polymorphism or heterogeneity in the case of these LS fibrils.

5.4. Chemical shift analysis of LS β_2 m fibrils

The chemical shifts of 51 of the 57 sequentially assigned residues were analyzed with the TALOS program⁵² and the Chemical Shift Index⁵³ (CSI) (Figure 5.7). TALOS provides predictions of the likely ϕ and ψ angles, while CSI gives an estimate of the secondary structure tendency based on the deviations of the chemical shifts from their random coil values. Six residues yielded no results due to incomplete assignments, and are excluded from Figure 5.7. Based on the predicted ϕ and ψ angles, and the chemical shifts of the C α and C β atoms, four major β -strand regions can be identified amongst the assigned regions of the sequence, namely residues 26-31, 44-55, 60-65 and 78-85 (Figure 5.8).

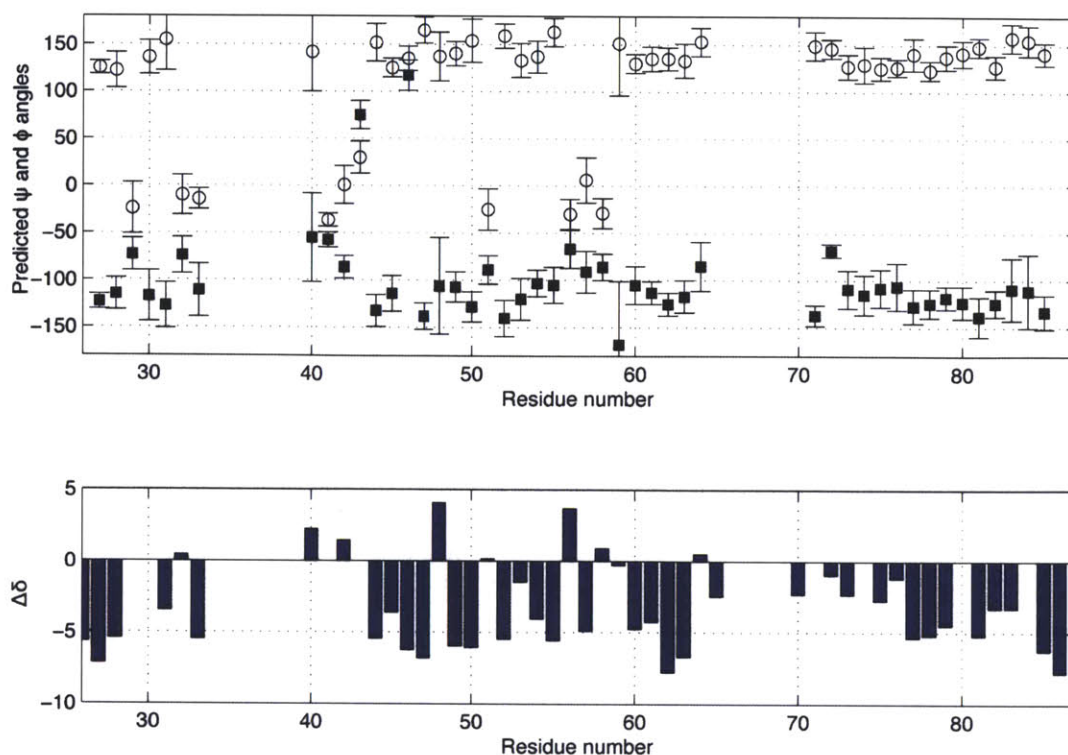


Figure 5.7. The Ψ and ϕ angles predicted by TALOS+ (top), and chemical shift analysis of the assigned $C\alpha$ and $C\beta$ atoms (bottom).

Analysis of the $C\beta$ and $C\gamma$ chemical shifts of the two assigned proline residues, P32 ($\Delta C\beta C\gamma = 4.3$ ppm) and P72 ($\Delta C\beta C\gamma = 5.1$ ppm), indicates that both residues are likely to adopt the more common *trans*-conformation in the fibril form.^{58,59} This is in contrast to the native state of β_2m , where the H31-P32 bond is *cis*.^{56,57} Although the exact conformation of the two proline residues can be determined only after the measurement of multiple distance constraints, the chemical shift data are consistent with biochemical experiments which indicate the presence of a *trans*-P32 folding intermediate on the fibril formation pathway at neutral pH,^{60,61} while P32 is also likely to be predominantly in the *trans* form in the unfolded ensemble from which fibril formation is initiated at pH 2.5.

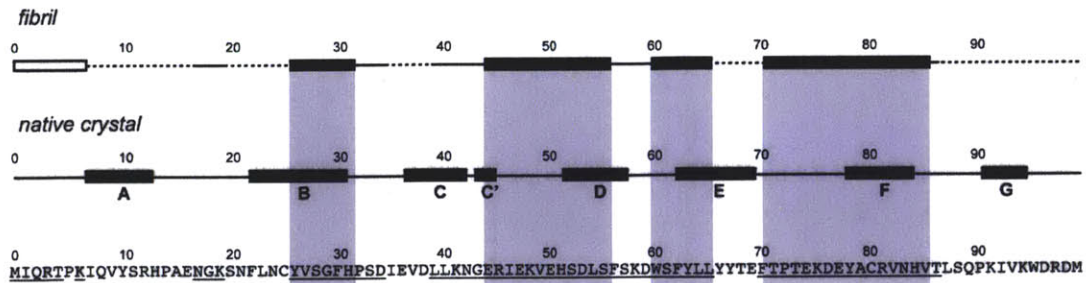


Figure 5.8. Secondary structure comparison of β_2m fibrils and native crystals (Trinh et al., Iwata et al.).

5.5. The majority of residues are involved in the rigid core structure of LS β_2m fibrils

The MAS NMR assignments presented above describe the first such information obtained for LS amyloid-like fibrils formed from full-length oxidized β_2m . Although an MAS NMR study has been performed previously on amyloid-like fibrils formed from a short peptide fragment of β_2m (residues 20-41),¹¹ these fibrils do not form the disulphide bond between C25 and C80 known to be vital for amyloid formation of the intact protein, and lack the remainder of the sequence that is intimately involved in the fibril structure as shown by EPR, HX and proteolysis.^{26,30,50} Furthermore, the 60-70 residue region has been shown by mutagenesis studies to be important in fibril formation from full-length β_2m under these conditions.^{64,65} Although at low pH monomeric β_2m is found initially in an acid unfolded and highly dynamic state^{21,22} approximately 70% of the residues^{*} appear in dipolar spectra of the fibrils and most likely participate in the rigid fibril core. This implies that upon aggregation there is a substantial reorganization within the polypeptide chain, in agreement with previous studies using methods such as hydrogen exchange, limited proteolysis and EPR, which show that the majority of residues, particularly those located between C25 and C80, are involved in the fibril core.^{25,26,30,66}

In our studies, a single set of resonances has been detected in MAS NMR spectra of LS fibrils, indicating that the observed residues reside in a homogeneous environment. Recently, a cryoEM study demonstrated that β_2m may form polymorphous LS fibril types under identical low pH conditions to those used here.²⁷ It was proposed that a complex architecture

* This estimate includes all observable residues in the dipolar spectra but not the 6 residues identified in through-bond (INEPT-TOBSY) experiments.

involving six protofilaments arranged as two crescent shaped units, each containing three protofilaments, formed and that within each protofilament there were at least three different subunit interfaces providing a complex superstructure. This is also demonstrated by the fact that hydrogen exchange studies of β_2m fibrils show that most backbone amide positions do not reach 100 % exchange, implying differing solvent exposure within a heterogeneous mixture where the same residue is protected differently depending on its molecular environment.^{67,68} Such heterogeneity is also observed in EPR measurements of β_2m fibrils spin labeled at the N-terminal residues R3 and R11, where both mobile and immobile components contribute to the spectra, but not at any other regions of the protein involved in the core fibrillar structure.³⁰ In combination with previous studies, our MAS NMR data suggest that the core residues of β_2m are in a homogeneous protected environment in most fibrils and the gross physiognomic differences observed by cryoEM can be explained by the macroscopic arrangement of subunits and/or protofibrils in relation to each other. These interactions may create different chemical environments and conformational variations for amino acid segments involved in the subunit interfaces. Such conformational disorder can lead to line broadening and weak signal intensities as observed for a fraction of the residues in the protein (in addition to dynamics).

Analysis of the fibrils using TOBSY experiments that are particularly sensitive to dynamics within the sample indicated that six of the ~30 residues not observed in the dipolar experiments are highly mobile compared to the rest of the sequence. The amino acid types of the mobile residues correspond to those found within the seven N-terminal residues in the sequence. The fact that this segment of fibrillar β_2m is prone to specific cleavage at V9 by pepsin (a non-specific protease that has been shown to digest acid unfolded β_2m at over twenty sites throughout the sequence) suggests that this region of the polypeptide chain is solvent exposed and dynamic.^{26,51,66} Indeed, Trp substitution and hydrogen exchange experiments of LS β_2m fibrils monitored by solution NMR spectroscopy have indicated that the N-terminus is exposed more than the rest of the protein, which is likely to be found in a protected core.^{25,69} Interestingly, disruption of the N-terminal region of the native protein by mutation or truncation has also been observed to promote amyloid fibril formation at neutral pH.^{60,61,70}

A recent study of the LS amyloid fibrils formed from β_2m at pH 2.5 using proteolysis and solution NMR spectroscopy has confirmed that residues 1-9 are cleaved by pepsin digestion and thus exposed, but are only seen to be dynamic by solution NMR when elongated with a sequence designed to favor random coil conformations.⁵¹ It is likely that the discrepancy between the results presented here and the solution NMR dataset is due to the fact that the solution NMR study measured backbone amide dynamics while the MAS INEPT-TOBSY experiments described here were optimized for aliphatic transfer and were therefore more sensitive to side chain motion. Since the mobility detected here is only limited to the very end of the N-terminus, the rest of the 20 N-terminal residues that present increased HX exchange rates⁵⁰ could still be part of the fibril core or play a role in the intermolecular assembly of the fibrils. This possibility is also corroborated by EPR, a method that also probes side chain mobility, which indicates that spin labels at residues 3 and 11 are highly dynamic.³⁰

5.6. β_2m is organized in a non-native manner in amyloid-like fibrils

The experiments discussed here, aided by the use of alternating labeling, have allowed the sequential assignment of 57 of the 100 residues present in the protein sequence and permit conclusions to be drawn concerning the structure of β_2m at an amino acid level within the fibril architecture. For instance, it is clear from the analysis of the chemical shifts (using TALOS and CSI) that the protein is organized in a non-native arrangement within these fibrils (Figures 5.7 and 5.8). Throughout the central portion of the sequence of β_2m (residues ~28-86) where assignments are available there is an increased prevalence of amino acids showing a β -sheet conformational preference (except for residues 43 and 56). This agrees with previous data for β_2m as well as other amyloid-like states of proteins, provided by techniques such as X-ray diffraction, which show an increase in β -structure as the proteins form cross- β arrangements upon aggregation.⁵ Furthermore, information from EPR and FTIR studies has also indicated that the β_2m polypeptide chain in LS fibrils is arranged in a parallel and in-register arrangement.^{28,30} Interestingly, the region encompassing residues 44-55 is found in a β -sheet conformation in the LS fibrils yet this segment of the protein contains bulges and loops in most structural studies of native β_2m .¹⁸ X-ray crystallography has indicated that rare conformations of the native state also exist where residues 51-56 of the protein form a

continuous β -strand without the bulge,^{56,70-72} although it has also been observed that straightening of β -strand D alone is insufficient for fibril formation.⁷³ These species have been proposed to be consistent with possible early structural changes that promote intermolecular strand-strand recognition in protein aggregation of β_2m at neutral pH.^{70,74,75} However, it is worth noting that no crystal structure of β_2m shows the extensive β -strand conformational propensity that is indicated by the chemical shift data described here suggesting that increased β -sheet structure in this region of the sequence is promoted during the aggregation reaction.

An interesting feature of the MAS NMR data presented here is that both assigned prolines (P32 and P72) adopt the *trans* conformer in the fibrillar state. A number of studies have described the conformational change of the H31-P32 peptide bond from *cis* to *trans* as a pivotal early step in the aggregation of β_2m at neutral pH.^{20,61,70} At the low pH conditions under which fibrils were formed in this study it would be expected that this peptide bond would populate predominantly a *trans* configuration (in ~80 % of the acid unfolded molecules).^{60,76} Therefore, the finding here that P32 adopts a *trans* conformation suggests that a *trans* P32 bond is a common feature of fibrils formed at both pH 2.5 and pH 7.

The divergence from native-like structure of the β_2m polypeptide chain in LS fibrils observed here is in good agreement with the cryoEM study of morphologically identical β_2m LS fibrils, which suggested that native-like monomers do not fit within the fibrillar architecture.²⁷ Other models founded on different types of biophysical information have also been proposed for LS fibrils formed from full-length β_2m . Based principally on analyses of the amyloid-forming abilities at low pH of variants of the human β_2m sequence, for instance, Ivanova and co-workers proposed that these fibrils are composed of a zipper-spine structure. In this model a tightly interdigitated core backbone is formed by residues 83-99 and the rest of the protein remains native-like and decorates the periphery of these fibrils.⁷⁷ Such an organization appears unlikely in the β_2m amyloid-like fibrils used in this study based on chemical shift analysis. Furthermore, a molecular dynamics study has proposed a domain swapping mechanism for propagation of β_2m fibrillation, where the N-terminal region of one monomer exchanges with that of another, leading to a chain reaction.⁷⁸ This model would lead

to a native-like structure of β_2m , which is not easily reconciled with the MAS NMR data presented here. The presence of native-like monomers within LS β_2m fibrils would also contradict data obtained from fiber diffraction, FTIR and EPR experiments.^{29,30,79}

A recently published MAS NMR study of full-length β_2m conjectured that the overall native structure is preserved in the fibrils, based on the observation of a fraction of similar ^{13}C signals between correlation spectra of fibrils formed at pH 2.5 and β_2m crystals.⁸⁰ In the absence of site-specific resonance assignments, such an inference is not consistent with the secondary structure in the fibril state presented in this article. The latter was derived from the analysis of chemical shifts in MAS spectra and shows important discrepancies between the fibrillar and native states. It may be possible that different fibril morphologies were studied in each case, as evidenced by large differences in MAS INEPT spectra, which in the sample analyzed here indicate a flexible N-terminus that is consistent with proteolysis and HX data.^{25,26}

5.7. Conclusions

We have presented the initial MAS NMR spectra recorded from fibrils formed from full-length β_2m . The data indicate that LS fibrils formed under low pH conditions exhibit an extensive fibril core, however, there is a significant portion of the sequence (~25 of 100 residues) that is not observed in either dipolar or through-bond experiments. The N-terminal region is observed to display increased mobility compared with the remainder of the sequence, which may explain its susceptibility to proteolysis and HX. Residues 27-86 display increased β -sheet content in the fibrillar form consistent with a wealth of other biophysical data that indicate that the protein does not retain a native-like structure in these assemblies. Interestingly, the data reveal that the prolyl bond at residue 32 is found in a non-native *trans* conformation, consistent with proposed changes in early structures formed *en route* to aggregation at neutral pH.^{20,70} The data indicate that the LS fibrils studied here contain a structurally unique and uniform organization within their core, and there is no evidence for gross structural polymorphism, at least within the regions of the sequence analyzed here. Experiments to investigate the tertiary and quaternary structure of β_2m within the fibril architecture are currently underway in our laboratory.

5.8. Methods

5.8.1. Protein Expression and Purification

Recombinant human β_2 -microglobulin (β_2m) was expressed in HCDM1 minimal media and purified as described elsewhere.⁸⁸ Uniformly ^{13}C - and ^{15}N -labelled β_2m samples were prepared by growing BL21(DE3) pLysS *Escherichia coli* in the presence of minimal media enriched with 1 gL^{-1} $^{15}NH_4Cl$ (Goss Scientific, UK) and 2 gL^{-1} D-glucose- $^{13}C_6$ (Sigma Aldrich, UK). Two biosynthetically site-directed ^{13}C -enriched samples were prepared by culturing bacteria in the presence of 1 gL^{-1} $^{15}NH_4Cl$ and either 2 gL^{-1} [1,3- ^{13}C] glycerol or 2 gL^{-1} [2- ^{13}C] glycerol and $NaH^{13}CO_3$ (Cambridge Isotope Laboratories, Andover, MA) to obtain labelling patterns consistent with those previously described.^{31,32}

5.8.2. Fibril formation

Long, straight (LS) fibrils were formed at 1 mg ml^{-1} in 25 mM sodium acetate, 25 mM sodium phosphate, 0.04% (w/v) NaN_3 at pH 2.5, 37 °C with shaking for 14 days. The fibrils were centrifuged at $265,000\times g$ for 1 hr and the resulting hydrated pellet was transferred into a MAS rotor using a tabletop centrifuge. Varian 3.2 mm rotors (Revolution NMR, Fort Collins, CO) as well as Bruker 2.5 mm and 3.2 mm rotors (Bruker BioSpin, Billerica, MA) were used for the experiments outlined below. The rotors contained $\sim 10\text{ mg}$, 5 mg and 15 mg fibril sample respectively.

The worm-like (WL) fibrils were formed at 3 mg ml^{-1} in 200 mM ammonium formate buffer at pH 3.6, 37 °C with no shaking for 2 days. These fibrils were transferred in 50 mM ammonium formate buffer (pH 3.6) and centrifuged at $176,000\times g$ for 1 hr and packed into a Bruker 2.5 mm rotor.

5.8.3. Solid-state NMR spectroscopy

Experiments were performed with custom designed spectrometers (courtesy of D.J. Ruben, Francis Bitter Magnet Laboratory, Massachusetts Institute of Technology, Cambridge, MA) operating at 700 and 750 MHz 1H Larmor frequency. The 700 MHz spectrometer was equipped with a triple-resonance $^1H/^{13}C/^{15}N$ Varian-Chemagnetics 3.2 mm probe (Varian,

Inc., Palo Alto, CA). The 750 MHz experiments were performed with triple-resonance Bruker probes (Bruker BioSpin, Billerica, MA) equipped with a 2.5 mm coil or a 3.2 mm E-free coil. The sample was cooled with a stream of dry air maintained at a temperature of -5 °C, while we estimate that the sample temperature during the MAS experiments was 10-15 °C higher.

1D CP experiments were recorded using 1.2-1.8 ms contact time and 83 kHz TPPM⁸⁹ ¹H decoupling during acquisition. A 2D ¹³C-¹³C correlation experiment of the LS fibrils was recorded with an RFDR sequence with $\tau_{\text{mix}} = 1.76$ ms at $\omega_r/2\pi = 18.2$ kHz, with 40 kHz π pulses on the ¹³C channel during mixing, and 83 kHz TPPM decoupling on the ¹H channel during evolution, mixing and acquisition. The acquisition time was 12.3 ms and 24 ms in the indirect and direct dimensions respectively. ¹⁵N-¹³C correlations on 2- β_2 m and 1,3- β_2 m LS fibril samples were recorded with TEDOR dipolar recoupling ($\tau_{\text{mix}} = 1.6$ ms) at $\omega_r/2\pi = 10$ kHz and 12.5 kHz respectively (40 kHz ¹⁵N pulses, 100 kHz ¹³C pulses and 83 kHz ¹H decoupling during mixing). The acquisition times were 12.8 ms for t_1 and 24 ms for t_2 for 2- β_2 m, and 11.2 ms and 24 ms respectively for 1,3- β_2 m fibrils. INEPT-TOBSY experiments were recorded at $\omega_r/2\pi = 16.667$ kHz, TOBSY mixing without decoupling ($\tau_{\text{mix}} = 5.77$ ms), 12 ms t_1 evolution and 24 ms t_2 evolution.

The ¹³C-¹³C correlation experiment of the WL fibrils was recorded with RFDR mixing ($\tau_{\text{mix}} = 2.56$ ms) at $\omega_r/2\pi = 12.5$ kHz, with 20 kHz π pulses on the ¹³C channel during mixing, and 83 kHz ¹H decoupling during mixing and acquisition. The carrier frequency was centred on the aliphatic region. The acquisition time in the indirect dimension was 8 ms, and 24 ms in the direct dimension respectively.

References

- (1) Westermark, P.; Benson, M. D.; Buxbaum, J. N.; Cohen, A. S.; Frangione, B.; Ikeda, S. I.; Masters, C. L.; Merlini, G.; Saraiva, M. J.; Sipe, J. D. *Amyloid* **2007**, *14*, 179-183.
- (2) Dobson, C. M. *Nature* **2003**, *426*, 884-890.
- (3) Jimenez, J. L.; Guijarro, J. L.; Orlova, E.; Zurdo, J.; Dobson, C. M.; Sunde, M.; Saibil, H. R. *EMBO J.* **1999**, *18*, 815-821.
- (4) Astbury, W. T.; Beighton, E.; Parker, K. D. *Biochim. Biophys. Acta* **1959**, *35*, 17-25.

- (5) Sunde, M.; Serpell, L. C.; Bartlam, M.; Fraser, P. E.; Pepys, M. B.; Blake, C. C. F. *J. Mol. Biol.* **1997**, *273*, 729-739.
- (6) LeVine, H. *Met. Enzymol.* **1999**, *309*, 274-284.
- (7) Nelson, R.; Sawaya, M. R.; Balbirnie, M.; Madsen, A. O.; Riek, C.; Grothe, R.; Eisenberg, D. *Nature* **2005**, *435*, 773-778.
- (8) van der Wel, P. C. A.; Lewandowski, J. R.; Griffin, R. G. *J. Am. Chem. Soc.* **2007**.
- (9) Wasmer, C.; Lange, A.; Van Melckebeke, H.; Siemer, A. B.; Riek, R.; Meier, B. H. *Science* **2008**, *319*, 1523-1526.
- (10) Petkova, A. T.; Yau, W. M.; Tycko, R. *Biochemistry* **2006**, *45*, 498-512.
- (11) Iwata, K.; Fujiwara, T.; Matsuki, Y.; Akutsu, H.; Takahashi, S.; Naiki, H.; Goto, Y. *Proc. Natl. Acad. Sci. U.S.A.* **2006**, *103*, 18119-18124.
- (12) Luca, S.; Yau, W. M.; Leapman, R.; Tycko, R. *Biochemistry* **2007**, *46*, 13505-13522.
- (13) Heise, H.; Hoyer, W.; Becker, S.; Andronesi, O. C.; Riedel, D.; Baldus, M. *Proc. Natl. Acad. Sci. U.S.A.* **2005**, *102*, 15871-15876.
- (14) Vilar, M.; Chou, H. T.; Luhrs, T.; Maji, S. K.; Riek-Loher, D.; Verel, R.; Manning, G.; Stahlberg, H.; Riek, R. *Proc. Natl. Acad. Sci. U.S.A.* **2008**, *105*, 8637-8642.
- (15) Cohen, F. E.; Kelly, J. W. *Nature* **2003**, *426*, 905-909.
- (16) Cherny, I.; Gazit, E. *Angew. Chem., Int. Ed.* **2008**, *47*, 4062-4069.
- (17) Gejyo, F.; Yamada, T.; Odani, S.; Nakagawa, Y.; Arakawa, M.; Kunitomo, T.; Kataoka, H.; Suzuki, M.; Hirasawa, Y.; Shirahama, T.; Cohen, A. S.; Schmid, K. *Biochem. Biophys. Res. Commun.* **1985**, *129*, 701-706.
- (18) Saper, M. A.; Bjorkman, P. J.; Wiley, D. C. *J. Mol. Biol.* **1991**, *219*, 277-319.
- (19) Radford, S. E.; Gosal, W. S.; Platt, G. W. *Biochim. Biophys. Acta, Proteins Proteomics* **2005**, *1753*, 51-63.
- (20) Eichner, T.; Radford, S. E. *J. Mol. Biol.* **2009**, *386*, 1312-1326.
- (21) Platt, G. W.; McParland, V. J.; Kalverda, A. P.; Homans, S. W.; Radford, S. E. *J. Mol. Biol.* **2005**, *346*, 279-294.
- (22) Katou, H.; Kanno, T.; Hoshino, M.; Hagihara, Y.; Tanaka, H.; Kawai, T.; Hasegawa, K.; Naiki, H.; Goto, Y. *Protein Sci.* **2002**, *11*, 2218-2229.
- (23) McParland, V. J.; Kad, N. M.; Kalverda, A. P.; Brown, A.; Kirwin-Jones, P.; Hunter, M. G.; Sunde, M.; Radford, S. E. *Biochemistry* **2000**, *39*, 8735-8746.

- (24) Smith, D. P.; Jones, S.; Serpell, L. C.; Sunde, M.; Radford, S. E. *J. Mol. Biol.* **2003**, *330*, 943-954.
- (25) Yamaguchi, K. I.; Katou, H.; Hoshino, M.; Hasegawa, K.; Naiki, H.; Goto, Y. *J. Mol. Biol.* **2004**, *338*, 559-571.
- (26) Myers, S. L.; Thomson, N. H.; Radford, S. E.; Ashcroft, A. E. *Rapid Commun. Mass Spectrom.* **2006**, *20*, 1628-1636.
- (27) White, H. E.; Hodgkinson, J. L.; Jahn, T. R.; Cohen-Krausz, S.; Gosal, W. S.; Muller, S.; Orlova, E. V.; Radford, S. E.; Saibil, H. R. *J. Mol. Biol.* **2009**, *389*, 48-57.
- (28) Fabian, H.; Gast, K.; Laue, M.; Misselwitz, R.; Uchanska-Ziegler, B.; Ziegler, A.; Naumann, D. *Biochemistry* **2008**, *47*, 6895-6906.
- (29) Jahn, T. R.; Tennent, G. A.; Radford, S. E. *J. Biol. Chem.* **2008**, *283*, 17279-17286.
- (30) Ladner, C. L.; Chen, M.; Smith, D. P.; Platt, G. W.; Radford, S. E.; Langen, R. *J. Biol. Chem.* **2010**, *285*, 17137-17147.
- (31) LeMaster, D. M.; Kushlan, D. M. *J. Am. Chem. Soc.* **1996**, *118*, 9255-9264.
- (32) Castellani, F.; van Rossum, B.; Diehl, A.; Schubert, M.; Rehbein, K.; Oschkinat, H. *Nature* **2002**, *420*, 98-102.
- (33) Castellani, F.; van Rossum, B. J.; Diehl, A.; Rehbein, K.; Oschkinat, H. *Biochemistry* **2003**, *42*, 11476-11483.
- (34) Bennett, A. E.; Ok, J. H.; Griffin, R. G.; Vega, S. *J. Chem. Phys.* **1992**, *96*, 8624-8627.
- (35) Bennett, A. E.; Rienstra, C. M.; Griffiths, J. M.; Zhen, W. G.; Lansbury, P. T.; Griffin, R. G. *J. Chem. Phys.* **1998**, *108*, 9463-9479.
- (36) Bayro, M. J.; Ramachandran, R.; Caporini, M. A.; Eddy, M. T.; Griffin, R. G. *J. Chem. Phys.* **2008**, *128*, 052321.
- (37) Jaroniec, C. P.; MacPhee, C. E.; Bajaj, V. S.; McMahon, M. T.; Dobson, C. M.; Griffin, R. G. *Proc. Natl. Acad. Sci. U.S.A.* **2004**, *101*, 711-716.
- (38) Bayro, M. J.; Maly, T.; Birkett, N. R.; Dobson, C. M.; Griffin, R. G. *Angew. Chem., Int. Ed.* **2009**, *48*, 5708-5710.
- (39) Bayro, M. J.; Huber, M.; Ramachandran, R.; Davenport, T. C.; Meier, B. H.; Ernst, M.; Griffin, R. G. *J. Chem. Phys.* **2009**, *130*, 114506.
- (40) Hing, A. W.; Vega, S.; Schaefer, J. *J. Magn. Reson.* **1992**, *96*, 205-209.
- (41) Jaroniec, C. P.; Filip, C.; Griffin, R. G. *J. Am. Chem. Soc.* **2002**, *124*, 10728-10742.

- (42) Maus, D. C.; Copie, V.; Sun, B. Q.; Griffiths, J. M.; Griffin, R. G.; Luo, S. F.; Schrock, R. R.; Liu, A. H.; Seidel, S. W.; Davis, W. M.; Grohmann, A. *J. Am. Chem. Soc.* **1996**, *118*, 5665-5671.
- (43) Long, J. R.; Sun, B. Q.; Bowen, A.; Griffin, R. G. *J. Am. Chem. Soc.* **1994**, *116*, 11950-11956.
- (44) Bajaj, V. S.; van der Wel, P. C. A.; Griffin, R. G. *J. Am. Chem. Soc.* **2009**, *131*, 118-128.
- (45) Petkova, A. T.; Ishii, Y.; Balbach, J. J.; Antzutkin, O. N.; Leapman, R. D.; Delaglio, F.; Tycko, R. *Proc. Natl. Acad. Sci. U.S.A.* **2002**, *99*, 16742-16747.
- (46) Siemer, A. B.; Arnold, A. A.; Ritter, C.; Westfeld, T.; Ernst, M.; Riek, R.; Meier, B. H. *J. Am. Chem. Soc.* **2006**, *128*, 13224-13228.
- (47) Helmus, J. J.; Surewicz, K.; Nadaud, P. S.; Surewicz, W. K.; Jaroniec, C. P. *Proc. Natl. Acad. Sci. U.S.A.* **2008**, *105*, 6284-6289.
- (48) Helmus, J. J.; Surewicz, K.; Surewicz, W. K.; Jaroniec, C. P. *J. Am. Chem. Soc.* **2010**, *132*, 2393-2403.
- (49) Andronesi, O. C.; Becker, S.; Seidel, K.; Heise, H.; Young, H. S.; Baldus, M. *J. Am. Chem. Soc.* **2005**, *127*, 12965-12974.
- (50) Hoshino, M.; Katou, H.; Hagihara, Y.; Hasegawa, K.; Naiki, H.; Goto, Y. *Nat. Struct. Biol.* **2002**, *9*, 332-336.
- (51) Platt, G. W.; Xue, W. F.; Homans, S. W.; Radford, S. E. *Angew. Chem., Int. Ed.* **2009**, *48*, 5705-5707.
- (52) Cornilescu, G.; Delaglio, F.; Bax, A. *J. Biomol. NMR* **1999**, *13*, 289-302.
- (53) Wishart, D. S.; Sykes, B. D. *J. Biomol. NMR* **1994**, *4*, 171-180.
- (54) Verdone, G.; Corazza, A.; Viglino, P.; Pettirossi, F.; Giorgetti, S.; Mangione, P.; Andreola, A.; Stoppini, M.; Bellotti, V.; Esposito, G. *Protein Sci.* **2002**, *11*, 487-499.
- (55) Khan, A. R.; Baker, B. M.; Ghosh, P.; Biddison, W. E.; Wiley, D. C. *J. Immunol.* **2000**, *164*, 6398 - 6405.
- (56) Trinh, C. H.; Smith, D. P.; Kalverda, A. P.; Phillips, S. E. V.; Radford, S. E. *Proc. Natl. Acad. Sci. U.S.A.* **2002**, *99*, 9771-9776.
- (57) Iwata, K.; Matsuura, T.; Sakurai, K.; Nakagawa, A.; Goto, Y. *J. Biochem.* **2007**, *142*, 413-419.

- (58) Sarkar, S. K.; Torchia, D. A.; Kopple, K. D.; Vanderhart, D. L. *J. Am. Chem. Soc.* **1984**, *106*, 3328-3331.
- (59) Schubert, M.; Labudde, D.; Oschkinat, H.; Schmieder, P. *J. Biomol. NMR* **2002**, *24*, 149-154.
- (60) Kameda, A.; Hoshino, M.; Higurashi, T.; Takahashi, S.; Naiki, H.; Goto, Y. *J. Mol. Biol.* **2005**, *348*, 383-397.
- (61) Jahn, T. R.; Parker, M. J.; Homans, S. W.; Radford, S. E. *Nat. Struct. Mol. Biol.* **2006**, *13*, 195-201.
- (62) Andersen, C. B.; Otzen, D.; Christiansen, G.; Rischel, C. *Biochemistry* **2007**, *46*, 7314-7324.
- (63) de Lacaillerie, J. B. D.; Jarry, B.; Pascui, O.; Reichert, D. *Solid State Nucl. Magn. Reson.* **2005**, *28*, 225-232.
- (64) Platt, G. W.; Routledge, K. E.; Homans, S. W.; Radford, S. E. *J. Mol. Biol.* **2008**, *378*, 251-263.
- (65) Routledge, K. E.; Tartaglia, G. G.; Platt, G. W.; Vendruscolo, M.; Radford, S. E. *J. Mol. Biol.* **2009**, *389*, 776-786.
- (66) Monti, M.; Principe, S.; Giorgetti, S.; Mangione, P.; Merlini, G.; Clark, A.; Bellotti, V.; Amoresano, A.; Pucci, P. *Protein Sci.* **2002**, *11*, 2362-2369.
- (67) Chatani, E.; Goto, Y. *Biochim. Biophys. Acta, Proteins Proteomics* **2005**, *1753*, 64-75.
- (68) Yamaguchi, K.; Naiki, H.; Goto, Y. *J. Mol. Biol.* **2006**, *363*, 279-288.
- (69) Kihara, M.; Chatani, E.; Iwata, K.; Yamamoto, K.; Matsuura, T.; Nakagawa, A.; Naiki, H.; Goto, Y. *J. Biol. Chem.* **2006**, *281*, 31061-31069.
- (70) Eakin, C. M.; Berman, A. J.; Miranker, A. D. *Nat. Struct. Mol. Biol.* **2006**, *13*, 202-208.
- (71) Rosano, C.; Zuccotti, S.; Mangione, P.; Giorgetti, S.; Bellotti, V.; Pettirossi, F.; Corazza, A.; Viglino, P.; Esposito, G.; Bolognesi, M. *J. Mol. Biol.* **2004**, *335*, 1051-1064.
- (72) Ricagno, S.; Colombo, M.; de Rosa, M.; Sangiovanni, E.; Giorgetti, S.; Raimondi, S.; Bellotti, V.; Bolognesi, M. *Biochem. Biophys. Res. Commun.* **2008**, *377*, 146-150.
- (73) Platt, G. W.; Radford, S. E. *FEBS Lett.* **2009**, *583*, 2623-2629.
- (74) Richardson, J. S.; Richardson, D. C. *Proc. Natl. Acad. Sci. U.S.A.* **2002**, *99*, 2754-2759.
- (75) Benyamini, H.; Gunasekaran, K.; Wolfson, H.; Nussinov, R. *J. Mol. Biol.* **2003**, *330*, 159-174.

- (76) Schmid, F. X. *Methods Enzymol.* **1986**, *131*, 70-82.
- (77) Ivanova, M. I.; Sawaya, M. R.; Gingery, M.; Attinger, A.; Eisenberg, D. *Proc. Natl. Acad. Sci. U.S.A.* **2004**, *101*, 10584-10589.
- (78) Chen, Y. W.; Dokholyan, N. V. *J. Mol. Biol.* **2005**, *354*, 473-482.
- (79) Jahn, T. R.; Makin, O. S.; Morris, K. L.; Marshall, K. E.; Tian, P.; Sikorski, P.; Serpell, L. C. *J. Mol. Biol.* **2010**, *395*, 717-727.
- (80) Barbet-Massin, E.; Ricagno, S.; Lewandowski, J. z. R.; Giorgetti, S.; Bellotti, V.; Bolognesi, M.; Emsley, L.; Pintacuda, G. *J. Am. Chem. Soc.*, *132*, 5556-5557.
- (81) Monti, M.; Amoresano, A.; Giorgetti, S.; Bellotti, V.; Pucci, P. *Biochim. Biophys. Acta* **2005**, *1753*, 44-50.
- (82) Relini, A.; De Stefano, S.; Torrassa, S.; Cavalleri, O.; Rolandi, R.; Gliozzi, A.; Giorgetti, S.; Raimondi, S.; Marchese, L.; Verga, L.; Rossi, A.; Stoppini, M.; Bellotti, V. *J. Biol. Chem* **2008**, *283*, 4912-4920.
- (83) Gosal, W. S.; Morten, I. J.; Hewitt, E. W.; Smith, D. A.; Thomson, N. H.; Radford, S. E. *J. Mol. Biol.* **2005**, *351*, 850-864.
- (84) Xue, W. F.; Homans, S. W.; Radford, S. E. *Proc. Natl. Acad. Sci. U.S.A.* **2008**, *105*, 8926-8931.
- (85) Lee, Y. H.; Chatani, E.; Sasahara, K.; Naiki, H.; Goto, Y. *J. Biol. Chem.* **2009**, *284*, 2169-2175.
- (86) Hiramatsu, H.; Lu, M.; Matsuo, K.; Gekko, K.; Goto, Y. J.; Kitagawa, T. *Biochemistry* **2010**, *49*, 742-751.
- (87) Toyama, B. H.; Kelly, M. J. S.; Gross, J. D.; Weissman, J. S. *Nature* **2007**, *449*, 233-237.
- (88) Kad, N. M.; Thomson, N. H.; Smith, D. P.; Smith, D. A.; Radford, S. E. *J. Mol. Biol.* **2001**, *313*, 559-571.
- (89) Bennett, A. E.; Rienstra, C. M.; Auger, M.; Lakshmi, K. V.; Griffin, R. G. *J. Chem. Phys.* **1995**, *103*, 6951-6958.

Chapter 6. Intermolecular Alignment in β_2 -Microglobulin Amyloid Fibrils

Adapted from "Intermolecular Alignment in β_2 -Microglobulin Amyloid Fibrils" by Debelouchina GT, Platt GW, Bayro MJ, Radford SE, Griffin RG, published in J. Am. Chem. Soc., 2010, 132, 17077-17079.

Summary

The deposition of amyloid-like fibrils, composed primarily of the 99-residue protein β_2 -microglobulin (β_2m), is one of the characteristic symptoms of dialysis-related amyloidosis. Fibrils formed in vitro at low pH and salt concentration share many properties with the disease related fibrils and have been extensively studied by a number of biochemical and biophysical methods. These fibrils contain a significant β -sheet core and present an unusually complex cryoEM electron density profile. Here, we investigate the intra-sheet arrangement of the fibrils by means of ^{15}N - ^{13}C MAS correlation spectroscopy. We utilize a fibril sample grown from a 50:50 mixture of ^{15}N , ^{12}C - and ^{14}N , ^{13}C -labeled β_2m monomers, the latter prepared using 2- ^{13}C glycerol as the carbon source. Together with the use of ZF-TEDOR mixing, this sample allowed us to observe intermolecular ^{15}N - ^{13}C backbone-to-backbone contacts with excellent resolution and good sensitivity. The results are consistent with a parallel, in-register arrangement of the protein subunits in the fibrils and suggest that a significant structural reorganization occurs from the native to the fibril state.

6.1. Introduction

β_2 -Microglobulin (β_2m) is a 99-residue protein that forms amyloid fibril deposits associated with dialysis-related amyloidosis (DRA).¹ Under acidic conditions (pH=2.5) and low salt concentration, the protein can also form amyloid fibrils *in vitro* through a nucleation-dependent mechanism.^{2,3} These fibrils are long, straight and unbranched in appearance, and share many properties with the fibrils isolated from tissues of DRA patients, including the same characteristic amide I' band in FTIR spectra.⁴ It has been shown that the fibrils themselves, and not the prefibrillar oligomeric species formed in the lag phase of assembly, can disrupt model membranes and are toxic to cells.⁵ While an atomic structural model for these fibrils is not yet available, structural details emerged first through methods like limited proteolysis,^{6,7} hydrogen exchange,^{8,9} and more recently by magic angle spinning (MAS) NMR,¹⁰ electron paramagnetic resonance (EPR)¹¹ and cryo-electron microscopy (cryoEM).¹² In particular, analysis of the chemical shifts of 64 assigned residues of β_2m fibrils has shown that the protein contains a rigid fibril core with substantially more β -sheet character than the native protein.¹⁰ CryoEM maps revealed a complex picture of the fibrils, where non-native globular β_2m monomers pack in “dimer-of-dimers” building blocks that associate asymmetrically into crescent-shaped units.¹² In addition, site-directed EPR spin labeling suggested that the major building block consists of six β_2m polypeptide chains, arranged in a parallel, in-register manner.¹¹

In the experiments described here, we investigate the tertiary structure of β_2m amyloid fibrils with ^{15}N - ^{13}C MAS NMR correlation spectroscopy. MAS NMR has been successfully used to obtain information about the inter- and intra-molecular interactions that form the β -sheet core of amyloid fibrils, including A β (1–40),¹³ a 22-residue fragment of β_2m ,¹⁴ Hets(218-289),¹⁵ and curli amyloid¹⁶. Various experiments and sample preparation techniques have been employed to achieve that end, including methods that rely on the incorporation of single labels^{17,18} or proton-mediated transfer.¹⁹ Here, we use ZF-TEDOR (z-filtered transfer echo double resonance) mixing^{20,21} to obtain inter-molecular ^{15}N - ^{13}C correlations that establish that the protein subunits in long, straight β_2m fibrils formed at pH 2.5 are arranged as parallel, in-register β -sheets.

6.2. Detection of backbone-to-backbone intermolecular interactions

Our experiments utilize fibrils formed from a 50:50 mixture of ^{15}N , ^{12}C - and ^{14}N , ^{13}C -labeled $\beta_2\text{m}$ monomers, the latter half being prepared using $[2\text{-}^{13}\text{C}]$ -glycerol as the carbon source. This sample, referred to as “mixed 2- $\beta_2\text{m}$ ”, offers improved resolution in the ^{13}C dimension²²⁻²⁴ (Figure 6.1a) as well as potential gains in experimental transfer efficiency due to the significantly reduced number of directly bonded ^{13}C atoms.²⁵ The absence of ^{13}C J-couplings, and the elimination of strong (intramolecular) dipolar ^{15}N - ^{13}C couplings as a result of the mixed nature of the sample improves the efficiency of ZF-TEDOR.^{20,26,27}

In a 100% uniformly ^{15}N , ^{13}C labeled $\beta_2\text{m}$ sample, the experimental one-bond ^{15}N - ^{13}C transfer efficiency after 1.76 ms of ZF-TEDOR mixing is typically ~20% of the ^{13}C CP signal. In the mixed 2- $\beta_2\text{m}$ sample, after such short mixing time, no significant buildup of ^{13}C polarization is observed, as shown in Figure 8.1b. This is due to the absence of ^{13}C nuclei in the ^{15}N , ^{12}C -labeled monomers, which were prepared using ^{13}C -depleted glucose (99.9% purity) to eliminate contributions from natural abundance. In particular, signals from one-bond ^{15}N - ^{13}C interactions are not detected. On the other hand, longer ZF-TEDOR mixing times lead to the buildup of ^{13}C intensity, which reaches a maximum at 18 ms (Figure 8.1c and Figure 6.2), and is consistent with ^{15}N - ^{13}C distances of ~5.0-5.5 Å. The maximum bulk transfer efficiency for the $\text{C}\alpha$ region is ~3%, which is better than the experimental transfer efficiencies observed for uniformly ^{13}C labeled samples (< 1% for similar distances).²⁰

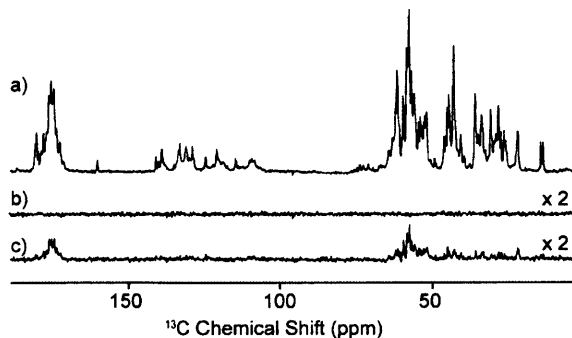


Figure 6.2. (a) ^{13}C CP spectrum of mixed 2- $\beta_2\text{m}$ fibrils, 512 scans, (b) ZF-TEDOR spectrum obtained with $\tau_{\text{mix}} = 1.76$ ms, 512 scans, (c) ZF-TEDOR with $\tau_{\text{mix}} = 18$ ms, 5120 scans.

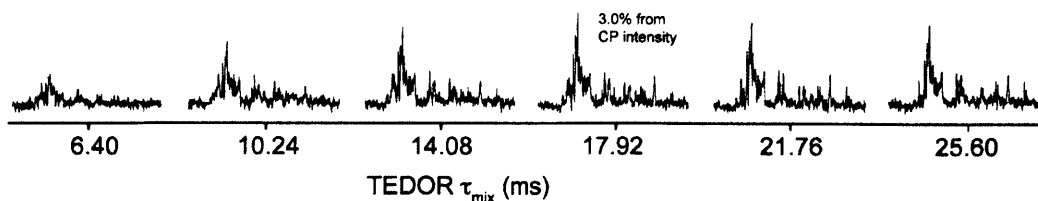


Figure 6.2. 1D TEDOR buildup of mixed 2- β_2 m fibrils obtained at 750 MHz, $\omega_r/2\pi = 12.5$ kHz, 5120 scans. The figure shows the aliphatic region of the spectra (10-70 ppm).

In order to obtain site-specific information regarding the origin of the ^{15}N - ^{13}C intermolecular contacts in mixed 2- β_2 m, we recorded a 2D ZF-TEDOR experiment with $\tau_{\text{mix}} = 16$ ms. This spectrum presents excellent resolution (^{13}C line widths ~ 50 Hz) and sufficient sensitivity after a long acquisition period, which was facilitated by the robustness of the TEDOR sequence. Overall, the positions of the observed cross-peaks in this mixed 2- β_2 m spectrum correspond exactly with the positions of cross-peaks in one-bond (Figure 6.2a) or two-bond TEDOR spectra (data not shown) of a β_2 m fibril sample prepared from 100% ^{15}N , 2- ^{13}C glycerol labeled material (2- β_2 m). The majority of the cross-peaks in the mixed 2- β_2 m sample could be readily assigned based on known chemical shifts of long, straight β_2 m fibrils¹⁰ and they correspond exclusively to *intermolecular* $\text{N}_i\text{-C}\alpha_i$, $\text{N}_i\text{-C}\alpha_{i-1}$, $\text{N}_i\text{-CO}_i$, or $\text{N}_i\text{-CO}_{i-1}$ transfer (Figure 6.3b). In particular, the following residues giving rise to intermolecular contacts in the mixed 2- β_2 m sample were assigned: H31-S33, N42, G43, R45, I46, V49, H51-F62, P72, T73, and Y78-V82. While P32, S33, G43, F56, S57, K58, F62 are part of well-ordered loops in the fibrils, the remainder of the residues represent all of the currently assigned fibril β -strands.

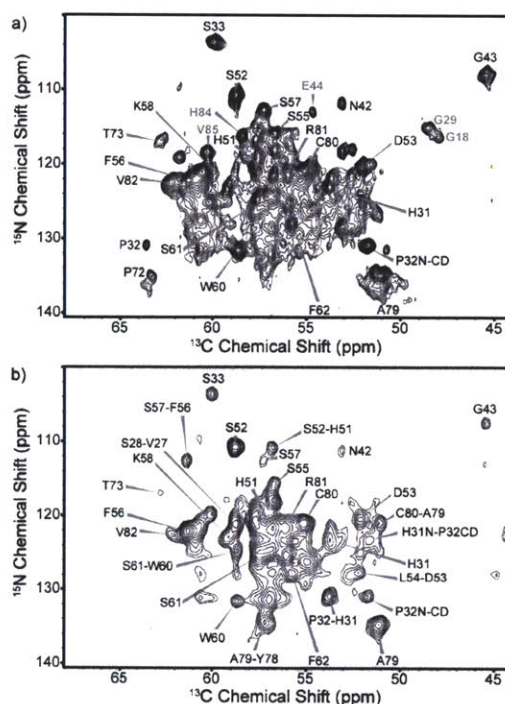


Figure 6.3. Comparison of the ^{15}N - $^{13}\text{C}\alpha$ region of correlation spectra obtained with ZF-TEDOR mixing for two differently labeled $\beta_2\text{m}$ fibril samples. (a) $2\text{-}\beta_2\text{m}$, $\tau_{\text{mix}} = 1.6$ ms, 12 mg of sample, 2 days of experimental time. Labels correspond to intramolecular $\text{N}_i\text{-C}\alpha_i$ transfer, unless otherwise noted, while labels in grey denote cross-peaks that appear only in the $2\text{-}\beta_2\text{m}$ spectrum. (b) mixed $2\text{-}\beta_2\text{m}$, $\tau_{\text{mix}} = 16$ ms, 16 mg of sample, 9 days of experimental time. Labels correspond to intermolecular $\text{N}_i\text{-C}\alpha_i$ or $\text{N}_i\text{-C}\alpha_{i-1}$ transfer, unless otherwise noted.

Some cross-peaks in Figure 6.3b (mixed $2\text{-}\beta_2\text{m}$) do not presently have assignments. Conversely, not all of the strong cross-peaks shown in Figure 6.3a ($2\text{-}\beta_2\text{m}$) appear in the mixed $2\text{-}\beta_2\text{m}$ spectrum. This includes G18, G29, E44, H84 and V85 (shown in grey in Figure 6.3a) among others. This is most likely due to differences in local dynamics and relaxation whose effects are exacerbated at long mixing times, resulting in large variations in the cross-peak intensities.³⁰

6.3. Parallel, in-register β -strand arrangement in $\beta_2\text{m}$ amyloid fibrils

The data presented above suggest that long, straight $\beta_2\text{m}$ fibrils grown at pH 2.5 and low salt concentration, form parallel, in-register β -sheets. In such case the average distances for intermolecular $\text{N}_i\text{-C}\alpha_i$ and $\text{N}_i\text{-C}\alpha_{i-1}$ contacts are ~ 5 Å and ~ 5.5 Å respectively, which is

consistent with the bulk ZF-TEDOR buildup (Figure 6.2). In order to accommodate such an arrangement, substantial reorganization of the native anti-parallel β -sheet structure³¹⁻³³ is required, indicating that the structure of the monomers within the fibrils must be highly non-native. Figure 6.4 highlights two clear pieces of evidence for the non-native structure of β_2m within fibrils: first, residues involved in loops/turns in native β_2m (Figure 6.4a) reorganize to form ordered β -strands in the fibrils (Figure 6.4b) and second, while all β -strands form anti-parallel β -sheet contacts with residues distant in sequence in native β_2m , β -strands in the fibrils are parallel and in register.

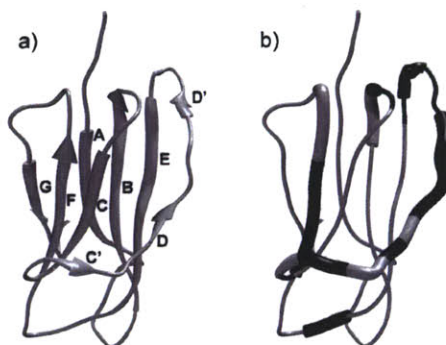


Figure 6.4. (a) Crystal structure of native monomeric β_2m (PDB ID: 1DUZ)²⁸ showing the anti-parallel β -sheet arrangement of the strands (labeled A to G). (b) Residues that form β -strands in fibrillar β_2m painted onto the native fold. β -strands in the fibrils¹⁰ are shown as thick tubes and the residues giving rise to assigned intermolecular $N_i-C\alpha_i$ cross-peaks are shown in black. The structures were prepared using the Chimera software.²⁹

The parallel arrangement of the β -strands in β_2m fibrils was predicted initially by FTIR experiments^{34,35} and is in agreement with data obtained by site-directed spin labeling and EPR.¹¹ The results described here verify and expand upon the latter, which indicates that spin labels attached to cysteine-substituted residues S33, S55, S61 and T73 among others give EPR spectra indicative of immobile, parallel and in-register stacked spin labels. Stacks of six β_2m monomers arranged in that manner are then required to fulfill the electron density maps obtained by cryoEM.¹² The site-specific information regarding the intermolecular arrangement of β_2m fibrils presented here provides an important step towards a full molecular

model of the fibrils. Additional experiments, particularly aimed at determining the quaternary fold of the fibrils, are in progress and should shed light on how this tertiary fibril arrangement fits into such a complex cryoEM electron density profile.

6.4. Methods

6.4.1. Sample Preparation

Mixed 2- β_2 m fibrils were grown from a 50:50 mixture w/w of monomers prepared in two different ways. Half of the monomers were prepared by growing BL21(DE3) pLysS *Escherichia coli* in the presence of minimal media enriched with 1 gL⁻¹ ¹⁵NH₄Cl (Goss Scientific, UK) and 2 gL⁻¹ D-glucose-¹²C₆ (99.9% purity, Cambridge Isotope Laboratories, Andover, MA).¹ The other half of the sample was prepared by culturing bacteria in the presence of 1 gL⁻¹ ¹⁴NH₄Cl, 2 gL⁻¹ [2-¹³C] glycerol, and 2 gL⁻¹ NaH¹³CO₃ (Cambridge Isotope Laboratories, Andover, MA).^{2,3}

2- β_2 m fibrils were grown from monomers prepared by culturing bacteria in the presence of 1 gL⁻¹ ¹⁵NH₄Cl, 2 gL⁻¹ [2-¹³C] glycerol, and 2 gL⁻¹ NaH¹³CO₃.

Fibrils were formed at 1 mg ml⁻¹ in 25 mM sodium acetate, 25 mM sodium phosphate, 0.04% (w/v) NaN₃ at pH 2.5, 37 °C with shaking for 14 days. This resulted in the expected long, straight fibril morphology. The fibrils were centrifuged at 265 000 x g for 1 hr and transferred to a Bruker 3.2 mm rotor (16 mg of mixed 2- β_2 m) or a Varian 3.2 mm rotor (12 mg of 2- β_2 m).

6.4.2. MAS NMR Spectroscopy

Spectra of mixed 2- β_2 m fibrils were obtained at a 750 MHz ¹H Larmor frequency spectrometer (courtesy of D.J. Ruben, Francis Bitter Magnet Laboratory, Massachusetts Institute of Technology, Cambridge, MA) equipped with a 3.2 mm Bruker E-free probe (Bruker BioSpin, Billerica, MA). The sample temperature was ~ 15 °C and $\omega_r/2\pi$ was set to 12.5 kHz.

1D ¹³C CP experiment was recorded with 1.6 ms contact time, and 91 kHz TPPM⁴ decoupling during acquisition. A series of 1D zf-TEDOR⁵ experiments were recorded with 40 kHz ¹⁵N pulses, 83 kHz ¹³C pulses, 100 kHz ¹H TPPM decoupling during mixing and 91 kHz during

acquisition. Similar parameters were employed for the 2D TEDOR experiment recorded with $\tau_{\text{mix}} = 16$ ms, 5.7 ms t_1 evolution and 24 ms t_2 evolution.

A 2D TEDOR experiment was recorded with the 2- β_2 m sample for comparison. This experiment was performed on a custom designed 700 MHz spectrometer (courtesy of D.J. Ruben, Francis Bitter Magnet Laboratory, Massachusetts Institute of Technology, Cambridge, MA) equipped with a triple resonance 3.2 mm Chemagnetics probe (Varian Inc., Palo Alto, CA). 40 kHz ^{15}N pulses, 100 kHz ^{13}C pulses, and 83 kHz ^1H TPPM decoupling were used during mixing, $\tau_{\text{mix}} = 1.6$ ms, $\omega_r/2\pi = 10$ kHz. The acquisition times were 12.8 ms for t_1 and 24 ms for t_2 , respectively.

References

- (1) Gejyo, F.; Yamada, T.; Odani, S.; Nakagawa, Y.; Arakawa, M.; Kunitomo, T.; Kataoka, H.; Suzuki, M.; Hirasawa, Y.; Shirahama, T.; Cohen, A. S.; Schmid, K. *Biochem. Biophys. Res. Commun.* **1985**, *129*, 701-706.
- (2) Platt, G. W.; Radford, S. E. *FEBS Lett.* **2009**, *583*, 2623-2629.
- (3) Xue, W. F.; Homans, S. W.; Radford, S. E. *Proc. Natl. Acad. Sci. U. S. A.* **2008**, *105*, 8926-8931.
- (4) Jahn, T. R.; Tennent, G. A.; Radford, S. E. *J. Biol. Chem.* **2008**, *283*, 17279-17286.
- (5) Xue, W. F.; Hellewell, A. L.; Gosal, W. S.; Homans, S. W.; Hewitt, E. W.; Radford, S. E. *J. Biol. Chem.* **2009**, *284*, 34272-34282.
- (6) Monti, M.; Amoresano, A.; Giorgetti, S.; Bellotti, V.; Pucci, P. *Biochim Biophys Acta, Proteins Proteomics* **2005**, *1753*, 44-50.
- (7) Myers, S. L.; Thomson, N. H.; Radford, S. E.; Ashcroft, A. E. *Rapid Commun. Mass Spectrom.* **2006**, *20*, 1628-1636.
- (8) Hoshino, M.; Katou, H.; Hagihara, Y.; Hasegawa, K.; Naiki, H.; Goto, Y. *Nat. Struct. Biol.* **2002**, *9*, 332-336.
- (9) Yamaguchi, K. I.; Katou, H.; Hoshino, M.; Hasegawa, K.; Naiki, H.; Goto, Y. *J. Mol. Biol.* **2004**, *338*, 559-571.

- (10) Debelouchina, G. T.; Platt, G. W.; Bayro, M. J.; Radford, S. E.; Griffin, R. G. *J. Am. Chem. Soc.* **2010**, *132*, 10414-10423.
- (11) Ladner, C. L.; Chen, M.; Smith, D. P.; Platt, G. W.; Radford, S. E.; Langen, R. *J. Biol. Chem.* **2010**, *285*, 17137-17147.
- (12) White, H. E.; Hodgkinson, J. L.; Jahn, T. R.; Cohen-Krausz, S.; Gosal, W. S.; Muller, S.; Orlova, E. V.; Radford, S. E.; Saibil, H. R. *J. Mol. Biol.* **2009**, *389*, 48-57.
- (13) Petkova, A. T.; Ishii, Y.; Balbach, J. J.; Antzutkin, O. N.; Leapman, R. D.; Delaglio, F.; Tycko, R. *Proc. Natl. Acad. Sci. U. S. A.* **2002**, *99*, 16742-16747.
- (14) Iwata, K.; Fujiwara, T.; Matsuki, Y.; Akutsu, H.; Takahashi, S.; Naiki, H.; Goto, Y. *Proc. Natl. Acad. Sci. U. S. A.* **2006**, *103*, 18119-18124.
- (15) Wasmer, C.; Lange, A.; Van Melckebeke, H.; Siemer, A. B.; Riek, R.; Meier, B. H. *Science* **2008**, *319*, 1523-1526.
- (16) Shewmaker, F.; McGlinchey, R. P.; Thurber, K. R.; McPhie, P.; Dyda, F.; Tycko, R.; Wickner, R. B. *J. Biol. Chem.* **2009**, *284*, 25065-25076.
- (17) Tycko, R. *J. Chem. Phys.* **2007**, *126*, 9.
- (18) Benzinger, T. L. S.; Gregory, D. M.; Burkoth, T. S.; Miller-Auer, H.; Lynn, D. G.; Botto, R. E.; Meredith, S. C. *Proc. Natl. Acad. Sci. U. S. A.* **1998**, *95*, 13407-13412.
- (19) Lange, A.; Luca, S.; Baldus, M. *J. Am. Chem. Soc.* **2002**, *124*, 9704-9705.
- (20) Jaroniec, C. P.; Filip, C.; Griffin, R. G. *J. Am. Chem. Soc.* **2002**, *124*, 10728-10742.
- (21) Hing, A. W.; Vega, S.; Schaefer, J. J. *Magn. Reson.* **1992**, *96*, 205-209.
- (22) LeMaster, D. M.; Kushlan, D. M. *J. Am. Chem. Soc.* **1996**, *118*, 9255-9264.
- (23) Castellani, F.; van Rossum, B.; Diehl, A.; Schubert, M.; Rehbein, K.; Oschkinat, H. *Nature* **2002**, *420*, 98-102.
- (24) Hong, M. *J. Magn. Reson.* **1999**, *139*, 389-401.
- (25) Bayro, M. J.; Maly, T.; Birkett, N. R.; Dobson, C. M.; Griffin, R. G. *Angew. Chem., Int. Ed.* **2009**, *48*, 5708-5710.
- (26) Nieuwkoop, A. J.; Wylie, B. J.; Franks, W. T.; Shah, G. J.; Rienstra, C. M. *J. Chem. Phys.* **2009**, *131*, 8.
- (27) Bayro, M. J.; Maly, T.; Birkett, N. R.; MacPhee, C. E.; Dobson, C. M.; Griffin, R. G. *Biochemistry* **2010**, *49*, 7474-7484.
- (28) Saper, M. A.; Bjorkman, P. J.; Wiley, D. C. *J. Mol. Biol.* **1991**, *219*, 277-319.

- (29) Pettersen, E. F.; Goddard, T. D.; Huang, C. C.; Couch, G. S.; Greenblatt, D. M.; Meng, E. C.; Ferrin, T. E. *J. Comput. Chem.* **2004**, *25*, 1605.
- (30) Debelouchina, G. T.; Bayro, M. J.; van der Wel, P. C. A.; Caporini, M. A.; Barnes, A. B.; Rosay, M.; Maas, W. E.; Griffin, R. G. *Phys. Chem. Chem. Phys.* **2010**, *12*, 5911-5919.
- (31) Trinh, C. H.; Smith, D. P.; Kalverda, A. P.; Phillips, S. E. V.; Radford, S. E. *Proc. Natl. Acad. Sci. U. S. A.* **2002**, *99*, 9771-9776.
- (32) Iwata, K.; Matsuura, T.; Sakurai, K.; Nakagawa, A.; Goto, Y. *J. Biochem.* **2007**, *142*, 413-419.
- (33) Verdone, G.; Corazza, A.; Viglino, P.; Pettirossi, F.; Giorgetti, S.; Mangione, P.; Andreola, A.; Stoppini, M.; Bellotti, V.; Esposito, G. *Protein Sci.* **2002**, *11*, 487-499.
- (34) Kardos, J.; Okuno, D.; Kawai, T.; Hagihara, Y.; Yumoto, N.; Kitagawa, T.; Zavodszky, P.; Naiki, H.; Goto, Y. *Biochim. Biophys. Acta* **2005**, *1753*, 108-120.
- (35) Fabian, H.; Gast, K.; Laue, M.; Misselwitz, R.; Uchanska-Ziegler, B.; Ziegler, A.; Naumann, D. *Biochemistry* **2008**, *47*, 6895-6906.

Chapter 7. Long-Range Structural Constraints in β_2 -Microglobulin Amyloid Fibrils

Summary

In this chapter, we present experiments and labeling schemes designed specifically to obtain long-range interactions in β_2 -microglobulin amyloid fibrils. This includes correlations useful for obtaining sequential assignments (i.e. $C\alpha$ - $C\alpha$), and correlations describing the quaternary structure of the fibrils, defined as the position and orientation of the β -sheets with respect to each other. We also present a strategy for obtaining efficient aromatic-to-aromatic and aromatic-to-aliphatic correlations, which play an important role in stabilizing the quaternary structure of the fibrils. Finally, we present experiments that allow us to distinguish between inter- and intra-molecular interactions, and to determine the relative orientation of the β -sheets along the long axis of the fibrils, also known as the β -sheet stagger.

7.1. Introduction

In recent years, MAS NMR has emerged as a high-resolution structural technique for complex insoluble biomolecular systems that cannot be studied by X-ray crystallography and solution NMR. This includes membrane protein systems in their native lipid environment and amyloid fibrils formed by a variety of proteins and peptides. High-resolution protein structure determination in NMR spectroscopy relies on the measurement of long-distance constraints in order to determine the fold of the protein. In MAS NMR this structural information is encoded in dipolar couplings and a large number of dipolar recoupling techniques have been developed to measure $^{15}\text{N}/^{13}\text{C}$ and $^{13}\text{C}/^{13}\text{C}$ distances in peptides and proteins. The recent advances in methodology, sample preparation and instrumentation, have made it possible to obtain *de novo* structural models of a variety of systems including the influenza-related M2 transmembrane domain,¹ the oligomers of the chaperone αB -crystallin² and the fibrils formed by Het-s(218-289)³ and A β (1-40).^{4,5} In some cases, truly atomic resolution has been possible, e.g. the structure of the TTR(105-115) amyloid fibrils presented in Chapter 4.

Despite the remarkable advances, however, the process of determining an unknown structure from MAS NMR data is still a formidable task. The distances necessary to obtain the 3D fold of the protein are usually quite long (4 – 8 Å), which means that sometimes very weak dipolar couplings need to be detected. The experimental observation of weak dipolar couplings in many cases is also hindered by a phenomenon known as dipolar truncation, where the presence of strongly coupled nearby spins can attenuate further the transfer to the distant spins of interest.^{6,7} Even in the cases when dipolar truncation can be circumvented, the unambiguous assignment of the long-range cross-peaks can still be very challenging due to spectral overlap and crowding. For example, constraining the “odd-even-odd-even” β -sheet interface in the TTR(105-115) amyloid fibrils (Chapter 4) required the use of specifically labeled samples and high field spectrometers in order to reduce the assignment ambiguity even for this relatively small system.

In this chapter, we present the experimental and labeling strategies that we have employed in order to obtain long-range correlations in β_2 -microglobulin ($\beta_2\text{m}$) amyloid fibrils formed at pH 2.5 and low ionic strength. In Chapter 5, we have shown that $\beta_2\text{m}$ fibrils contain an extensive rigid core with four known β -strands encompassing residues 26-31, 44-55, 60-64, 71-82.⁸ These β -strands are arranged in a parallel, in-register manner as described in Chapter

6.⁹ Here, we focus our attention on long-range correlations useful for obtaining sequential assignments and on correlations describing the quaternary structure of the fibrils, defined as the position and orientation of the β -sheets with respect to each other.¹⁰

7.2. Alternating labeling scheme

The standard method for producing isotopically enriched proteins involves *E. coli* expression in M9-rich media, where the ^{13}C and ^{15}N sources are ^{13}C -labeled glucose and ^{15}N labeled ammonium chloride, respectively.^{11,12} This provides a relatively inexpensive procedure for introducing ^{13}C and ^{15}N labels uniformly throughout the protein sequence. While uniformly labeled samples are an essential starting point for the structural studies of biological systems, they present certain disadvantages in the measurement of long-distance structural constraints. In particular, the dense network of strongly coupled ^{13}C atoms provides ideal conditions for dipolar truncation, where the one- and two-bond dipolar couplings dominate the recoupling dynamics and severely attenuate the transfer to the distant spins of interest. Neighboring ^{13}C atoms are also J-coupled ($J_{cc} = 30 - 60 \text{ Hz}$),¹² which leads to line broadening, and in some cases attenuation of the cross-peak intensity. In the rings of aromatic residues, the strong one-bond dipolar ^{13}C - ^{13}C couplings can serve as “polarization sinks” and aromatic cross-peaks are usually not observed in 2D ^{13}C - ^{13}C correlation spectra of uniformly labeled $\beta_2\text{m}$ amyloid fibrils. In addition, when the size of the protein becomes large, the number of expected cross-peaks increases and spectral overlap and crowding become a problem that cannot always be solved with the use of higher dimensional experiments.

The problems listed above can be partially resolved by utilizing the so-called alternating labeling scheme, where 2- ^{13}C or 1,3- ^{13}C glycerol is supplied as the carbon source in *E. coli* cultures. This method, first implemented by Le Master and Kushlan in the dynamics studies of thioredoxin by solution NMR,¹³ and later introduced to MAS NMR by Hong,¹⁴ leads to the placement of a ^{13}C label at every other position for the majority of the residues. The two types of glycerol give complementary labeling patterns, where a large number of the $\text{C}\alpha$ positions are labeled when 2- ^{13}C glycerol is utilized (supplemented with an equimolar amount of ^{13}C -labeled sodium bicarbonate), while the majority of the CO and $\text{C}\beta$ positions are labeled when the 1,3- ^{13}C glycerol form is used. In some amino acid types (E, Q, P, R, D, N, M, T, I, K, P), partial labeling of the $\text{C}\alpha$, $\text{C}\beta$, and CO positions occurs but as long as the expression time is

kept relatively short, adjacent positions are rarely labeled concurrently in the same molecule.¹⁵ The alternating placement of ^{13}C atoms eliminates the one-bond J-couplings and greatly reduces the line width for some cross-peaks, thus enhancing their intensity.^{15,16} For example, in $\beta_2\text{m}$ amyloid fibrils, G18 is only observed with sufficient intensity in 2- ^{13}C glycerol labeled samples. The elimination of many one-bond ^{13}C - ^{13}C couplings also mitigates the effects of dipolar truncation, and results in more efficient long-range polarization transfer as exemplified by the spectra discussed in the following sections.

7.3. Experiments for efficient recoupling of long-range correlations

7.3.1. BASE-RFDR

A large number of dipolar recoupling sequences, such as RFDR (radio frequency-driven recoupling),¹⁷ generate an effective Hamiltonian that contains zero-quantum (ZQ) and double-quantum (DQ) terms truncated to the zeroth-order. These pulse sequences are therefore particularly susceptible to the effects of dipolar truncation. A modified version of the RFDR experiment called BASE-RFDR (band-selective RFDR),¹⁸ shows a much improved performance over the broadband experiment with respect to the recoupling of distant spins. This experiment relies on the application of low-power, band-selective π pulses during the mixing period, with a band-width large enough to cover only the aliphatic region of the spectrum. This effectively excludes the CO atoms from participating in the polarization dynamics, improving the transfer efficiency between distant aliphatic spins. The use of alternating labeling further enhances the polarization transfer, resulting, for example, in efficient $\text{C}\alpha$ - $\text{C}\alpha$ recoupling, as shown in Figure 7.1. This spectrum, recorded with a $\beta_2\text{m}$ sample labeled with 2- ^{13}C glycerol as the carbon source (2- $\beta_2\text{m}$) shows many sequential $\text{C}\alpha$ - $\text{C}\alpha$ cross-peaks with an average ^{13}C - ^{13}C distances of ~ 4.5 Å. In principle, intermolecular interactions between adjacent layers of the β -sheets (distances $\sim 5.0 - 5.5$ Å) should also be detected in this type of experiment. However, due to the parallel, in-register arrangement of the β -strands in $\beta_2\text{m}$ fibrils, these interactions result in cross-peaks identical to the intramolecular $\text{C}\alpha$ - $\text{C}\alpha$ correlations.

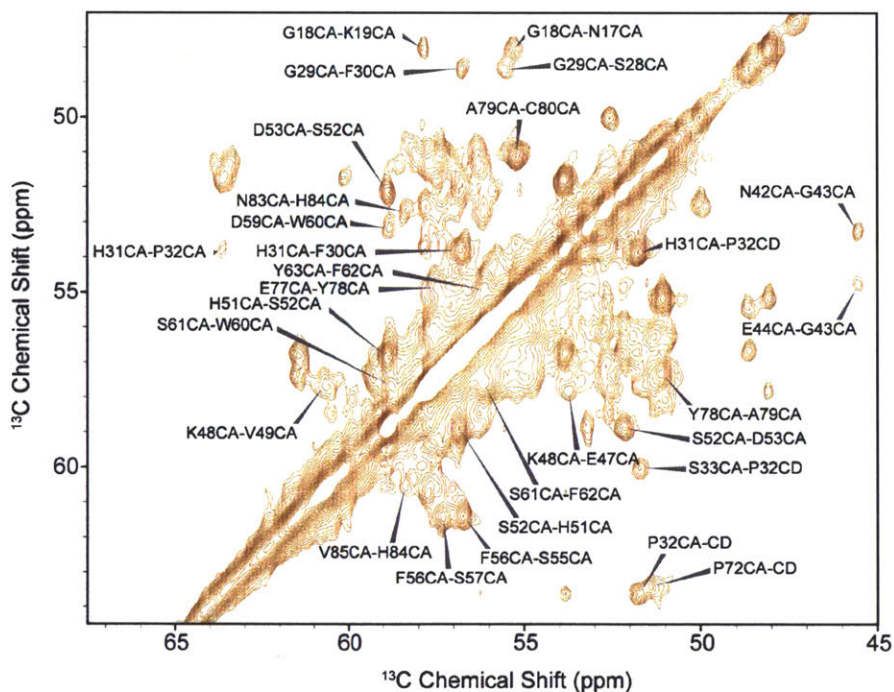


Figure 7.1: The C α region of a ^{13}C - ^{13}C correlation spectrum obtained with BASE-RFDR mixing ($\tau_{\text{mix}} = 18$ ms, $\omega_r/2\pi = 12.5$ kHz, 700 MHz ^1H Larmor frequency) with a 2- $\beta_2\text{m}$ amyloid fibril sample.

7.3.2. PDS/DARR

The proton-driven spin diffusion (PDS) experiment¹⁹ and its variant, the dipolar assisted rotational resonance (DARR) experiment,²⁰ are perhaps the most widely used ^{13}C - ^{13}C recoupling experiments in protein MAS NMR spectroscopy. They are easy to implement, work well at moderate MAS frequencies, and since they rely on second order effects, they are less susceptible to dipolar truncation. In particular, the ^{13}C - ^{13}C transfer is promoted by the second-order cross-terms $(^1\text{H} - ^{13}\text{C}) \times (^{13}\text{C} - ^{13}\text{C})$ and $(^{13}\text{C} - ^{13}\text{C}) \times (^{13}\text{C} - ^{13}\text{C})$ and occurs on the time scale of milliseconds to seconds.²¹ The recoupling efficiency of the mechanism arises from a relayed transfer through the ^{13}C spins, which allows the polarization to reach spins that are far away in space. This process, however, also makes it very difficult to quantify the transfer and extract distances from the cross-peak volumes. Therefore, these experiments are usually used similarly to the NOE experiments in solution NMR, where the structural constraints are divided into distance bins based on the mixing time when they first appear in the spectra.^{16,22}

While these experiments can yield a large number of long-range cross-peaks in the spectra, they are sometimes very difficult to identify and assign unambiguously. The use of alternating labeling can partially simplify the spectra, although the cross-peak assignment can still remain a formidable task. Several procedures for automated assignments of such spectra in combination with structure calculation have been published in the literature; however, they have only been applied to model proteins with well-known structures.²³⁻²⁵ In order to determine the *de novo* quaternary structure of a biological molecule like β_2 m amyloid fibrils, a reliable set of unambiguous distant constraints is necessary, and the manual assignment of spectra like the ones presented in Figures 7.2 and 7.3 cannot be avoided.

Figure 7.2 presents the PDS spectrum of a β_2 m fibril sample expressed with 1,3-¹³C glycerol as the carbon source (1,3- β_2 m). With this labeling scheme, only the Leu residues are completely labeled at the C α position, while several residue types (E, R, D, I, T) are partially labeled. This results in a well-resolved C α -C α region where sequential C α -C α cross-peaks between these residues can be easily identified and assigned. Many more complementary C α -C α cross-peaks have been identifying with the 2- β_2 m sample using BASE-RFDR¹⁸ (Figure 7.1) and a similar PDS experiment (see Figure 7.6).

The side-chains of hydrophobic residues like Val, Leu and Ile are important in the formation of β -sheet interactions in many proteins and since they comprise a large number of the residues in the β_2 m sequence, identifying any potential contacts between them in the spectra is important for defining the quaternary structure of the fibrils as well. The C γ atoms of the Val and Ile residues, and the C δ atoms of the Leu residues are labeled under the 1,3-¹³C glycerol scheme and provided that they can be assigned unambiguously (see discussion below), Val-Leu and Leu-Ile contacts should be identifiable in the PDS spectrum in Figure 7.2. This is indeed the case, and some of those contacts are labeled in blue in the spectrum. In particular, cross-peaks between the side-chain atoms of I46, V49 and L54 have been identified and assigned, indicating a possible turn around residue V49. In addition a contact between S52 C β and V49 C γ has been identified, corroborating this possibility.

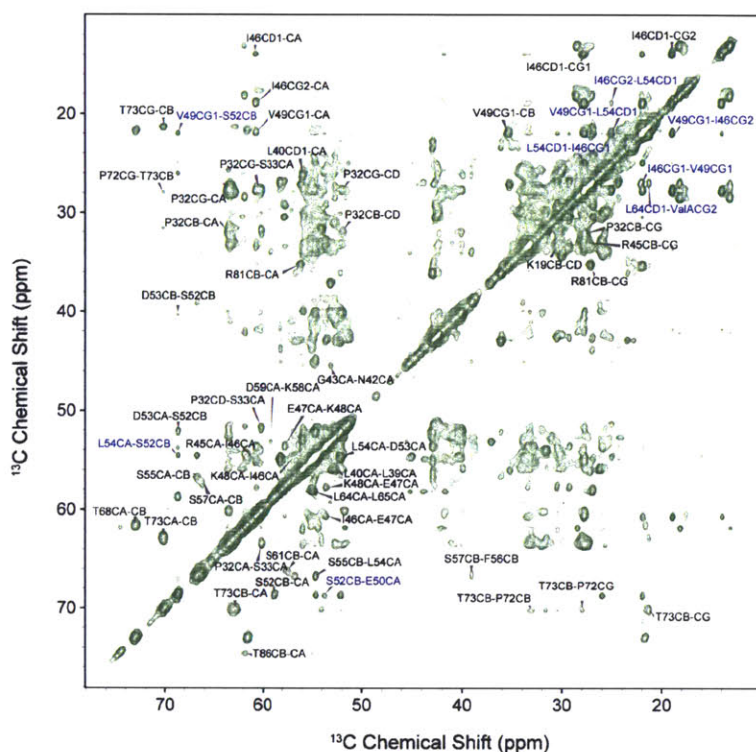


Figure 7.2: The aliphatic region of a ^{13}C - ^{13}C correlation spectrum obtained with PDSM mixing ($\tau_{\text{mix}} = 700$ ms, $\omega_r/2\pi = 15.7$ kHz, 750 MHz ^1H Larmor frequency) with a 1,3- $\beta_2\text{m}$ amyloid fibril sample. Correlations between residues distant in sequence are shown in blue.

7.3.3. Efficient recoupling of aromatic residues

Hydrophobic interactions involving aromatic residues and aromatic ring stacking can play an important role in stabilizing the structure of amyloid fibrils.²⁶ For example, in TTR(105-115) amyloid fibrils, the tyrosine residues are not only important in defining the β -sheet interface, but they also participate in the protofibril-to-protofibril arrangement (see Chapter 4). In $\beta_2\text{m}$, the hydrophobic stretch between residues 60 and 68 contains five aromatic residues with an important role in fibril formation.²⁷ Aromatic residues, however, are notoriously difficult to observe in uniformly labeled samples due to their large dipolar couplings of the adjacent atoms. They also have relatively large chemical shift anisotropies,²⁸ which affects the resolution and intensity at low and moderate MAS frequencies. In some cases, the motion of the aromatic rings, e.g. ring flips and librations,²⁹⁻³² can occur on the time scale of the experiment and interfere with the polarization transfer and/or the heteronuclear

decoupling, and thus cause line broadening and further attenuation of the signals with any labeling scheme.

PDS experiments on samples labeled with 1,3- and 2-glycerol show improved aromatic-to-aromatic and aromatic-to-aliphatic transfer (Figure 7.3). Surprisingly, however, the largest number of aromatic cross-peaks occurs at experimental conditions different from those optimal for aliphatic-to-aliphatic transfer. For β_2 m fibril samples, performing PDS experiments at $\omega_r/2\pi = 12.5$ kHz and $\tau_{\text{mix}} = 500$ ms results in the optimal trade-off between resolution and long-range transfer efficiency for the aliphatic region (Figure 7.2), however, these are not the best parameters for the aromatic region (Figure 7.3). We evaluated the performance of the PDS aromatic transfer efficiency as a function of the MAS frequency and found that the most favorable conditions were $\omega_r/2\pi = 15.7$ kHz and $\tau_{\text{mix}} = 700$ ms for both 1,3- β_2 m and 2- β_2 m labeled fibril samples. This observation is quite unexpected since spin diffusion is in principle attenuated at higher MAS frequencies, which reduce the effective dipolar couplings central to the spin diffusion process. In the aromatic case, however, higher MAS frequency leads to better averaging of the chemical shift anisotropy and better linewidth, which partly compensates for the loss in polarization efficiency. Aromatic rings in peptides and proteins can also experience slow-motion librations in the range of 1-10 kHz,³² and it is possible that these motions interfere with the polarization transfer at lower MAS frequencies.

The complementary sets of data performed with the 1,3- β_2 m and 2- β_2 m labeled fibril samples are shown in Figure 7.3, where many more correlations between aromatic side-chains and the side-chains of non-aromatic residues can be observed with $\omega_r/2\pi = 15.7$ kHz and $\tau_{\text{mix}} = 700$ ms. Some of these correlations occur between residues that are far away in sequence, e.g. Y78 to V27, that are, however, placed in proximity to each other in the quaternary arrangement of the fibrils by the disulfide bridge between C25 and C80. Other cross-peaks indicate the proximity of the side-chains of residues W60 and F56, implying the presence of a turn and a hydrophobic pocket in this region of the sequence.

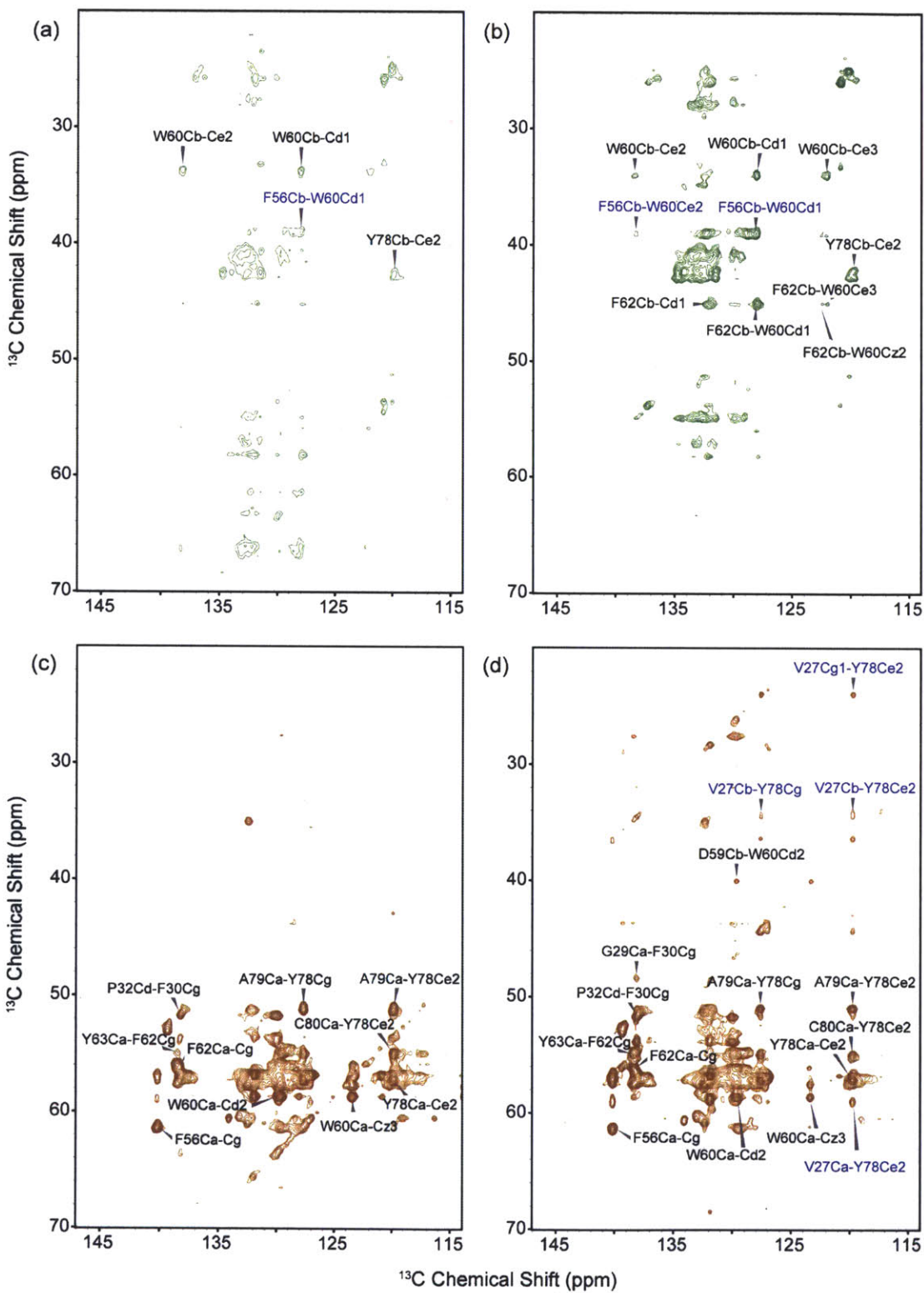


Figure 7.3: The aromatic regions of ^{13}C - ^{13}C correlation spectra obtained with PDSM mixing with (a) and (b) 1,3- $\beta_2\text{m}$ and (c) and (d) 2- $\beta_2\text{m}$ amyloid fibril sample. The spectra shown in (a) and (c) were obtained with $\tau_{\text{mix}} = 500$ ms and $\omega_r/2\pi = 12.5$ kHz, while the spectra in (b) and (d) were obtained with $\tau_{\text{mix}} = 700$ ms and $\omega_r/2\pi = 15.7$ kHz. Identified long-range correlations are shown in blue.

7.3.4. TSAR-based experiments

Another set of experiments relying on second-order effects and thus less susceptible to dipolar truncation, are based on the third-spin assisted recoupling (TSAR) mechanism.³³⁻³⁵ In this case, the terms that mediate the transfer are of the form $C_1^\pm C_2^\mp H_z$ for ^{13}C - ^{13}C recoupling, and $N^\pm C_2^\mp H_z$ for ^{15}N - ^{13}C recoupling. This implies that the transfer between two ^{13}C atoms or between a ^{15}N and a ^{13}C atom is mediated by a nearby ^1H spin. The homonuclear version of the experiment is known as proton assisted recoupling (PAR),³³ while the heteronuclear form is called proton assisted insensitive nuclei cross-polarization (PAIN-CP).^{34,35} Since these experiments do not involve direct ^{13}C - ^{13}C or ^{15}N - ^{13}C couplings, relayed polarization transfer is minimal. The size of the cross-terms, however, also depends on the geometry of the three-spin system, and is therefore not directly proportional to the distance of the two spins of interest. Thus, these experiments are also hard to quantify and the obtained constraints are used in a similar fashion as the ones obtained by the PDSM/DARR type of experiments. The TSAR based-experiments, however, offer several advantages: they are efficient at high MAS frequencies; they usually yield less crowded spectra than the spin-diffusion based experiments due to the absence of relayed transfer; and the transfer occurs on the 2-20 ms time scale, as opposed to the 200 ms – 1 sec mixing times required for PDSM experiments.

Figure 7.4 shows PAIN-CP spectra obtained with 1,3- $\beta_2\text{m}$ and 2- $\beta_2\text{m}$ labeled fibril samples, while Figure 7.5 shows a section of a PAR spectrum, obtained with a specifically labeled $\beta_2\text{m}$ sample (see discussion below). The N $\text{C}\alpha$ correlations observed in the PAIN-CP spectra can be very helpful for the sequential assignment of the backbone atoms in the $\beta_2\text{m}$ sequence, as one C α atom can give correlations to its directly bonded ^{15}N atom, and the ^{15}N atoms of the preceding and following residues. For example, G29 C α gives rise to cross-peaks corresponding to G29N-C α , F30N-G29C α and S28N-G29C α , as illustrated in Figure 7.4a. While in principle the one-bond N-C α correlations should be relatively weak at this long-

mixing time, in β_2 m fibril samples their intensity arises also from intermolecular interactions between the parallel, in-register β -strands. While the majority of the cross-peaks in the NC α region of the PAIN-CP spectra are sequential, some weak cross-peaks attributed to residues that are relatively far away in sequence can be observed. For example, the S28N-P32C α cross-peak in Figure 7.4a indicates the presence of a turn around the P32 residue.

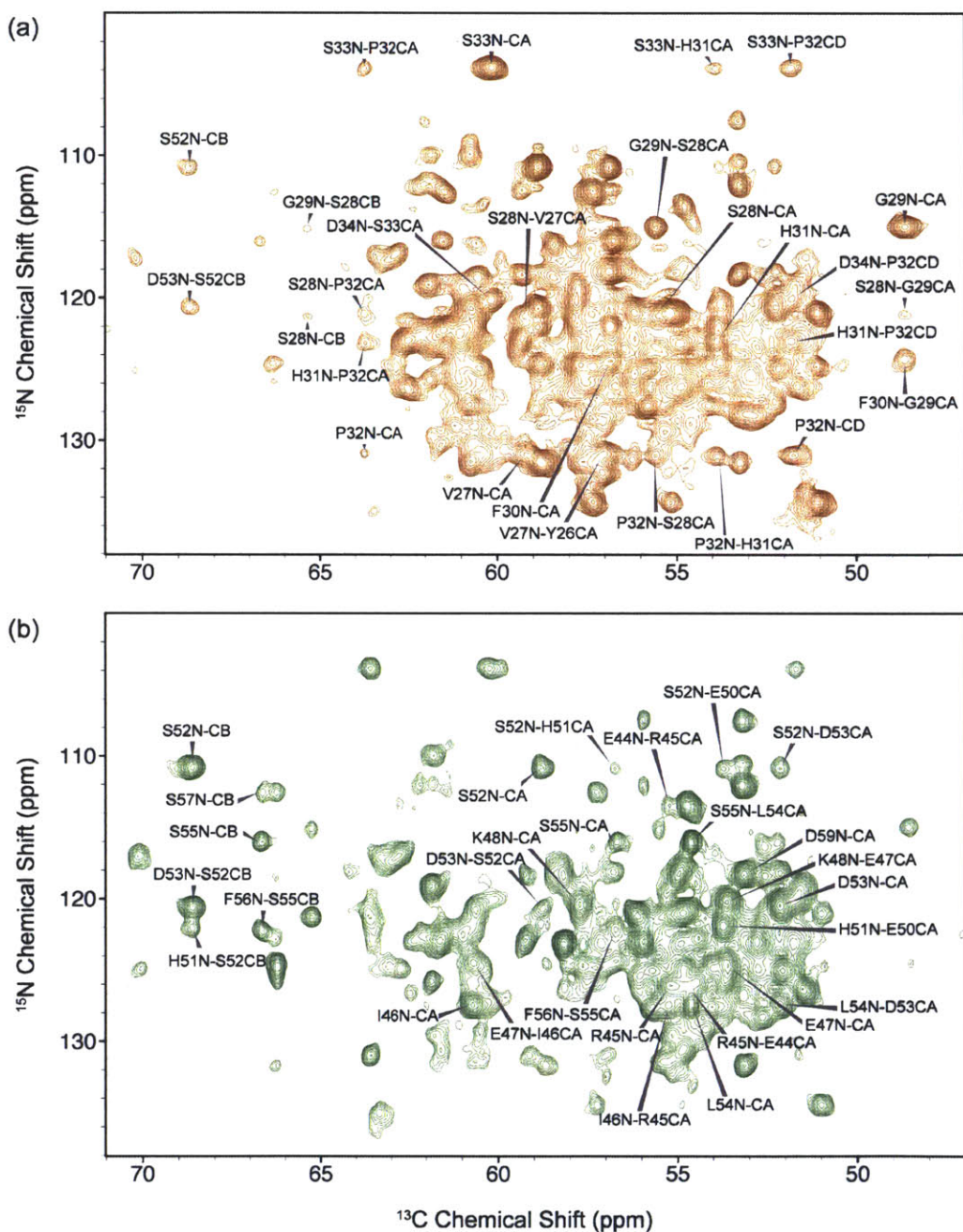


Figure 7.4: The NC α regions of ^{15}N - ^{13}C correlation spectra obtained with PAINCP mixing ($\tau_{\text{mix}} = 8$ ms, $\omega_r/2\pi = 20$ kHz, 900 MHz ^1H Larmor frequency) with (a) 2- β_2 m, and (b) 1,3- β_2 m amyloid fibril sample. Peak assignments for residues 27-34 and 44-56 are shown in (a) and (b) respectively.

7.4. Specific labeling for unambiguous assignments

The use of the alternating labeling scheme provides improved resolution and efficiency that are crucial in obtaining long-range contacts in many biological systems. Even with this scheme, however, the spectral overlap can still be quite significant. In addition, since only some atoms are labeled per residue, e.g. the Val C γ 1 and C γ 2, but not the Val C β in 1,3- ^{13}C glycerol samples, and since the chemical shifts for the Val C γ 1 and C γ 2 atoms can be similar, it might not be possible to distinguish between the different Val residues in 1,3- $\beta_2\text{m}$ spectra. In order to complement the data obtained with the 1,3- $\beta_2\text{m}$ and 2- $\beta_2\text{m}$ labeled fibril samples, we also used a sample specifically labeled with ^{13}C only at the Val, Leu and Tyr residues (VYL- $\beta_2\text{m}$). These residues represent 19 out of the 99 residues in the $\beta_2\text{m}$ sequence. While, in principle, these residues are uniformly labeled in this sample, and therefore more likely to lead to dipolar truncation, the PAR experiment described above works well and several cross-peaks for residues distant in space can be observed in the spectrum (Figure 7.5). The aliphatic side-chain region of the spectrum provides excellent resolution for the Val and Leu side-chains, significantly simplifying the assignment procedure.

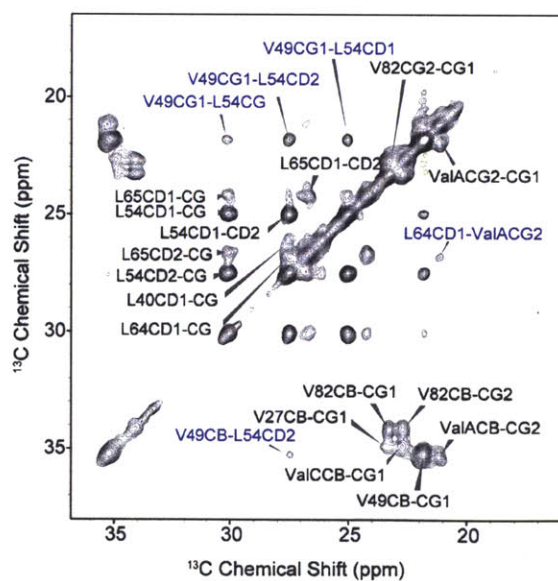


Figure 7.5: The aliphatic region of a ^{13}C - ^{13}C correlation spectrum obtained with PAR mixing ($\tau_{\text{mix}} = 10$ ms, $\omega_r/2\pi = 20$ kHz, 900 MHz ^1H Larmor frequency) with a VYL- $\beta_2\text{m}$ amyloid fibril sample. Long-range correlations are shown in blue.

7.5. Distinguishing between *inter*-molecular and *intra*-molecular interactions

The experiments presented so far have been performed with 100% isotopically enriched samples, i.e. all the molecules in the sample are in principle labeled in the same fashion. Therefore, it is not possible to determine whether the quaternary contacts observed in the spectra arise from *inter*- or *intra*-molecular interactions. This is an important question in the context of quaternary amyloid fibril structure, as evidence for the staggering of the β -sheets has been observed in some systems. For example, in the amyloid fibrils formed by the A β (1-40) peptide, each β -strand interacts with a β -strand from the opposite β -sheet formed by a different A β (1-40) molecule, leading to the so-called STAG(\pm 2) arrangement.¹⁰ Similar staggering has also been observed in the fibrils formed by the K3 β_2 m segment (residues 20-41).³⁶ Other, more complicated arrangements involving inter-molecular interactions might also be possible.

In order to distinguish between inter-molecular and intra-molecular cross-peaks, we prepared two additional samples: a mixture of 2- β_2 m labeled monomers diluted with monomers prepared with ¹³C-depleted glucose in a ratio of 1:1 (dilute 2- β_2 m), and a similar sample using 1,3- β_2 m labeled monomers (dilute 1,3- β_2 m). We recorded long-range PDS experiments ($\tau_{\text{mix}} = 500$ ms) and compared the spectra of the dilute and 100% labeled samples with the expectation that peaks due to inter-molecular interactions will be absent or much weaker in the dilute preparation. Figure 9.6 presents the comparison for the two 2- β_2 m samples, where the spectrum of the fully labeled preparation was recorded with 64 scans per t_1 point, and the spectrum of the dilute sample was recorded with 128 scans. The same contour levels were plotted for each spectrum. A similar data set for the 1,3- β_2 m samples is shown in Figure 7.7.

A brief look at Figures 7.6 and 7.7 reveals that many of the cross-peaks preserve their intensity in the isotopically dilute preparations, implying that many of the observed correlations arise from intramolecular interactions. This includes the structurally interesting correlations between I46, V49, S52 and L54. There are, of course, cross peaks that disappear or have much attenuated intensities in the dilute samples, but we attribute their behavior mostly to the peculiarities of the glycerol labeling. For example, the cross-peaks assigned to V49C α -C γ 1 (2- β_2 m samples), A79C α -C β , and L54C α -C β (1,3- β_2 m samples) are present in the fully labeled samples due to scrambling. However, as adjacent positions like C α and C β

are rarely labeled concurrently in the same molecule,¹⁶ these correlations are intermolecular and due to the parallel, in-register arrangement of the β -strands in β_2 m fibrils. Therefore, these cross-peaks should be absent from the spectra of dilute samples, as is indeed the case. The analysis of the presented spectra is still ongoing, however, the data so far indicates the absence of significant staggering of the β -sheets in the fibrils, and that the majority of the structurally relevant correlations are intramolecular. This observation is also consistent with the presence of a disulfide bond between residues C25 and C80, which places the β -strands centered around these residues in close proximity to each other, including in the vertical direction.

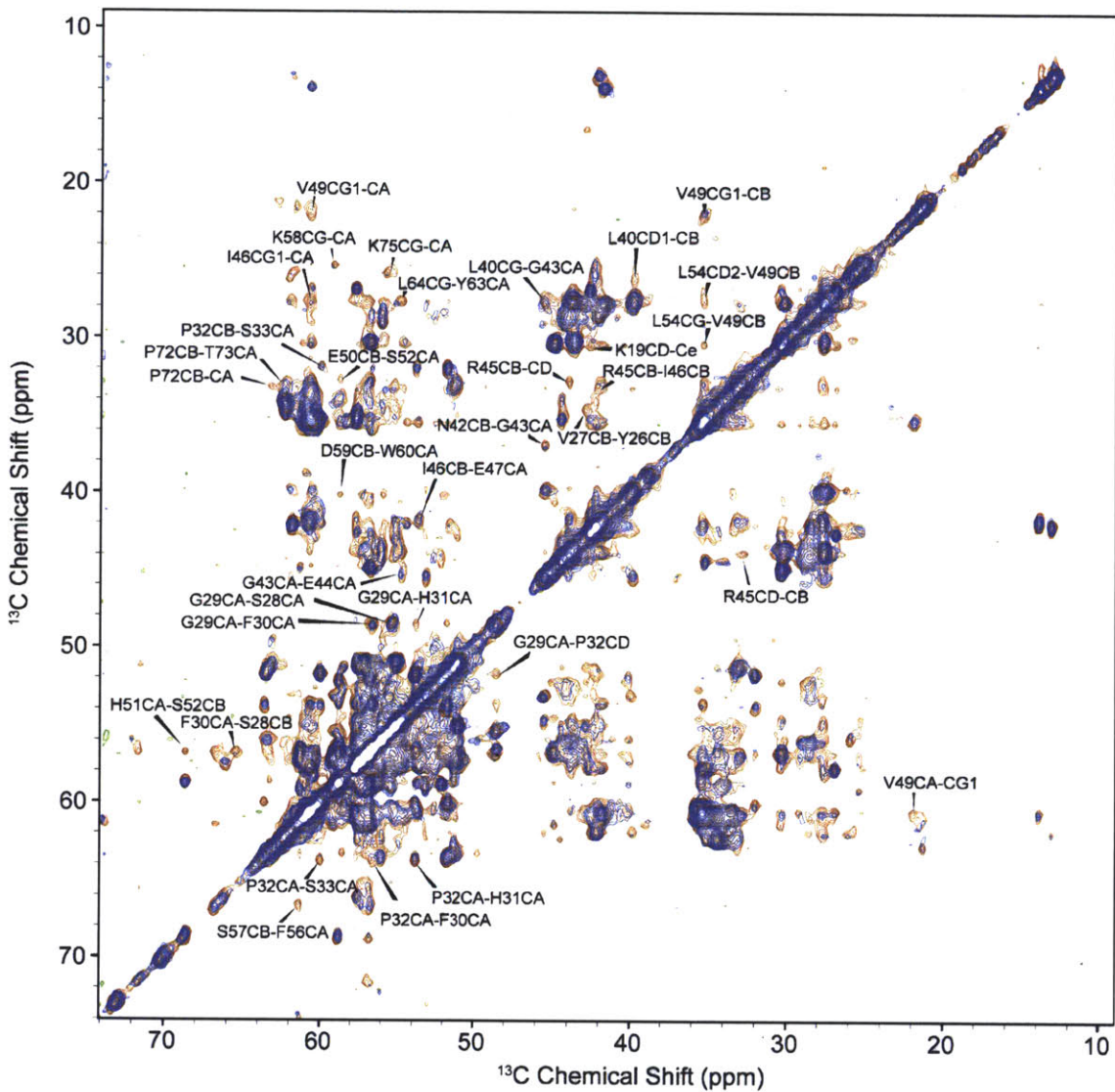


Figure 7.6: Comparison of ^{13}C - ^{13}C correlation spectra obtained with PSD mixing ($\tau_{\text{mix}} = 500$ ms, $\omega_r/2\pi = 12.5$ kHz, 750 MHz ^1H Larmor frequency) of a 100% labeled 2- $\beta_2\text{m}$ sample (brown) and a dilute 2- $\beta_2\text{m}$ sample (blue). Labels correspond to assigned cross-peaks that appear with much greater intensity in the 100% labeled sample or cross-peaks that are important for determining the quaternary structure of the fibrils.

7.6. Summary of observed quaternary structural constraints in β_2 m fibrils

The disulfide-bond between residues C25 and C80 places an important quaternary structural constraint by bringing the backbones of neighboring residues within 6-7 Å of each other in space. Therefore, long-range cross-peaks for residues in these regions should be expected. Such contacts between residues Y78 and V27 are indeed observed in the 1,3- β_2 m PDS spectrum optimized for aromatic transfer (Figure 7.3). This experiment also contains cross-peaks between residues F56, K58, W60, and F62 (not all shown in Figure 7.3), thus defining a turn around residues 58 and 59, potentially stabilized by numerous hydrophobic aromatic-to-aromatic interactions. The existence of this turn was also predicted by the secondary structure analysis of the β_2 m fibrils, as shown in Chapter 5.

The long-range correlation spectra of the 1,3- β_2 m, 2- β_2 m and VYL- β_2 m samples contain many cross-peaks connecting residues I46, V49, S52, and L54. The analysis of the dilute 1,3- β_2 m and 2- β_2 m samples confirms that many of these cross-peaks arise from intramolecular interactions, and therefore suggests that an intramolecular turn exists in this part of the sequence as well. This is perhaps surprising as the secondary structure analysis in Chapter 5 overall predicts that this region is a part of a long β -sheet. While many residues in this segment, including V49 and L54 do have N, C α , CO and C β chemical shifts and predicted torsion angles consistent with a β -sheet, several other residues (I46, K48 and S52) give more ambiguous results. Since no additional information was available at the time, this region was overall predicted to be a part of a β -sheet. The new information available from the long-range experiments presented here can help resolve such ambiguities and provide much more detailed and subtle structural constraints.

Acknowledgements

The samples described in this chapter were prepared by Dr. Geoffrey Platt and Theodoros Karamanos in Prof. Sheena Radford's group at the University of Leeds. The outlined experiments were designed and performed in collaboration with Dr. Marvin Bayro. We thank Ajay Thakkar and Dr. David Ruben for assistance and maintenance of the NMR spectrometers used in this study, and Mathew Eddy, Loren Andreas, Dr. Gael de Paepe, Dr. Patrick van der Wel, and Dr. Kendra Frederick for many helpful discussions.

References:

- (1) Cady, S. D.; Schmidt-Rohr, K.; Wang, J.; Soto, C. S.; DeGrado, W. F.; Hong, M. *Nature* **2010**, *463*, 689-U127.
- (2) Jehle, S.; Rajagopal, P.; Bardiaux, B.; Markovic, S.; Kuhne, R.; Stout, J. R.; Higman, V. A.; Klevit, R. E.; van Rossum, B. J.; Oschkinat, H. *Nature Structural & Molecular Biology* **2010**, *17*, 1037-U1.
- (3) Wasmer, C.; Lange, A.; Van Melckebeke, H.; Siemer, A. B.; Riek, R.; Meier, B. H. *Science* **2008**, *319*, 1523-1526.
- (4) Petkova, A. T.; Ishii, Y.; Balbach, J. J.; Antzutkin, O. N.; Leapman, R. D.; Delaglio, F.; Tycko, R. *Proc. Natl. Acad. Sci. U. S. A.* **2002**, *99*, 16742-16747.
- (5) Paravastu, A. K.; Leapman, R. D.; Yau, W. M.; Tycko, R. *Proc. Natl. Acad. Sci. U. S. A.* **2008**, *105*, 18349-18354.
- (6) Bayro, M. J.; Huber, M.; Ramachandran, R.; Davenport, T. C.; Meier, B. H.; Ernst, M.; Griffin, R. G. *J. Chem. Phys.* **2009**, *130*.
- (7) Hohwy, M.; Rienstra, C. M.; Griffin, R. G. *J. Chem. Phys.* **2002**, *117*, 4973-4987.
- (8) Debelouchina, G. T.; Platt, G. W.; Bayro, M. J.; Radford, S. E.; Griffin, R. G. *J. Am. Chem. Soc.* **2010**, *132*, 10414-10423.
- (9) Debelouchina, G. T.; Platt, G. W.; Bayro, M. J.; Radford, S. E.; Griffin, R. G. *J. Am. Chem. Soc.* **2010**, *132*, 17077-17079.
- (10) Petkova, A. T.; Yau, W. M.; Tycko, R. *Biochemistry* **2006**, *45*, 498-512.
- (11) McIntosh, L. P.; Dahlquist, F. W. *Quart. Rev. Biophys.* **1990**, *23*, 1-38.
- (12) Cavanagh, J.; Fairbrother, W.; Palmer, A. G.; Skelton, N. J. *Protein NMR Spectroscopy: Principles and Practice*; Academic Press: New York, 1996.
- (13) LeMaster, D. M.; Kushlan, D. M. *J. Am. Chem. Soc.* **1996**, *118*, 9255-9264.
- (14) Hong, M. *J. Magn. Reson.* **1999**, *139*, 389-401.
- (15) Castellani, F.; van Rossum, B.; Diehl, A.; Schubert, M.; Rehbein, K.; Oschkinat, H. *Nature* **2002**, *420*, 98-102.
- (16) Castellani, F.; van Rossum, B. J.; Diehl, A.; Rehbein, K.; Oschkinat, H. *Biochemistry* **2003**, *42*, 11476-11483.
- (17) Bennett, A. E.; Ok, J. H.; Griffin, R. G.; Vega, S. *J. Chem. Phys.* **1992**, *96*, 8624-8627.

- (18) Bayro, M. J.; Maly, T.; Birkett, N. R.; Dobson, C. M.; Griffin, R. G. *Angew. Chem., Int. Ed.* **2009**, *48*, 5708-5710.
- (19) Szeverenyi, N. M.; Sullivan, M. J.; Maciel, G. E. *J. Magn. Reson.* **1982**, *47*, 462-475.
- (20) Takegoshi, K.; Nakamura, S.; Terao, T. *Chem. Phys. Lett.* **2001**, *344*, 631-637.
- (21) Grommek, A.; Meier, B. H.; Ernst, M. *Chem. Phys. Lett.* **2006**, *427*, 404-409.
- (22) Zech, S. G.; Wand, A. J.; McDermott, A. E. *Journal of the American Chemical Society* **2005**, *127*, 8618-8626.
- (23) Manolikas, T.; Herrmann, T.; Meier, B. H. *J. Am. Chem. Soc.* **2008**, *130*, 3959-3966.
- (24) Loquet, A.; Bardiaux, B.; Gardienet, C.; Blanchet, C.; Baldus, M.; Nilges, M.; Malliavin, T.; Bockmann, A. *J. Am. Chem. Soc.* **2008**, *130*, 3579-3589.
- (25) Fossi, M.; Castellani, T.; Nilges, M.; Oschkinat, H.; van Rossum, B. J. *Angew. Chem., Int. Ed.* **2005**, *44*, 6151-6154.
- (26) Sawaya, M. R.; Sambashivan, S.; Nelson, R.; Ivanova, M. I.; Sievers, S. A.; Apostol, M. I.; Thompson, M. J.; Balbirnie, M.; Wiltzius, J. J. W.; McFarlane, H. T.; Madsen, A. O.; Riek, C.; Eisenberg, D. *Nature* **2007**, *447*, 453.
- (27) Platt, G. W.; Routledge, K. E.; Homans, S. W.; Radford, S. E. *J. Mol. Biol.* **2008**, *378*, 251-263.
- (28) Ye, C. H.; Fu, R. Q.; Hu, J. Z.; Hou, L.; Ding, S. W. *Magn. Reson. Chem.* **1993**, *31*, 699-704.
- (29) Rice, D. M.; Wittebort, R. J.; Griffin, R. G.; Meirovitch, E.; Stimson, E. R.; Meinwald, Y. C.; Freed, J. H.; Scheraga, H. A. *J. Am. Chem. Soc.* **1981**, *103*, 7707-7710.
- (30) Rice, D. M.; Meinwald, Y. C.; Scheraga, H. A.; Griffin, R. G. *J. Am. Chem. Soc.* **1987**, *109*, 1636-1640.
- (31) Gall, C. M.; Cross, T. A.; Diverdi, J. A.; Opella, S. J. *Proc. Natl. Acad. Sci. U. S. A.* **1982**, *79*, 101-105.
- (32) Kameda, T.; Ohkawa, Y.; Yoshizawa, K.; Nakano, E.; Hiraoki, T.; Ulrich, A. S.; Asakura, T. *Macromolecules* **1999**, *32*, 8491-8495.
- (33) De Paepe, G.; Lewandowski, J. R.; Loquet, A.; Bockmann, A.; Griffin, R. G. *J. Chem. Phys.* **2008**, *129*.
- (34) Lewandowski, J. R.; De Paepe, G.; Griffin, R. G. *J. Am. Chem. Soc.* **2007**, *129*, 728-729.

- (35) De Paepe, G.; Lewandowski, J. R.; Loquet, A.; Eddy, M.; Megy, S.; Bockmann, A.; Griffin, R. G. *J. Chem. Phys.* **2011**, *134*.
- (36) Iwata, K.; Fujiwara, T.; Matsuki, Y.; Akutsu, H.; Takahashi, S.; Naiki, H.; Goto, Y. *Proc. Natl. Acad. Sci. U. S. A.* **2006**, *103*, 18119-18124.

Chapter 8. Structural Comparison of Three Distinct β_2 -Microglobulin Amyloid Fibril Morphologies

Section 8.2 was adapted from from “Magic Angle Spinning NMR Analysis of β_2 -Microglobulin Fibrils in Two Distinct Morphologies” by Debelouchina GT, Platt GW, Bayro MJ, Radford SE, Griffin RG, published in J. Am. Chem. Soc. 2010, 132, 10414-10423.

Summary

Fibril polymorphism is a characteristic feature of many amyloidogenic proteins and peptides and represents one of the most challenging aspects of studying amyloid fibril structure. β_2 -Microglobulin (β_2 m) forms amyloid fibrils with different morphologies when different growth conditions are used. The long, straight (LS) fibrils formed at pH 2.5 and low salt concentration are the best characterized morphology, but β_2 m can also form curved, worm-like (WL) fibrils at pH 3.6 and high ionic strength. Here, we compare MAS NMR spectra of the two morphologies and conclude that the two forms share a common fibril core, but that the WL fibrils display a much higher degree of dynamics. We also investigate the structure of a truncation variant of β_2 m, lacking the first six residues of the sequence (Δ N6). Unlike the full-length protein, Δ N6 easily forms fibrils at physiological conditions. Here, we show evidence that this truncation variant has a different structure from the LS fibrils.

8.1. Fibril polymorphism

Fibril polymorphism is a characteristic feature of many amyloidogenic proteins and peptides and represents one of the most challenging aspects of studying amyloid fibril structure.¹⁻³ For fibrils formed *in vitro*, changes in the experimental conditions like varying the salt concentration, pH and temperature can lead to fibrils with distinct morphological appearance as recognized by cryoEM and AFM.⁴ Sometimes, even subtle changes in the growth condition can produce dramatic structural differences. For example, depending on whether the A β (1-40) peptide solution is agitated or not during fibril growth, fibrils with a striated ribbon appearance or twisted morphology form, and the structural models determined by MAS NMR spectroscopy also indicate that these morphological differences are propagated at the atomic level.^{3,5,6} Even in the case when fibrils with homogeneous appearance can be obtained under a certain growth condition, however, different chemical environments within the fibril can lead to the appearance of several sets of chemical shifts in the spectra that can complicate spectral interpretation and structure determination. A case in point is the GNNQQNY peptide, which not only can form both crystals and fibrils just depending on the concentration of peptide used, but the homogenous fibril samples always display three sets of chemical shifts in the MAS NMR spectra.^{7,8} Fibril polymorphism, however, also forms the basis of conformation-based inheritance in prions and therefore can have a very important role in many organisms and diseases.^{9,10}

Although associated with the disease dialysis-related amyloidosis, native β_2 -microglobulin does not aggregate under physiological conditions even at high concentration. Fibrillization is initiated only with the addition of trigger molecules such as Cu²⁺, glycosaminoglycans, proteoglycans and collagen, in solvents containing TFE or SDS, at high temperature or with ultrasonication.^{11,12} A truncated variant of the protein, however, lacking the six N-terminal residues (Δ N6) is highly amyloidogenic, can form amyloid fibrils spontaneously, and in catalytic amounts can convert the native protein into a rare amyloidogenic conformation.¹³

At pH 2.5 and low ionic strength, an acid unfolded state of β_2 -microglobulin is highly populated and fibril formation proceeds rapidly with a lag-dependent kinetics.¹⁴ The fibrils formed under these conditions are highly homogeneous, they are long and straight (LS) in appearance, and are the best characterized morphology of β_2 m amyloid species (Figure 8.1).¹⁵⁻

¹⁹ At slightly higher pH (pH = 3.6), worm-like (WL) or rod-like fibrils can be formed

depending on the ionic strength of the solution.⁴ The WL fibrils form with lag-independent kinetics, bind amyloid-specific dyes such as Congo Red and Thioflavin T, but produce fiber diffraction patterns indicative of a less organized fibril core.²⁰⁻²² EPR studies of spin-labeled WL fibrils also indicated that their structural organization is very different from the organization of the LS fibrils.¹⁹

In this chapter, we try to understand the basis for structural polymorphism in β_2 m fibrils, and we compare the MAS NMR spectra of the well-characterized LS fibrils to the WL fibrils, and to the fibrils formed by the truncation variant Δ N6.

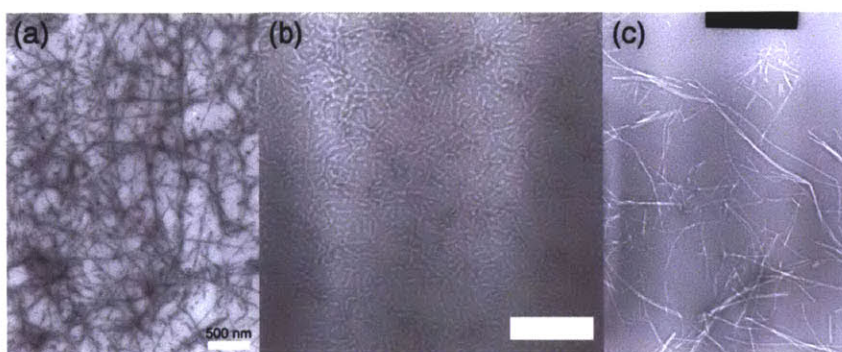


Figure 8.1. CryoEM images of β_2 -microglobulin fibrils with distinct morphologies: (a) long, straight (LS) fibrils formed at pH 2.5 and 50 mM ionic strength; (b) worm-like (WL) fibrils formed at pH 3.6 and 200 mM salt. (c) CryoEM image of the fibrils formed by the Δ N6 variant of β_2 m at pH 6.2 and 175 mM ionic strength. Scale bars correspond to 500 nm, 200 nm, and 1000 nm respectively.

8.2. Comparison of LS and WL fibrils

In this section we investigate the structural and dynamic differences and similarities of the LS fibrils formed by β_2 m at pH 2.5 and low ionic strength (50 mM), and the WL fibrils formed at pH 3.6 and high ionic strength (200 mM).⁴ Buffers containing high concentrations of ions can significantly decrease the RF performance of conventional MAS NMR probes and increase the potential to overheat and damage the sample during data collection.²³ In order to avoid this problem, after formation and ultracentrifugation in 200 mM formate buffer, the WL fibrils were washed and repelleted in 50 mM buffer. The EM images of the fibrils before and approximately three weeks after the change of ionic strength did not reveal any detectable differences in their length and morphology.

Figure 8.2 compares 1D spectra recorded with CP (cross polarization) and INEPT ^{13}C magnetization preparation steps for both fibril forms. As was observed for the LS fibrils, the WL fibrils also contain a rigid fibril core as shown by their CP spectrum (Figure 8.2b), although the resolution of this spectrum is lower than that observed in the CP spectrum of the LS fibrils (Figure 8.2a). The INEPT spectrum of the WL fibrils (Figure 8.2d) contains more peaks than that of the LS fibrils (Figure 8.2c), indicating that the WL fibrils are characterized by enhanced mobility. Specifically, the WL fibrils seem to exhibit increased mobility in the backbone, as shown by the presence of more lines in the $\text{C}\alpha$ region (40-60 ppm) of their INEPT spectrum, and in a few aromatic side-chains (110-140 ppm).

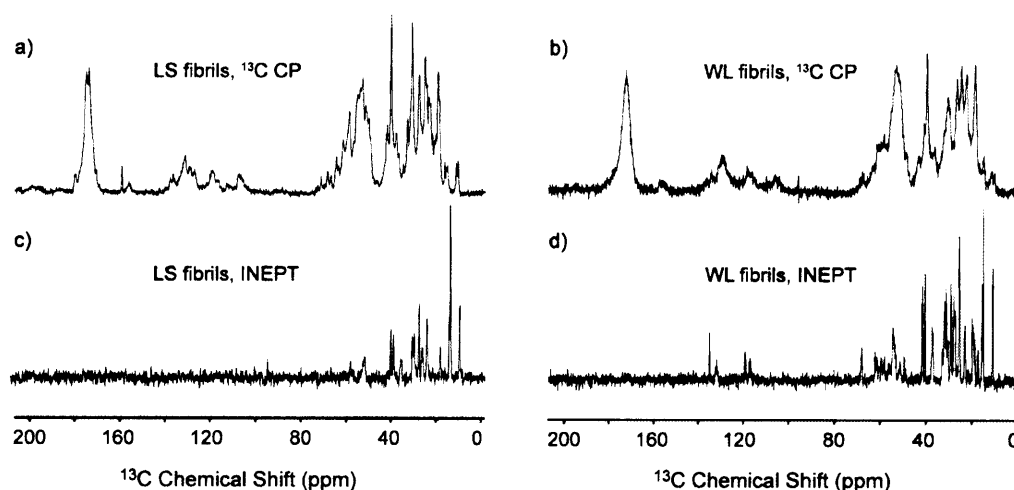


Figure 8.2. Comparison of CP (a and b) and INEPT (c and d) spectra of the LS U- $\beta_2\text{m}$ fibrils (a and c) and WL U- $\beta_2\text{m}$ fibrils (b and d). All spectra were obtained at 750 MHz in a 2.5 mm rotor (~ 5 mg of sample). The spectra in a), b) and d) were recorded with $\omega_r/2\pi = 12.5$ kHz and 128 scans, while c) was recorded with $\omega_r/2\pi = 16.7$ kHz with 32 scans.

To compare the rigid cores of the two fibril forms, we recorded a ^{13}C - ^{13}C correlation spectrum of the WL fibrils with $\tau_{\text{mix}} = 2.56$ ms in an RFDR experiment. Figure 8.3 depicts a superposition of this spectrum with the RFDR spectrum of the LS fibrils (labels corresponding to the LS fibril assignments). The $\text{C}\alpha$ - $\text{C}\beta$ region of the WL fibrils is noticeably less resolved, and the relative intensities of some cross-peaks are significantly different. For example, only one of the five threonine residues present in the $\beta_2\text{m}$ sequence (T73) appears as a clearly resolved peak in the WL fibril spectrum, while the unassigned serine $\text{C}\alpha$ - $\text{C}\beta$ cross-

peak (marked with asterisks) is much stronger than in the LS fibril spectrum. On the other hand, the positions of many cross-peaks coincide for the two samples, including cross-peaks that belong to P32, S33, I46, K48, S52, A79, and V85 in the LS fibrils. These residues span all assigned regions of the LS fibrils, implying that the two fibril forms share a similar core. The WL fibrils, however, display a higher level of molecular disorder that compromises the resolution and the sensitivity of the dipolar spectra. This low sensitivity did not allow us to perform further experiments on this sample (Figure 10.2a and b). Nevertheless, our findings suggest that the rigid core of the WL fibrils may involve similar residues but is shorter in length than the core of the LS fibrils.

The LS and WL fibrils are distinct classes and each is formed by divergent and competitive assembly pathways from the unfolded/partially folded monomers in equilibrium under the assembly conditions employed. As a consequence, the fibril type(s) that result from assembly can be modulated by alteration of the conditions under which the protein is incubated. Accordingly, pure LS fibrils form at low ionic strength and low pH, pure WL fibrils form at pH 3.6 at high ionic strength, while mixtures of the two are formed under conditions between these extremes.²⁰ Thus, by careful control of the solution conditions samples containing each morphologically dissimilar species can be prepared exclusively. WL fibrils are a kinetically trapped species formed *via* a non-nucleated reaction, whereas the LS fibrils form with classic amyloid-like nucleation dependent kinetics.^{4,20,24,25} The MAS NMR data presented here show that, in common with LS fibrils, WL fibrils exhibit a protected core that is rigid and hence amenable to solid-state NMR methods. Many chemical shifts located throughout the polypeptide sequence are similar to those found in LS fibrils, suggesting that there could be a high degree of structural similarity between these two fibril types. However, there are also differences between the spectra of LS and WL fibrils, which indicate that the WL fibrils are more dynamic and less organized than the LS fibrils. This agrees with hydrogen exchange and proteolysis data, which show that although WL fibrils have a protected core, it is not as extensive as that of LS fibrils.^{26,27} Furthermore, experiments using densitometry indicate that WL fibrils have a strong core but a more loosely packed exterior than LS fibrils, consistent with the MAS NMR data presented here.²⁸ FTIR experiments also indicate that there are differences at an atomic level between LS and WL fibrils, in that different amide I' absorbance maxima are observed.²⁹ In addition, recent studies using EPR,

FTIR and Raman spectroscopies have proposed that the side chains of LS fibrils have a more fixed spatial arrangement in the core than those of WL fibrils.^{19,30}

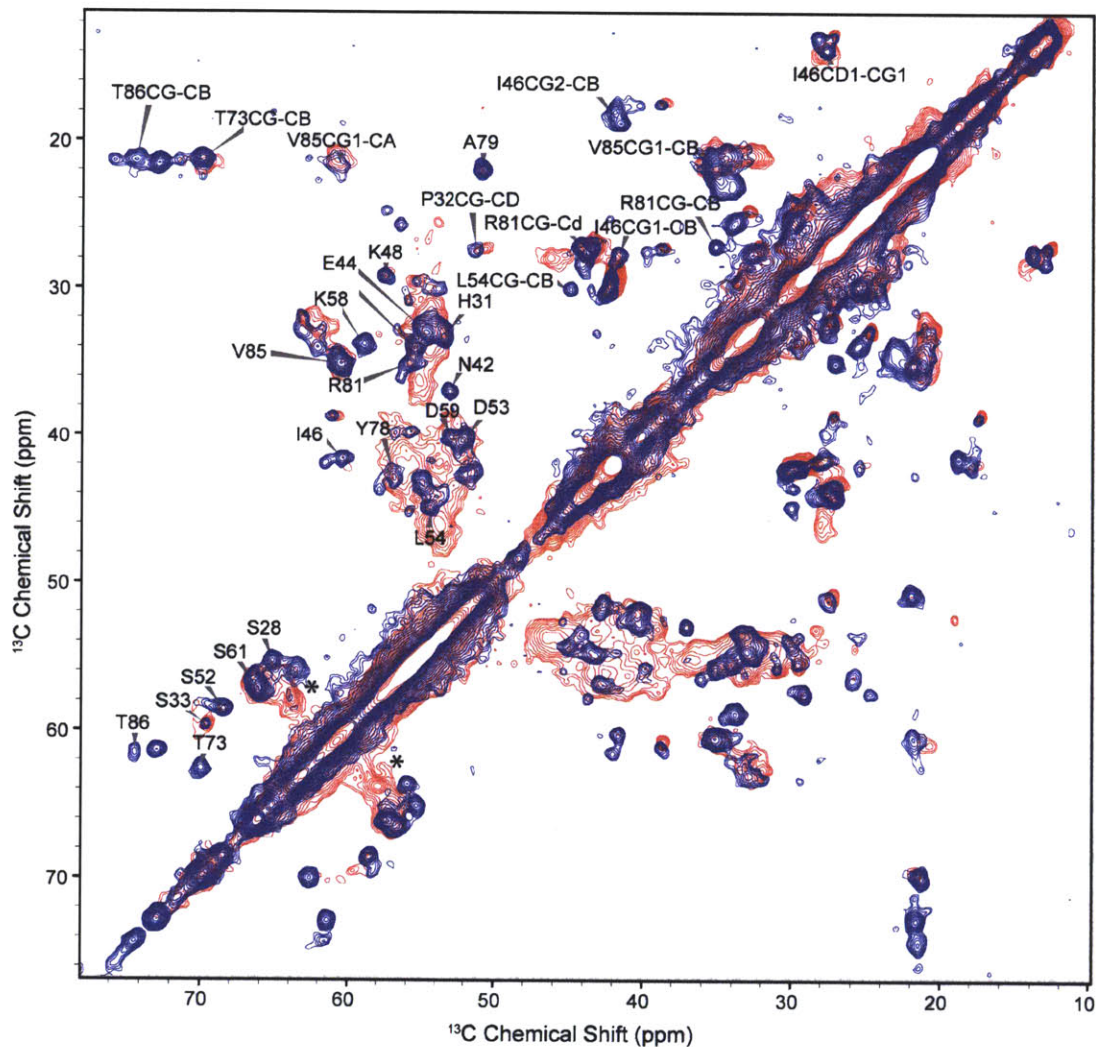


Figure 8.3. ^{13}C - ^{13}C correlation spectra comparing U- $\beta_2\text{m}$ WL (red) and U- $\beta_2\text{m}$ LS fibrils (blue) (RFDR $\tau_{\text{mix}} = 2.56$ ms, $\omega_r/2\pi = 12.5$ kHz for the WL fibrils, and RFDR $\tau_{\text{mix}} = 1.76$ ms, $\omega_r/2\pi = 18.182$ kHz for the LS fibrils). The labels represent the LS fibril assignments. The asterisk denotes a Ser C α -C β cross-peak that is much more prominent in the WL fibril spectrum.

Importantly, the data presented here support the idea that the distinct macroscopic morphological features of the $\beta_2\text{m}$ fibrils of different type, and perhaps the differences in their thermodynamic stability and reactivity to the amyloid specific dyes Congo Red and ThT as well as anti-amyloid antibodies,^{20,21} result from variation in structure and dynamics at the

molecular level, rather than from different association patterns starting from identical units. This is analogous to the fibril strain phenomena of prions, where the same protein sequences adopt alternative structures at a residue level leading to changes in fibril morphology, stability and ability to replicate.³¹

8.3. Comparison of LS and Δ N6 fibrils

The truncation variant Δ N6 is an important culprit in dialysis-related amyloidosis, since ~26 % of β_2 -microglobulin fibrils found in patients lack the six N-terminal residues.³² While it is not known whether the cleavage occurs before or after fibril formation, Δ N6 is highly amyloidogenic and can convert human β_2 m into an amyloid-competent state.¹³ The solution structure of Δ N6 is known, and while it retains a native backbone conformation, there is a significant repacking of the side-chains to accommodate the non-native *trans*-Pro32 conformer.¹³ More surprisingly, however, the structure of the variant in solution is amazingly similar to the structure of a slow-folding intermediate of the full-length protein,³³ indicating that a *cis/trans* proline isomerization may be an important step on the pathway to fibril formation for β_2 m. In particular, the N-terminus might play an important role in stabilizing the native but energetically non-favorable *cis*-conformation of Pro32. Therefore, when the N-terminus has been cleaved off or the side-chain interactions that fold it onto the rest of the protein structure have been disrupted due to changes in pH, the *trans*-Pro32 conformer is stabilized, and this provides a route for fibril formation. It is then perhaps not surprising that these six N-terminal residues do not participate in the fibril core of LS β_2 m fibrils, but are quite mobile and can be detected in solution NMR based experiments.¹⁷

In this section, we provide preliminary MAS NMR results aimed at obtaining insights into the structure of the Δ N6 fibrils, and comparing them to the structure of the better-characterized LS β_2 m fibrils. Figure 10.4 shows ^{13}C - ^{13}C correlation spectra of both fibril forms, obtained with RFDR mixing. At the mixing time used in this experiment ($\tau_{\text{mix}} = 1.7$ ms), primarily one-bond correlations are observed. The Δ N6 fibril spectrum presents good sensitivity, with some fairly well-resolved regions (i.e. in the Ser $\text{C}\alpha$ - $\text{C}\beta$ region eight cross-peaks can be observed) and some regions with a relatively broad intensity. The LS fibril spectrum presents fairly good resolution but a large number of the correlations expected based on the sequence are not observed. For example, only six of the nine expected Ser spin systems

give strong $\text{C}\alpha\text{-C}\beta$ correlations. While currently there are no chemical shift assignments available for the ΔN6 form, the inspection of the spectra in Figure 8.4 reveals that the majority of the cross-peaks are shifted between the two data sets.

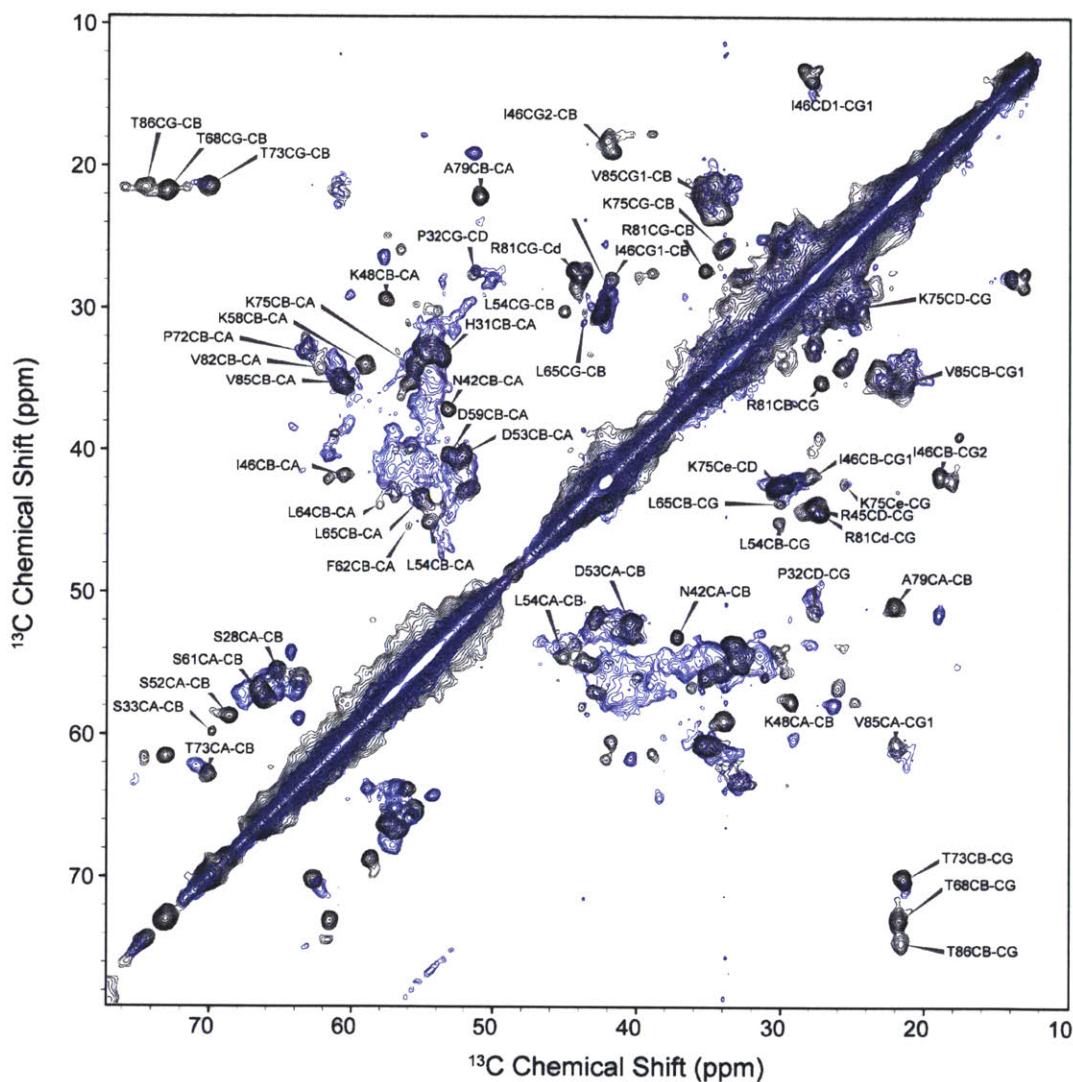


Figure 8.4. ^{13}C - ^{13}C correlation spectra of LS (black) and ΔN6 (blue) $\beta 2\text{m}$ fibrils. Spectra were acquired with RFDR mixing ($\tau_{\text{mix}} = 1.7$ ms) at 750 MHz ^1H Larmor frequency. At this mixing time, primarily one-bond correlations are observed. Labels correspond to assigned LS $\beta 2\text{m}$ fibrils peaks.

While some differences, especially in the protonated side-chains, might arise from the difference in pH (6.2 vs 2.5), there seem to be general differences in the backbone conformation as well. This is especially evident from the TEDOR spectrum (Figure 8.5),

which reports on the backbone N and C α conformation. For example, all of the glycine residues in the Δ N6 fibrils have chemical shifts similar to the LS fibril G43 (circles in Figure 10.5b), while LS fibril G29 and G18 are quite different. It is also interesting to note that for the Δ N6 sample, all three (and maybe a small extra peak) glycine residues are observed, while in the LS fibrils under very similar experimental conditions and uniform- ^{13}C labeling, one strong (G43) and one weak (G29) cross-peak are observed. G18 usually appears in LS fibrils prepared with 2-glycerol labeling (its usual position marked with an asterisks in Figure 8.5b).

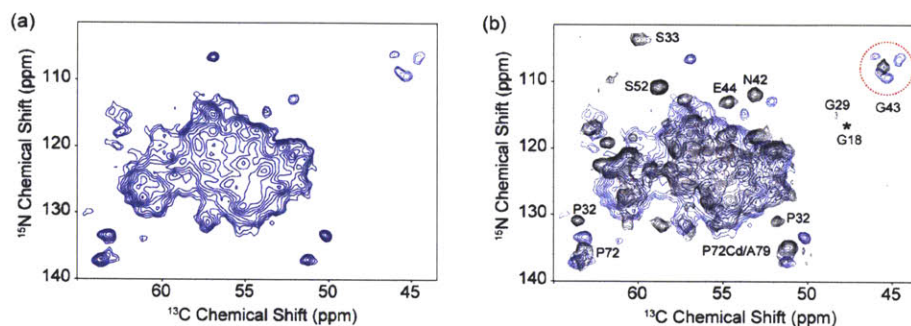


Figure 8.5. ^{15}N - ^{13}C correlation spectrum of Δ N6 (blue) β 2m fibrils (a) superimposed on a spectrum of the LS (black) β 2m fibrils (b). Spectra were acquired with TEDOR mixing ($\tau_{\text{mix}} = 1.6$ ms) at 750 MHz ^1H Larmor frequency. Labels correspond to $\text{N}_i\text{-C}\alpha_i$ correlations of some of the assigned LS β 2m fibrils peaks.

It is important to note that both the RFDR and TEDOR spectra contain more peaks in the Δ N6 case, than in the LS fibril case, i.e. the fibril core is perhaps more extensive. The additional signals, however, are sometimes less resolved and broad (e.g. in the C α -C β region in the RFDR spectrum), which could be due to dynamics. Using 2- ^{13}C and 1,3- ^{13}C glycerol as the carbon source could improve the resolution in the broader regions by reducing the spectral overlap, and by narrowing the line width due to the elimination of ^{13}C - ^{13}C J-couplings. There is no INEPT signal in the Δ N6 case, which excludes the possibility of very mobile regions present in this fibril form.

8.4. Materials and Methods.

8.4.1. Protein Expression and Purification

Recombinant human β_2 -microglobulin (β_2m) was expressed in HCDM1 minimal media and purified as described elsewhere.⁸⁸ Uniformly ^{13}C - and ^{15}N - labelled β_2m samples were prepared by growing BL21(DE3) pLysS *Escherichia coli* in the presence of minimal media enriched with 1 gL⁻¹ $^{15}NH_4Cl$ (Goss Scientific, UK) and 2 gL⁻¹ D-glucose- $^{13}C_6$ (Sigma Aldrich, UK).

8.4.2. Fibril Formation

The worm-like (WL) fibrils were formed at 3 mg ml⁻¹ in 200 mM ammonium formate buffer at pH 3.6, 37 °C with no shaking for 2 days. These fibrils were transferred in 50 mM ammonium formate buffer (pH 3.6) and centrifuged at 176,000 x g for 1 hr and packed into a Bruker 2.5 mm rotor.

8.4.3. MAS NMR Spectroscopy

Experiments were performed with a custom designed spectrometer (courtesy of D.J. Ruben, Francis Bitter Magnet Laboratory, Massachusetts Institute of Technology, Cambridge, MA) operating at 750 MHz 1H Larmor frequency. The spectrometer was equipped with triple-resonance Bruker probes (Bruker BioSpin, Billerica, MA) equipped with a 2.5 mm coil or a 3.2 mm E-free coil. The sample was cooled with a stream of dry air maintained at a temperature of -5 °C, while we estimate that the sample temperature during the MAS experiments was 10-15 °C higher.

1D CP experiments were recorded using 1.2-1.8 ms contact time and 83 kHz TPPM 1H decoupling during acquisition. A 2D ^{13}C - ^{13}C correlation experiment of the LS fibrils was recorded with an RFDR sequence with $\tau_{mix} = 1.76$ ms at $\omega_r/2\pi = 18.2$ kHz, with 40 kHz π pulses on the ^{13}C channel during mixing, and 83 kHz TPPM decoupling on the 1H channel during evolution, mixing and acquisition. The acquisition time was 12.3 ms and 24 ms in the indirect and direct dimensions respectively. The ^{13}C - ^{13}C correlation experiment of the WL fibrils was recorded with RFDR mixing ($\tau_{mix} = 2.56$ ms) at $\omega_r/2\pi = 12.5$ kHz, with 20 kHz π

pulses on the ^{13}C channel during mixing, and 83 kHz ^1H decoupling during mixing and acquisition. The carrier frequency was centred on the aliphatic region. The acquisition time in the indirect dimension was 8 ms, and 24 ms in the direct dimension respectively.

Acknowledgements

Samples were prepared by Dr. Geoffrey Platt and Dr. Claire Sarell in Prof. Sheena Radford's group at the University of Leeds, Leeds, UK.

References:

- (1) Chiti, F.; Dobson, C. M. *Annu. Rev. Biochem.* **2006**, *75*, 333-366.
- (2) Pedersen, J. S.; Andersen, C. B.; Otzen, D. E. *FEBS Journal* **2010**, *277*, 4591-4601.
- (3) Tycko, R. *Annu. Rev. Phys. Chem.* **2011**, *62*, 279-299.
- (4) Radford, S. E.; Gosal, W. S.; Platt, G. W. *BBA - Proteins Proteom.* **2005**, *1753*, 51-63.
- (5) Petkova, A. T.; Yau, W. M.; Tycko, R. *Biochemistry* **2006**, *45*, 498-512.
- (6) Paravastu, A. K.; Leapman, R. D.; Yau, W. M.; Tycko, R. *Proc. Natl. Acad. Sci. U. S. A.* **2008**, *105*, 18349-18354.
- (7) van der Wel, P. C. A.; Lewandoswki, J.; Griffin, R. G. *Biochemistry* **2010**, submitted.
- (8) van der Wel, P. C. A.; Lewandowski, J. R.; Griffin, R. G. *J. Am. Chem. Soc.* **2007**, 5117-5130.
- (9) Morales, R.; Abid, K.; Soto, C. *BBA - Mol. Basis Dis.* **2007**, *1772*, 681-691.
- (10) Baxa, U.; Cassese, T.; Kajava, A. V.; Steven, A. C.; Andrey Kajava, J. M. S.; David, A. D. P. In *Adv. Protein Chem*; Academic Press: 2006; Vol. Volume 73, p 125-180.
- (11) Calabrese, M. F.; Miranker, A. D. *Prion* **2009**, *3*, 1-4.
- (12) Platt, G. W.; Radford, S. E. *FEBS Lett.* **2009**, *583*, 2623-2629.
- (13) Eichner, T.; Kalverda, A. P.; Thompson, G. S.; Homans, S. W.; Radford, S. E. *Mol. Cell* **2011**, *41*, 161-172.
- (14) Platt, G. W.; McParland, V. J.; Kalverda, A. P.; Homans, S. W.; Radford, S. E. *J. Mol. Biol.* **2005**, *346*, 279-294.
- (15) Hoshino, M.; Katou, H.; Hagihara, Y.; Hasegawa, K.; Naiki, H.; Goto, Y. *Nat. Struct. Biol.* **2002**, *9*, 332-336.

- (16) White, H. E.; Hodgkinson, J. L.; Jahn, T. R.; Cohen-Krausz, S.; Gosal, W. S.; Muller, S.; Orlova, E. V.; Radford, S. E.; Saibil, H. R. *J. Mol. Biol.* **2009**, *389*, 48-57.
- (17) Debelouchina, G. T.; Platt, G. W.; Bayro, M. J.; Radford, S. E.; Griffin, R. G. *J. Am. Chem. Soc.* **2010**, *132*, 10414-10423.
- (18) Debelouchina, G. T.; Platt, G. W.; Bayro, M. J.; Radford, S. E.; Griffin, R. G. *J. Am. Chem. Soc.* **2010**, *132*, 17077-17079.
- (19) Ladner, C. L.; Chen, M.; Smith, D. P.; Platt, G. W.; Radford, S. E.; Langen, R. *J. Biol. Chem.* **2010**, *285*, 17137-17147.
- (20) Gosal, W. S.; Morten, I. J.; Hewitt, E. W.; Smith, D. A.; Thomson, N. H.; Radford, S. E. *J. Mol. Biol.* **2005**, *351*, 850-864.
- (21) Smith, D. P.; Jones, S.; Serpell, L. C.; Sunde, M.; Radford, S. E. *J. Mol. Biol.* **2003**, *330*, 943-954.
- (22) McParland, V. J.; Kad, N. M.; Kalverda, A. P.; Brown, A.; Kirwin-Jones, P.; Hunter, M. G.; Sunde, M.; Radford, S. E. *Biochemistry* **2000**, *39*, 8735-8746.
- (23) de Lacaillerie, J. B. D.; Jarry, B.; Pascui, O.; Reichert, D. *Solid State Nucl. Magn. Reson.* **2005**, *28*, 225-232.
- (24) Platt, G. W.; Routledge, K. E.; Homans, S. W.; Radford, S. E. *J. Mol. Biol.* **2008**, *378*, 251-263.
- (25) Xue, W. F.; Homans, S. W.; Radford, S. E. *Proc. Natl. Acad. Sci. U.S.A.* **2008**, *105*, 8926-8931.
- (26) Yamaguchi, K. I.; Katou, H.; Hoshino, M.; Hasegawa, K.; Naiki, H.; Goto, Y. *J. Mol. Biol.* **2004**, *338*, 559-571.
- (27) Myers, S. L.; Thomson, N. H.; Radford, S. E.; Ashcroft, A. E. *Rapid Commun. Mass Spectrom.* **2006**, *20*, 1628-1636.
- (28) Lee, Y. H.; Chatani, E.; Sasahara, K.; Naiki, H.; Goto, Y. *J. Biol. Chem.* **2009**, *284*, 2169-2175.
- (29) Jahn, T. R.; Tennent, G. A.; Radford, S. E. *J. Biol. Chem.* **2008**, *283*, 17279-17286.
- (30) Hiramatsu, H.; Lu, M.; Matsuo, K.; Gekko, K.; Goto, Y. J.; Kitagawa, T. *Biochemistry* **2010**, *49*, 742-751.
- (31) Toyama, B. H.; Kelly, M. J. S.; Gross, J. D.; Weissman, J. S. *Nature* **2007**, *449*, 233-237.

- (32) Bellotti, V.; Stoppini, M.; Mangione, P.; Sunde, M.; Robinson, C.; Asti, L.; Brancaccio, D.; Ferri, G. *Eur. J. Biochem.* **1998**, *258*, 61-67.
- (33) Eichner, T.; Radford, S. E. *J. Mol. Biol.* **2009**, *386*, 1312-1326.

CURRICULUM VITAE

EDUCATION

Colby College, B.A. Chemistry, Mathematics, *summa cum laude* 2001-2005
Massachusetts Institute of Technology, Ph.D. Physical Chemistry 2005-2011

PUBLICATIONS

“Intermolecular Structure Determination of Amyloid Fibrils by Magic-Angle Spinning NMR Spectroscopy and Dynamic Nuclear Polarization” Bayro MJ, Debelouchina GT, Eddy MT, Birkett, NR, Rosay M, Maas WE, Dobson CM, Griffin RG, *Journal of the American Chemical Society*, DOI:10.1021/ja203756x (2011).

“Quantum Mechanical Theory of Dynamic Nuclear Polarization in Solid Dielectrics” Hu KN, Debelouchina GT, Smith AA, Griffin RG, *The Journal of Chemical Physics*, 134, 125105 (2011).

“Intermolecular Alignment in β_2 -Microglobulin Amyloid Fibrils” Debelouchina GT, Platt GW, Bayro MJ, Radford SE, Griffin, RG, *Journal of the American Chemical Society*, 132, 17077 (2010).

“Magic Angle Spinning NMR Analysis of β_2 -Microglobulin Amyloid Fibrils in Two Distinct Morphologies” Debelouchina GT, Platt GW, Bayro MJ, Radford SE, Griffin RG, *Journal of the American Chemical Society*, 132, 10414 (2010).

“Dynamic Nuclear Polarization Enhanced Solid-State NMR Spectroscopy of GNNQQNY Crystals and Amyloid Fibrils” Debelouchina GT, Bayro MJ, van der Wel PCA, Caporini MA, Barnes AB, Rosay M, Maas WE, Griffin RG, *Physical Chemistry Chemical Physics*, 12, 5911 (2010).

“Z-Selective and Syndioselective Ring-Opening Metathesis Polymerization (ROMP) Initiated by Monoaryloxidepyrrolide (MAP) Catalysts” Flook MM, Gerber LCH, Debelouchina GT, Schrock R, *Macromolecules* 43, 7515 (2010).

“Synthesis of a BDPA-TEMPO Biradical” Dane EL, Maly T, Debelouchina GT, Griffin RG, Swager TM, *Organic Letters*, 11, 1871 (2009).

“Dynamic Nuclear Polarization at High Magnetic Fields” Maly T, Debelouchina GT, Bajaj VS, Hu KN, Joo CG, Mak-Jurkauskas ML, Sirigiri JR, van der Wel PCA, Herzfeld J, Temkin RJ, Griffin RG, *Journal of Chemical Physics*, 128, 052211 (2008).